

Self-heating hydrogel for mechanically-controlled drug release

THÈSE N° 6354 (2015)

PRÉSENTÉE LE 12 MARS 2015

À LA FACULTÉ DES SCIENCES ET TECHNIQUES DE L'INGÉNIEUR
LABORATOIRE DE BIOMÉCANIQUE EN ORTHOPÉDIE EPFL-CHUV-DAL
PROGRAMME DOCTORAL EN MÉCANIQUE

ÉCOLE POLYTECHNIQUE FÉDÉRALE DE LAUSANNE

POUR L'OBTENTION DU GRADE DE DOCTEUR ÈS SCIENCES

PAR

Mohamadreza NASSAJIAN MOGHADAM

acceptée sur proposition du jury:

Prof. J.-F. Molinari, président du jury
Prof. D. Pioletti, directeur de thèse
Dr O. Jordan, rapporteur
Dr C. Wandrey, rapporteuse
Prof. M. Zenobi-Wong, rapporteuse



ÉCOLE POLYTECHNIQUE
FÉDÉRALE DE LAUSANNE

Suisse
2015

Acknowledgements

I would like to express all my thanks to my thesis director, Prof. Dominique Pioletti, who gave me this opportunity to accomplish this thesis, for his guidance throughout the work and for all I learnt from him. Every day working with him was a precious experience. I am grateful for the liberty he gave me in this work and for his trust.

I would like to thank the members of my dissertation committee, Dr. Christine Wandrey, Prof. Marcy Zenobi-Wong and Dr. Olivier Jordan who have dedicated their precious time and expertise to examine my work. Also I would like to thank my mentor and the president of my exam Prof. Jean-François Molinari.

I would like to thank all the members of the Laboratory of Biomechanical Orthopedics (LBO) who were like my second family. Special thanks to Dr. Alexandre Terrier for his advises to develop the numerical models in this thesis. In particular, I would like to thank Dr. Arne Vogel for his advices. Special thanks for Sandra Jaccoud for her technical support for the cell culture, and to Dr. Philippe Abdel-Sayed, for his collaboration and fruitful discussions in biological aspects. Likewise, special thanks for Caroline Sieger Fernandes for her helps in statistical analysis. I am also grateful to the rest of the LBO family, Virginie Kokocinski, Dr. Salim Darwiche, Dr. Ulrike Kettenberger and Tanja Hausherr, Adeliya Latypova, Christoph Engelhardt, Antoine Dewarrat, Valérie Malfroy Camine, Naser Nasrollahzadeh and Valérie Parvex.

I would like to thank the people of the Laboratory of Polymer specially Prof. Harm-Anton Klok and Dr. Vitaliy Kolesov for their collaboration and preparing Thermosensitive nanoparticles for this project.

My special thanks to the students I have supervised during this thesis, for their great job and their influence in accomplishing this work.

Likewise thanks to Marc Jeanneret and team of the workshop, for their technical advices in designing and manufacturing the mechanical set-ups required for experiments.

Finally, I would like to thank my family who were far from me, but always were available for me, always believed in me and supported me all along this PhD thesis and thanks to my friends who were always with me where my family were far and let me feel like home.

Abstract

Due to our active lifestyle, knee cartilage is at risk for focal defects. Unfortunately, the native healing properties of the articular cartilage are very limited. New strategies to treat cartilage defects are then developed such as the local delivery of growth factors. For this particular approach, the delivery mode and timing are essential. In parallel, mechanical loading has been demonstrated to activate growth factor receptors involved in the healing process of the cartilage. It is thus proposed that using mechanical loading to control the growth factor release can increase its efficiency. However, a delay of 5 to 20 minutes is necessary for the activation of cell receptors following the initiation of a mechanical stimulation. The synergic effect between the mechanical loading and the delivery of growth factor could then be maximized by delaying the delivery of the growth factor following the initiation of the mechanical stimulation. The development of a hydrogel system allowing to delay the delivery of a pay-load following a mechanical stimulation is the primary objective of this thesis.

The main conceptual idea for developing the delayed delivery is to utilize the viscous dissipated energy of the hydrogel submitted to cyclic mechanical loading. Under specific conditions, the dissipated energy will induce a temperature increase in the hydrogel after a certain amount of time, and will then locally trigger the release of a drug incorporated in the hydrogel. With this approach, a new concept of drug release following a mechanical stimulation is developed, where the duration of the mechanical stimulation, before the drug release, can be controlled by the dissipative properties of the hydrogel. The proposed hydrogel system is composed of two components: a hydrogel matrix and thermosensitive nanogel particles. The hydrogel matrix is a chemically cross-linked hydrogel with high dissipative properties. The dissipation of the hydrogel under loading conditions results in a certain temperature increase several minutes after cyclic loading. Incorporated in this hydrogel matrix are thermosensitive nanogel particles, which can respond to the temperature increase when the temperature surpasses their Least Critical Solution Temperature

(LCST) and trigger the drug release. In this way, we can provide a time delay between the initiation of the mechanical load and the release of the drug.

We followed four steps to develop such a smart drug delivery system. In the first step, we developed a finite element model to study the heat transfer mechanism in knee cartilage. We also used this model to estimate the heat power required by the hydrogel under several minutes of mechanical loading to reach a local temperature increase of about 2°C. In the second step, we designed and optimized a self-heating hydrogel structure based on Hydroxyethyl Methacrylate (HEMA) with high dissipative properties and resistance to fracture under load. The developed hydrogel could dissipate sufficiently to cause an increase in temperature several minutes after the initiation of a mechanical load. In the third step we demonstrated the proof of concept for delayed drug release following a mechanical loading by combining the developed self-heating HEMA-based hydrogel with the thermosensitive poly(N-isopropyl acrylamide) (PNIPAM) nanogel particles. We showed that after 5 minutes of loading, the temperature surpassed the LCST of the nanoparticles due to the dissipation of the hydrogel. At this temperature, the PNIPAM nanoparticles shrank and thus increased the permeability of the hydrogel and expedited the release of a model drug by a factor of 3. In the last step, we improved our hydrogels to obtain a degradable version of the HEMA-based hydrogels with enhanced mechanical properties.

The developed dissipation-driven drug delivery system is a new approach, which allows us to take into account in the delivery mode the mechanical history to which the hydrogel will be exposed. This approach provides a temporal control over the drug release process, which should maximize the cell response to the release factor. This kind of temporal control is not possible with conventional drug delivery systems.

Keywords: drug delivery system, controlled release, hydrogel, viscous dissipation, mechanical loading, thermosensitive nanoparticles.

Résumé

En raison de notre mode de vie active, le cartilage du genou est sujet à des lésions localisées. Malheureusement, la capacité de régénération du cartilage articulaire est très limitée. Ainsi, de nouvelles stratégies pour traiter les lésions du cartilage ont été développées telles que l'administration locale de facteurs de croissance. Concernant cette approche, le mode d'acheminement et le contrôle temporel de la délivrance de ces facteurs de croissance sont cruciaux. Parallèlement, la stimulation mécanique du cartilage induit une activation des récepteurs des facteurs de croissance impliqués dans le processus de guérison de ce tissu. Il est donc proposé dans ce travail d'utiliser la stimulation mécanique pour contrôler la délivrance locale des facteurs de croissance. Néanmoins, il est important de noter qu'un délai de 5 à 20 minutes est nécessaire après une stimulation mécanique pour que les cellules puissent activer ses récepteurs. L'effet synergétique entre la stimulation mécanique et la délivrance des facteurs de croissance pourrait donc être maximisé si les facteurs de croissance étaient délivrés avec un certain retard suivant l'initiation de la stimulation mécanique. Le développement d'un hydrogel qui permet de délivrer un agent biologique quelques minutes après l'initiation d'une stimulation mécanique est l'objet principal de cette thèse.

L'idée centrale pour obtenir un retard de la délivrance d'un facteur de croissance est d'utiliser l'énergie visqueuse dissipée par l'hydrogel lorsque celui-ci est soumis à une stimulation mécanique cyclique. Sous des conditions particulières, l'énergie dissipée induit une augmentation de la température dans l'hydrogel après un certain temps et déclenchera localement la libération du facteur de croissance incorporé dans cet hydrogel. Avec cette approche, un nouveau concept de délivrance locale d'un agent biologique par une stimulation mécanique est développé. Ceci nous permet également de lier la durée de la stimulation mécanique aux propriétés dissipatives de l'hydrogel pour contrôler le délai de la délivrance des facteurs de croissance après l'initiation de la stimulation mécanique. Le système d'hydrogel proposé est constitué de deux composants: une matrice d'hydrogel et des particules de type nanogel thermosensibles. La matrice d'hydrogel est

obtenue par un procédé de réticulation chimique ce qui induit des propriétés dissipatives élevées pour l'hydrogel. La dissipation de l'hydrogel génère une augmentation de la température plusieurs minutes après la stimulation mécanique. Les particules de type nanogel thermosensibles sont incorporées dans la matrice d'hydrogel. Au-delà d'un certain seuil, elles réagissent à l'augmentation de température et libèrent le facteur de croissance. Ainsi, un délai est obtenu entre le début de la stimulation mécanique et la délivrance du facteur de croissance.

Nous avons suivi quatre étapes pour développer un tel système de délivrance locale. Dans la première étape, nous avons développé un modèle d'éléments finis pour étudier le mécanisme de transfert de chaleur dans le cartilage du genou. Nous avons ensuite utilisé ce modèle pour estimer la chaleur à produire par l'hydrogel pendant plusieurs minutes de stimulation mécanique pour atteindre une augmentation locale de la température d'environ 2°C. Dans la seconde étape, nous avons conçu et optimisé une structure d'hydrogel auto-chauffante basée sur de l'Hydroxyethyl Methacrylate (HEMA) présentant des propriétés dissipatives élevées et résistant aux fractures sous chargement. Cet hydrogel peut dissiper suffisamment d'énergie pour induire une augmentation de la température quelques minutes après le début de la stimulation mécanique. Dans la troisième étape, nous avons apporté la démonstration du concept de la délivrance retardée d'un agent après une stimulation mécanique en combinant l'hydrogel auto-chauffant basé sur du HEMA avec des particules thermosensibles de nanogel poly(N-isopropyl acrylamide) (PNIPAM). Nous avons montré qu'après 5 minutes de stimulation, la température a dépassé la valeur seuil des nanoparticules. À cette température, les nanoparticules de PNIPAM se rétractent ce qui augmente la perméabilité de l'hydrogel et accélère par un facteur 3 la délivrance d'un agent incorporé dans l'hydrogel. Dans la dernière étape, nous avons amélioré notre hydrogel pour obtenir une version dégradable et présentant des propriétés mécaniques augmentées.

Le système de délivrance d'un agent thérapeutique par dissipation est une nouvelle approche qui nous permet de prendre en compte, dans la mode de délivrance, l'historique mécanique auquel l'hydrogel est soumis. Cette approche permet le contrôle temporel du processus de libération de l'agent ce qui devrait maximiser la réponse cellulaire à l'agent délivré. Ce genre de contrôle temporel n'est pas possible avec un système conventionnel.

Mots-clés: Système de délivrance de médicament, relargage contrôlé, hydrogel, dissipation visqueuse, chargement mécanique, nanoparticules thermosensibles.

Table of Contents

Acknowledgements	i
Abstract	iii
Résumé	v
Chapter 1 Introduction.....	1
1.1 Articular Cartilage.....	3
1.1.1 Composition and Structure of Articular Cartilage.....	3
1.1.2 Cartilage Focal Defects.....	4
1.1.3 Cartilage Treatment.....	4
1.1.4 Effect of Growth Factor Delivery on Cartilage Regeneration.....	6
1.2 Controlled Drug Delivery System for Cartilage Treatment	7
1.2.1 Hydrogels as Drug Carriers.....	7
1.2.2 Environmental Variables to Control Drug Release	8
1.2.3 Effects of Mechanical Load on the Delivery of Growth Factors to Cartilage Cells	9
1.2.4 Coupling Drug Release with Mechanical Stimulation	11
1.2.5 Temporal Control of Drug Release via Mechanical Stimulation	12
1.2.5.1 Viscous Dissipation and Hysteresis Loop.....	12
1.2.5.2 Viscous Dissipation as a New Environmental Variable to Control Drug Delivery	12
1.3 Thesis Objectives	13
1.3.1 Overall Goal	13
1.3.2 Specific Aims	14
1.4 References.....	16
Chapter 2 Modeling the Heat Transfer in Articular Cartilage	23
2.1 Impact of Synovial Fluid Flow on Temperature Regulation in Knee Cartilage *	25
2.1.1 Abstract.....	25
2.1.2 Introduction	26
2.1.3 Methods.....	27
2.1.3.1 Model of Heat Transfer in Cartilage	27
2.1.3.2 Experimental Determination of the Model Parameters.....	29
2.1.4 Results.....	31

2.1.4.1	Experimental Determination of the Model Parameters.....	31
2.1.4.2	Model of Heat Transfer in Cartilage	31
2.1.5	Discussion	33
2.1.6	Conclusion.....	35
2.1.7	Acknowledgments.....	35
2.1.8	References	36
2.2	Estimation of the Required Heat Power for a Relevant Temperature Increase in Hydrogels to Activate Thermosensitive Nanoparticles	38
2.2.1	Introduction	38
2.2.2	Methods.....	38
2.2.3	Results and Discussion	39
2.2.4	References	39
Chapter 3	Developing a Self-heating Hydrogel Structure with High Dissipative Properties.....	41
3.1	Abstract.....	43
3.2	Introduction	44
3.3	Materials and Methods	45
3.3.1	Materials.....	45
3.3.2	Hydrogel Preparation.....	46
3.3.2.1	PHEMA hydrogels.....	46
3.3.2.2	HEMA-PEGM hydrogels.....	46
3.3.3	Hydrogel Mechanical Characterization	47
3.3.3.1	Dissipation measurement	47
3.3.3.2	Damping ratio measurement	47
3.4	Results.....	48
3.4.1	Effect of Cross-Linker	48
3.4.2	Effect of Water Ratio	50
3.4.3	Effect of Hydrophobicity	50
3.5	Discussion.....	52
3.6	Conclusion.....	55
3.7	Acknowledgment.....	55
3.8	References.....	56
Chapter 4	Controlled Release from Composite Hydrogel	59
4.1	Abstract.....	61
4.2	Introduction	62

4.3	Materials and Methods	63
4.3.1	Principle of Dissipation Used as an Environmental Variable.....	63
4.3.2	Materials	64
4.3.3	Preparation of the Nanoparticles	64
4.3.4	Preparation of the Composite Hydrogel	65
4.3.5	Quantification of Xylene Cyanole FF Release.....	66
4.3.6	Mechanical Loading	67
4.3.7	Effective Diffusion Coefficient Measurement.....	67
4.4	Results.....	68
4.4.1	Temperature Response of Nanoparticles	68
4.4.2	Composite Hydrogels.....	69
4.4.3	Self-Heating of Hydrogels Due to Dissipation	69
4.4.4	Drug Release Due to Dissipation.....	70
4.4.5	Effective Diffusion Coefficient.....	71
4.5	Discussion.....	72
4.6	Conclusion.....	74
4.7	Acknowledgments	74
4.8	References.....	74
Chapter 5	Improving Self-Heating Hydrogels for Clinical Application	77
5.1	Abstract.....	79
5.2	Introduction	80
5.3	Materials and Methods	81
5.3.1	Materials	81
5.3.2	DMHA Synthesis.....	82
5.3.3	Hydrogels Synthesis	82
5.3.4	Swelling and Mechanical Evaluation of Hydrogels.....	84
5.3.5	Accelerated Degradation Study	85
5.3.6	Mechanical Stiffness and Weight Lost of Hydrogels Under Cyclic Loading.....	85
5.3.7	Molecular Weight of Degradation Products	86
5.3.8	Structure of Hydrogels Obtained by SEM	86
5.3.9	Biocompatibility of Hydrogels and Degradation Products.....	86
5.3.10	Statistical Test.....	87
5.4	Results.....	87
5.4.1	Swelling and Mechanical Evaluation of Hydrogels.....	87

5.4.2	Accelerated Degradation Study	88
5.4.3	Mechanical Stiffness and Weight Lost by Hydrogels under Cyclic Loading	89
5.4.4	Molecular Weight of Degradation Products	91
5.4.5	Structure of Hydrogels Obtained by SEM	92
5.4.6	Biocompatibility of Hydrogels and Degradation Products.....	93
5.5	Discussion.....	94
5.6	Conclusion	97
5.7	Acknowledgments	97
5.8	References.....	97
Chapter 6	Conclusion	101
6.1	Summary of Findings	103
6.2	General Discussion	104
6.3	Future Works.....	106
6.3.1	Improvement of the Thermosensitive Nanoparticles	106
6.3.2	Improving the Mesh Size of Hydrogels to Deliver Larger Drugs.....	106
6.3.3	HEMA Hydrogels as a Mechanically Controlled Drug Delivery System	107
6.3.4	Clinical Application.....	108
6.4	References.....	109
Chapter 7	APPENDIX	111
7.1	APPENDIX for Chapter 3.....	113
7.1.1	Supplementary Tables	113
7.1.2	Supplementary Methods: Mesh Size Measurement.....	114
7.2	APPENDIX for Chapter 4.....	115
7.2.1	Supplementary Figures	115
7.3	APPENDIX for Chapter 6.....	117
7.3.1	Supplementary Methods: Lysozyme Release form HEMA-DMHA-Tetrakis Hydrogels	117
7.4	Reference	117
Curriculum Vitae	119

Chapter 1

Introduction

1.1 Articular Cartilage

1.1.1 Composition and Structure of Articular Cartilage

Articular cartilage is a connective tissue, which covers the surface of joints and allows them to slide over one another. Articular cartilage is composed of cells called chondrocytes with a specific round shape morphology. The chondrocytes are dispersed in a biphasic extracellular matrix (ECM), which is composed mainly of water (65%-80% wet weight) and two protein macromolecules: collagen and proteoglycans (Cohen et al., 1998, Mow et al., 1984). The mechanical behavior of articular cartilage is determined by the interaction of these two predominant components. Over half of the dry weight of cartilage is made of type II collagen, which is the most prevalent type of collagen in articular cartilage. The other main macromolecule of cartilage is proteoglycan made of a protein core covalently bonded to polysaccharide chains, called glycosaminoglycans (GAGs). The most common proteoglycan in articular cartilage is aggrecan (Athanasίου et al., 2009, Bobick et al., 2009), which is made of hyaluronan with numerous GAG side chains, mainly chondroitin sulfate and keratan sulfate (Figure 1.1A). Articular cartilage also has a small fraction of proteins, including oligomeric proteins, fibronectin, link proteins, thrombospondin and chondrocalcin (Cohen et al., 1998).

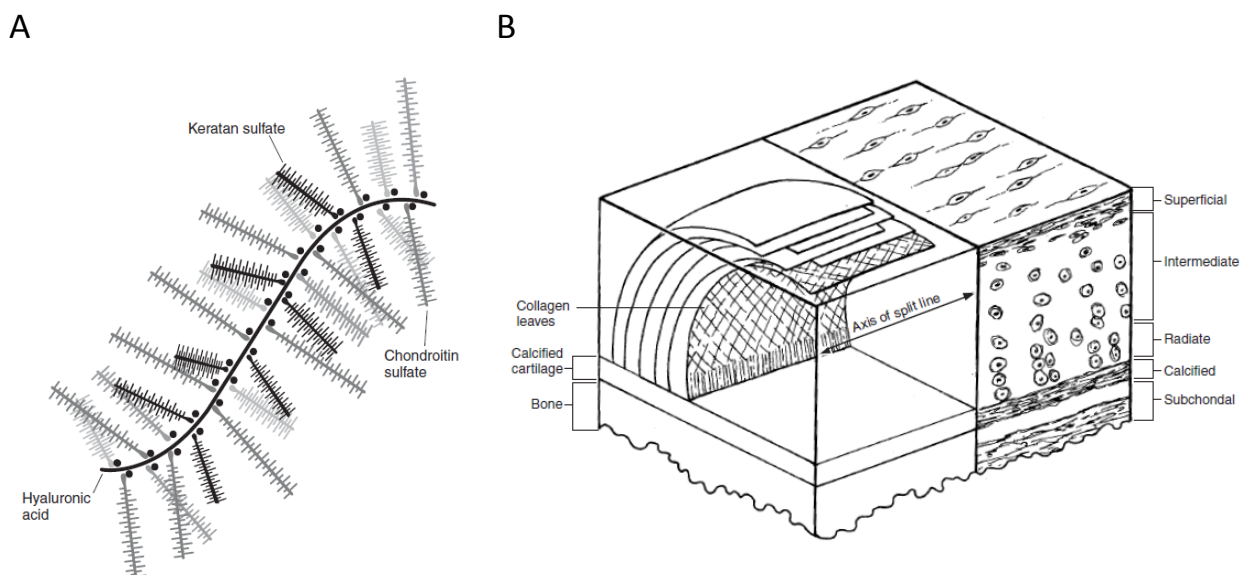


Figure 1.1. (A) A proteoglycan aggregate and (B) cross sections cut through the thickness of articular cartilage on two mutually orthogonal planes showing the four zones of the cartilage as well as the organization of collagen fibers with varying organization through the thickness of the cartilage (Mansour, 2003).

Articular cartilage structure is described by four zones (Figure 1.1B): first is the superficial tangential zone composed of densely packed collagen fibrils oriented parallel to the articular surface. Second is the intermediate zone, composed of randomly orientated fibers with high proteoglycan content, and they have larger diameters. The third zone is the deep zone composed of bundles of perpendicularly orientated collagen fibers anchoring tissue to the bony interface. The final zone is the calcified zone, which makes the transition into the subchondral bone. In the deep zone, water content is the lowest and the proteoglycan content is the highest of all the zones (Clark, 1990, Radin and Rose, 1986).

1.1.2 Cartilage Focal Defects

Articular cartilage serves as a load-bearing and shock-absorbing material for synovial joints. Due to the active lifestyle of humans, knee cartilage is especially at risk for focal defect. When a knee injury occurs, some focal defects can be created in the tibial or femoral cartilage. The size of these defects can vary from several square millimeters to several square centimeters. Defects smaller than 2 cm² are considered small (Figure 1.2). Regardless of defect size, it has been shown that damage to articular cartilage can lead to the accelerated onset of osteoarthritis (Athanasίου et al., 2009, Gillogly et al., 1998).

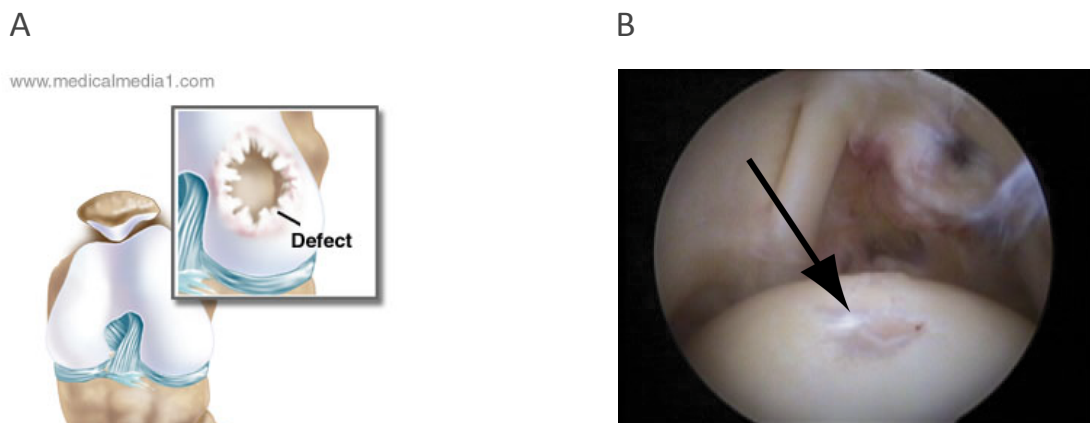


Figure 1.2. Cartilage focal defect. (A) Cartoon view (B) Arthroscopic view of the humeral head with a focal cartilage defect (arrow) (Ruckstuhl et al., 2008).

1.1.3 Cartilage Treatment

Unfortunately, the native healing properties of articular cartilage are very limited. This is due to two main factors: first is a lack of vascularity, and consequently the exchanges between articular

cartilage and surrounding tissues rely on transport phenomena. The second factor is a lack of progenitor cells and a sparse and highly differentiated cell population (Holland and Mikos, 2003, Van Osch et al., 2009).

During the past several decades, several techniques have been developed to address the problem of cartilage healing. Some of these techniques like subchondral drilling (Pridie and Gordon, 1959), abrasion (Johnson, 1986), and microfracture (Steadman et al., 1997) (Figure 1.3A) are based on the stimulation of articular cartilage healing through breaching the subchondral bone. In these methods, pluripotent stem cells from the bone marrow can remodel the fibrin clot. However, penetrating to the subchondral bone results in the formation of fibrocartilage instead of hyaline cartilage (Magnussen et al., 2008). Fibrocartilage is made to resist tension forces, while the hyaline cartilage, which is the correct tissue for knee cartilage, is made to resist compression forces (Gomoll et al., 2010). More recently, some techniques have been proposed that are independent to the recruitment of pluripotent cells. A technique called Osteochondral Autograft Transfer (OAT) has been developed to replace articular cartilage defects with osteochondral grafts. In this technique, one large graft or multiple smaller cylinders are harvested from minimal weight bearing parts of the distal femur and transplanted to fill defects in higher weight bearing areas (mosaicplasty) (Hangody et al., 1998) (Figure 1.3B). Another method is Autologous Chondrocyte Implantation (ACI) which is based on the implantation of cultured chondrocytes in the articular cartilage defect (Haddo et al., 2004) (Figure 1.3C).

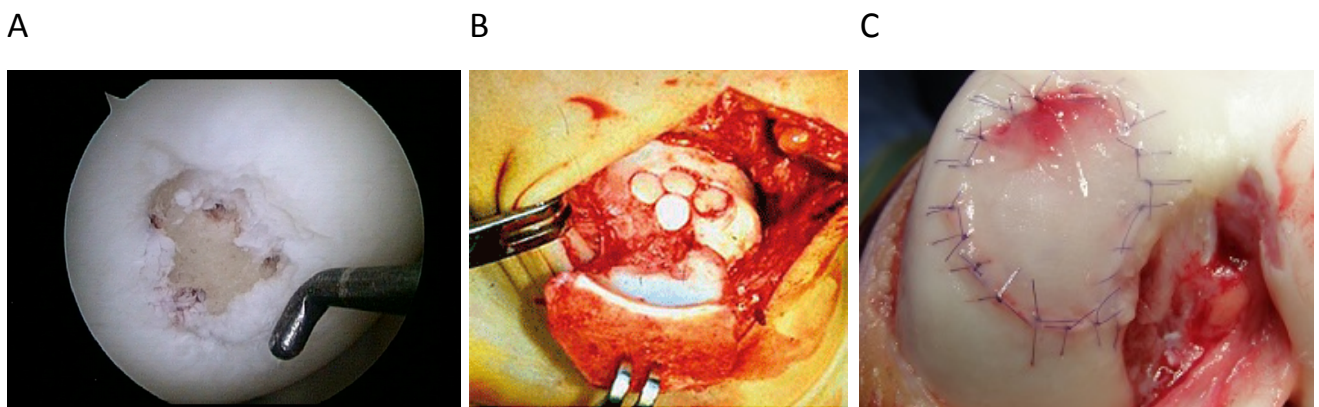


Figure 1.3. (A) Microfracture technic for cartilage therapy (<http://www.drkhalfayan.com>) (B) Osteochondral Autograft Transfer (OAT) for a moderate osteochondral defect (Chuckpaiwong, 2009) (C) Autologous Chondrocyte Implantation (ACI) for a moderate osteochondral defect (<http://www.brighamandwomens.org>).

1.1.4 Effect of Growth Factor Delivery on Cartilage Regeneration

Most of the existing cartilage repair techniques have not yet been proven successful. Therefore the treatment options are limited and the long-term outcomes are still uncertain (Magnussen et al., 2008). Scientists hoping to improve cartilage regeneration have demonstrated that the delivery of a number of different growth factors has an impact on articular cartilage repair (Mauck et al., 2003).

Growth factors are essential signaling molecules capable of stimulating cell growth in order to increase cell mass and play an important role in initiating the repair response. They are synthesized and secreted by cells in a large range of tissues and usually act in a paracrine or autocrine manner on the target-cell, as opposed to hormones that act in an endocrine manner (Alberts et al., 2013). Growth factors stimulate cell growth by binding to receptors on the surface of the target-cell and activating intracellular signaling pathways. By increasing the rate of the protein synthesis and decreasing its degradation rate, these pathways stimulate the accumulation of proteins and some other macromolecules. They also trigger the increased uptake of nutrients and production of ATP, which is required to fuel increased protein synthesis (Alberts et al., 2013, Lima et al., 2007).

One of the most important growth factors is Transforming Growth Factor-beta (TGF- β). TGF- β is a multifunctional peptide, which controls cell proliferation and differentiation. The TGF- β super-family includes bone morphogenetic protein (BMP), which induces the formation of bone and cartilage. In particular, it has been reported that TGF- β 3 is more responsible than other types of TGF- β super-families in the formation of cartilage (Chimal-Monroy and Diaz de Leon, 1999, Lima et al., 2007).

Although TGF- β growth factors are released from the subchondral cells, it has been shown that the delivery of these growth factors highly enhances the healing process of tissues in different organs of body, like the intervertebral discs (Masuda and An, 2006) or articular cartilage (Chung and Burdick, 2008, Elder and Athanasiou, 2008). On the other hand, over-expression of TGF- β can cause some problems including kidney disease, diabetes, renal fibrosis, and end-stage renal disease (ESRD). Therefore, it is how these growth factors are delivered that holds the key for tissue regeneration (Getgood et al., 2009). The timing and delivery of these factors remain a challenge, and designing an efficient and controlled drug delivery system is of great interest.

1.2 Controlled Drug Delivery System for Cartilage Treatment

1.2.1 Hydrogels as Drug Carriers

It is generally accepted that drug delivery may enhance the healing process of defected tissues in different parts of body. In this context, the most successful drug carriers have been based on hydrogels (Hoffman, 2002, Kamath and Park, 1993). Hydrogels are water swollen polymer networks that are widely used in biomedical applications. Due to the porous structure of hydrogels and their high water content, they can mimic biological tissues. They can be produced in the form of thin films, nanoparticles or scaffolds, for a wide range of biomedical applications (Peppas et al., 2000, Peppas et al., 2006). In order to prevent the dissolution of hydrogels in an aqueous environment, cross-links have to be employed in the hydrogel structure. With chemical cross-linking (covalent bonds) (Hennink and Van Nostrum, 2012) or physical interactions, hydrogels present a unique three-dimensional structure with tunable swelling behavior, degradation and mechanical properties (Hennink and van Nostrum, 2012, Klouda and Mikos, 2008). Physical interactions include crystallite formation (Kenawy et al., 2014), secondary forces like hydrophobic, electrostatic, or hydrogen-bonding forces (De Jong et al., 2001, Sun et al., 2012) or chain entanglements (Han et al., 2008). Physically cross-linked hydrogels have better swelling and degradation properties, but they are mechanically poor. In contrast, covalently bonded hydrogels can exhibit high stability and mechanical properties, but due to strong covalent bonds their degradation is limited (Hennink and Van Nostrum, 2012). However, by introducing hydrolytically cleavable or enzymatically labile bonds, their degradation properties can be improved to some extent (Atzet et al., 2008, Moffat and Marra, 2004). Hydrogels can be formed in situ and provide a tool for special therapeutics in the form of injectable biomaterials. For example, a polymer solution can form hydrogel in situ, via photo-polymerization (Baker et al., 2009), ionic crosslinking (Kuo and Ma, 2001), chemical crosslinking (Ossipov and Hilborn, 2006, Shu et al., 2006), or in response to an environmental stimulus such as temperature or pH (Qiu and Park, 2012).

The porous structure of hydrogels can be controlled by changing certain polymerization parameters, like the type and amount of a cross-linker, in order to trigger the release of a specific drug with a specific molecular size (Baker et al., 2009, Peppas et al., 2000). Different mechanisms can be used to trigger the drug release; for example swelling behaviors, degradation, or environmental stimuli like pH or temperature (Figure 1.4) (Peppas et al., 2006). In thermo-responsive hydrogels,

temperature change acts as the trigger to determines the behavior of the gel (Klouda and Mikos, 2008).

In the context of the delivery of growth factors, most research has been focused on direct drug loading in hydrogels, microspheres or microparticles, which undergo slow hydrolytic degradation. With direct drug loading, the release profile can be dictated by degradation and diffusion (Chung and Burdick, 2008). For example, an emulsion-coated scaffold has been shown to tailor the release of TGF- β 3 from 12 to 50 days (Van Osch et al., 2009).

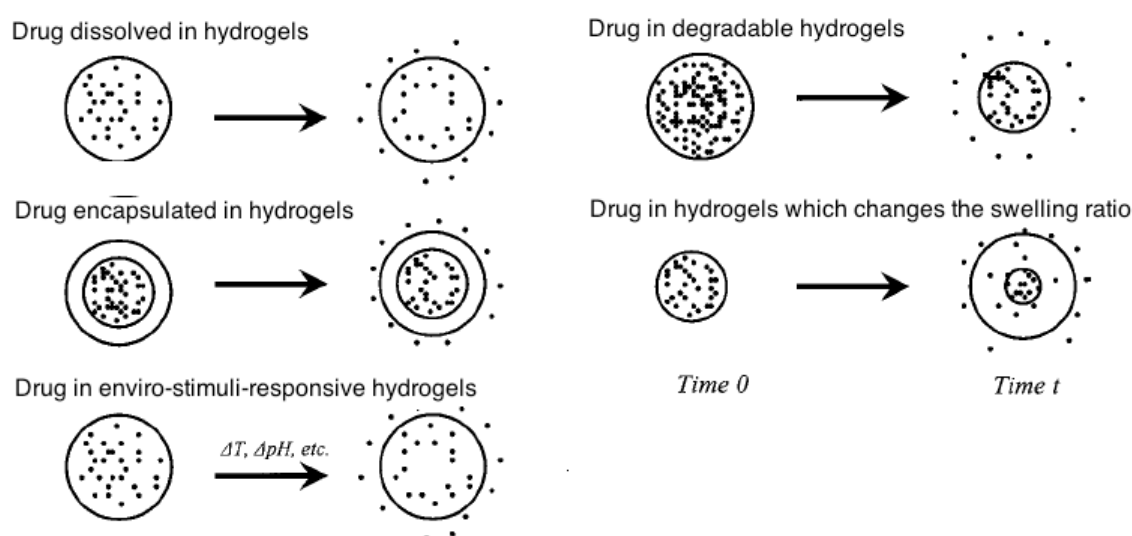


Figure 1.4. Various delivery and release mechanism of hydrogels (Peppas et al., 2006).

1.2.2 Environmental Variables to Control Drug Release

Controlling the drug release is of great importance since it can prevent an overdose and allow drug delivery over a longer time period, thus increasing release efficiency. Most research in the field of controlled drug release has focused on smart drug delivery systems and the development of environmentally stimulated hydrogels (Qiu and Park, 2012). Temperature and pH are the two most commonly used environmental variables that control drug delivery by increasing or decreasing the degree of polymer swelling (Gil and Hudson, 2004, Lin and Metters, 2006, Park et al., 2001). While pH is coupled with variations within the body (Priya James et al., 2014), temperature-responsive drug delivery systems are designed to control the drug release when their temperature is altered by an external heat source (Schmaljohann, 2006). They are often based on hydrogels containing polymers with a Lower Critical Solution Temperature (LCST), around 38°C,

so that the drug is released when the tissue surrounding the hydrogel reaches a temperature slightly above the physiological value (Zhang and Misra, 2007). However, using an external heat source limits their application in controlling the drug release at the defects in deep tissues (Klouda and Mikos, 2008).

While such environmentally stimulated hydrogel-based approaches can be interesting for growth factor delivery, by using these methods there is no guarantee that the growth factor will reach an available receptor on a cell on time. Indeed, to design an effective drug delivery system, we should consider the environment in which it is supposed to function. Considering the environment of a synovial joint and the fact that articular cartilage works under cyclic mechanical loading, mechanical loading may be a suitable parameter to use as a driver for drug release. Moreover, mechanical loading has been identified as a key factor in improving the activation of growth factors for the treatment of such tissues (Li et al., 2010, Neu et al., 2007), which is discussed in the following section.

1.2.3 Effects of Mechanical Load on the Delivery of Growth Factors to Cartilage Cells

Mechanical loading stimulates some cellular response and can trigger several molecular cascades. A synergetic effect exists between mechanical loading and the delivery of growth factors to the cell (Li et al., 2010). Growth factor delivery via mechanical loading can be accomplished in two ways: either by enhancing the expression of TGF- β receptors on cells so that cells can accept more TGF- β , or by increasing the amount of TGF- β molecules available to cells (Buscemi et al., 2011). This synergy was initially observed in bone with growth factors systemically injected (Chow et al. 1998). More recently, it has been shown that sequential cyclic stretching and TGF- β 3 supplementation lead to both improved mechanical properties and increased elastin deposition in engineered connective tissues (Syedain and Tranquillo, 2011). With respect to TGF- β 3 receptors, it has been demonstrated that the synergetic effect of mechanical stimulus and TGF- β 3 on nucleus pulposus cells is due to an increase in the expression of TGF- β 3 receptors following mechanical stimulation (Hiyama et al., 2007, Stadelmann et al., 2008). It is interesting to note that although these cells produce TGF- β 3, the produced amount was not enough to saturate receptors. But, exogenous addition of TGF- β 3 still increased the positive effect on extracellular matrix synthesis.

Similar results were found for cartilage (Neu et al., 2007, Ohno et al., 2005). One of the first studies describing synergetic effects between mechanical stimulus and growth factors in cartilage tissue engineering involved combining dynamic compression loading with IGF-1 delivery (Bonassar et al., 2001). IGF-1, which is stored in the extracellular matrix, is the main anabolic growth factor of articular cartilage (Getgood et al., 2009) and increases the production of proteoglycans and type II collagen (Chung and Burdick, 2008). In the study of Bonassar *et al.*, it was also mentioned that dynamic compression by itself might play a role in improving the access of soluble growth factors to these isolated cells through a convection effect (Bonassar et al., 2001). Apart from IGF-1, TGF- β 3 was also demonstrated to have a synergetic effect with mechanical loading, specifically on proteoglycan and collagen content and the equilibrium aggregate modulus of chondrocytes cultured in agarose hydrogels (Mauck et al., 2003). These synergetic effects have also been confirmed between hydrostatic pressure and TGF- β 3 on engineered articular cartilage constructs (Elder and Athanasiou, 2008, Syedain and Tranquillo, 2011). To induce a biological response, the growth factor must activate a cascade of events, starting with binding to a specific cell receptor (Figure 1.5). This signaling pathway takes some time and therefore cell receptors are not immediately activated following mechanical loading. Indeed, a delay of 5 to 20 minutes has been observed between the initiation of mechanical loading and the activation of cell receptors (Cheng et al., 1996, HU et al., 2008, Tschumperlin et al., 2004).

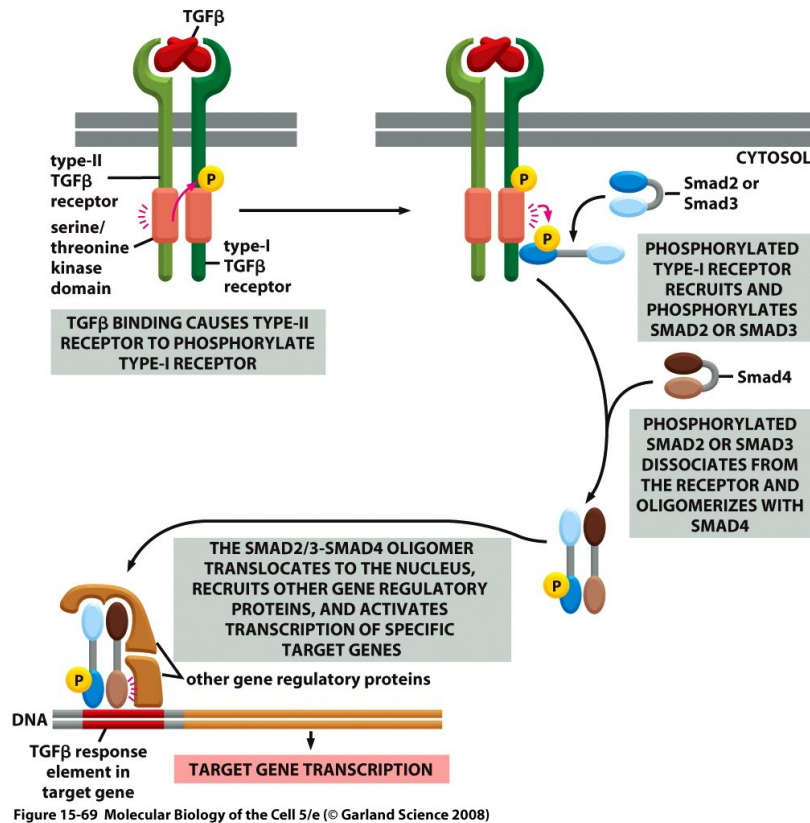


Figure 1.5. TGF- β signaling pathway. This signaling passway takes some time since a cascade of events must be activated before getting a response to an external stimulation (Albert et al. 2008).

1.2.4 Coupling Drug Release with Mechanical Stimulation

Considering the environment of the synovial joint where articular cartilage is permanently subjected to mechanical loading and the corresponding effect of mechanical loading on TGF- β delivery to cartilage cells, it seems that mechanical loading can be a promising environmental variable to control the release of growth factors. In this context, there have been only a limited number of investigations on systems, which were designed to release a drug based on a direct hydrogel matrix deformation either by mechanical loading or by magnetic field (Edelman et al., 1992, Lee et al., 2000). For example, Lee and co-workers showed that the release of vascular growth factors is correlated with direct mechanical loading (Lee et al., 2000). The study further showed that the release was dependent on the magnitude of the input load. However, no tailoring of this delivery was performed. As mentioned in previous sections, cells need time to respond to mechanical loading. Indeed, the major drawback of currently proposed systems is that it is not possible to delay the release of grow factors to match the delay in cell receptor activation (Lin and Metters, 2006).

In order to maximize the biological efficiency of growth factor delivery, it would be advantageous to release the growth factors only after a mechanical stimulation of known duration has been applied. In other words, if we have a mechanically controlled system which releases its payload without any delay after loading, the maximum potency of the treatment will not be reached.

1.2.5 Temporal Control of Drug Release via Mechanical Stimulation

1.2.5.1 Viscous Dissipation and Hysteresis Loop

Under cyclic loading, viscoelastic materials exhibit hysteresis, which leads to the dissipation of mechanical energy. The dissipated energy is transformed into heat, which can increase the temperature of the material. Considering the force-displacement graph of a material under cyclic loading, (Figure 1.6) the integral of the area within the hysteresis loop on the graph represents the dissipated energy during one loading cycle. A larger hysteresis loop indicates a material with greater dissipation properties. Furthermore, the total energy given to material during loading is represented by the integral of the total area under the loading curve in this graph (Lakes, 1999, Li and Xu, 2007).

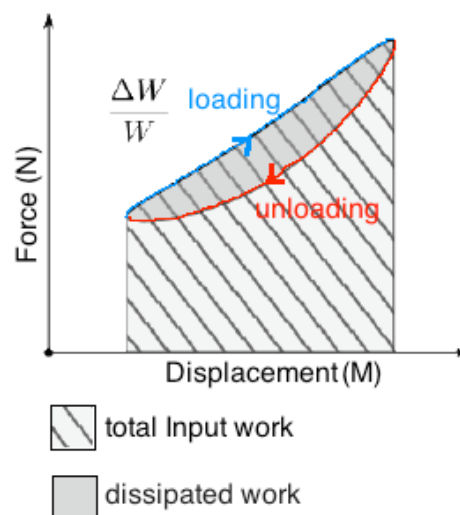


Figure 1.6. Hysteresis curve of viscoelastic material under cyclic mechanical loading.

1.2.5.2 Viscous Dissipation as a New Environmental Variable to Control Drug Delivery

To achieve the delay in drug release following mechanical loading, we suggest the use of the internal dissipation as a new environmental variable. With this strategy, the drug will not be re-

leased unless we reach the required dissipation amount, and this dissipation will not be met unless the material experiences mechanical loading for several minutes.

Having such a drug delivery system, there is a high potential to improve growth factor therapy by delivering growth factors when their respective receptors are available. In this situation, less growth factor would be needed and higher biological activity would certainly be obtained. This new approach is attractive from a clinical point of view. In the following section we will explain how viscous dissipation can be utilized for this purpose.

1.3 Thesis Objectives

1.3.1 Overall Goal

The primary objective of this project is to utilize the dissipated “lost” energy from cyclic loading which induces a temperature increase in order to locally trigger and/or accelerate, and allow temporal control of the release of a drug or growth factor incorporated in a hydrogel. We propose a new concept of drug release following a mechanical stimulation, where the duration of the mechanical stimulation, before the drug release, can be controlled. In this way we can provide a couple of minutes delay between the initiation of load and the release of the drug.

Indeed, since energy dissipation leads to temperature increase, we want to exploit the temperature increase generated by internal viscous dissipation to design a self-heating hydrogel system for local drug delivery. The proposed *“self-heating hydrogel for mechanically-controlled drug release”* consists of two components: a hydrogel matrix with high viscoelastic properties and thermosensitive biohybrid nanogel particles.

The hydrogel matrix that we propose is a chemically cross-linked polymer network with high viscoelastic properties. The viscoelastic properties will be optimized to result in a relevant temperature increase under physiological loading conditions. Incorporated in this matrix will be thermosensitive nanogel particles loaded with a drug, which will dissociate and release their payload when the temperature increases to their Lower Critical Solution Temperature (LCST) due to viscous dissipation of hydrogel (Figure 1.7). These nanoparticles will be developed at the Polymer Laboratory (LP) at EPFL.

In the absence of a mechanical stimulus, the temperature decreases to less than the LCST of the nanogel and the reserved drug can be encapsulated in the nanogel particles, which are physically entrapped in the hydrogel matrix. Since temperature increase due to dissipation depends on the frequency and number of loading cycles, the use of viscous dissipation to control drug release allows us to take into account the mechanical history to which the hydrogel will be exposed, and provides a temporal control over the drug release process. This kind of temporal control is not possible with conventional drug delivery systems. Here, our target drug will be the growth factor TGF- β or IGF-1. This approach is completely different from what has been done so far, i.e. delivering a growth factor simultaneously to a mechanical stimulation.

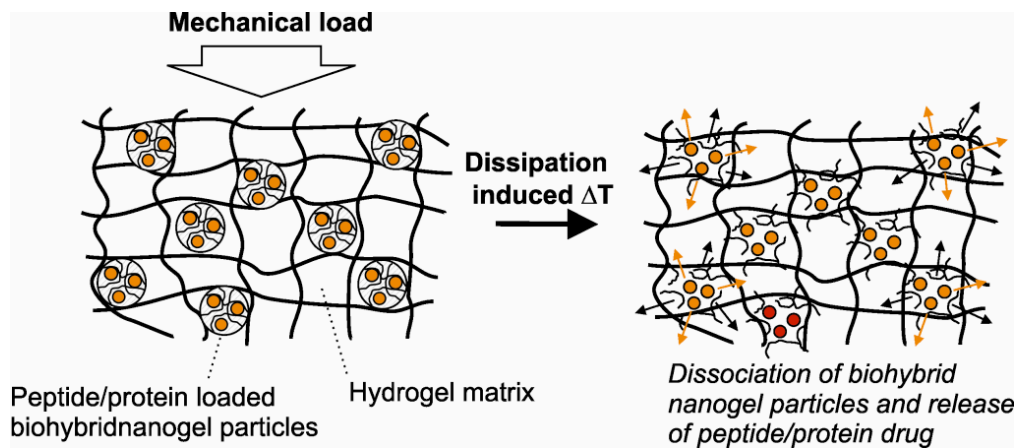


Figure 1.7. Mechanically-controlled drug release from a thermosensitive two-component hydrogel. Mechanical loading results in a relevant temperature increase in viscoelastic hydrogel due to viscous dissipation and the temperature increase results in the dissociation of biohybrid nanogel particles and the release of their payload.

1.3.2 Specific Aims

Based on the overall goal of this project, we followed four specific aims each presented in a chapter and a publication:

First aim (Chapter 2): modeling the heat transfer in articular cartilage.

In this chapter, we developed a poroelastic Finite Element (FE) model of knee cartilage to study the heat transfer mechanisms of articular cartilage. In the first step, we specifically focused on the effect of energy dissipation in cartilage under cyclic loading and the effect of synovial fluid flow on cartilage heat regulation. Having such a model, in the next step we estimated how much heat power must be produced by dissipative properties of a cylindrical hydrogel placed in the

middle of a cartilage defect to increase the local temperature by 2°C. This is the value of temperature increase needed to activate the thermosensitive nanogel particles.

Second aim (Chapter 3): developing a self-heating hydrogel structure with high dissipative properties.

In this chapter, we first studied the viscoelastic properties of different hydrogel structures and identified parameters involved in increasing the dissipative properties of these structures. We also introduced dissipation as a means to increase material resistance to crack propagation and fracture under mechanical loading, which is necessary for a biomaterial to be applicable in load bearing tissues like cartilage. Based on these results, then we optimized the dissipation of developed hydrogels to be able to produce the required energy dissipation estimated from the previous chapter.

Third aim (Chapter 4): controlled release from composite hydrogel.

In this chapter, we present how to combine the developed self-heating hydrogel with thermosensitive nanogel particles, which were developed with Polymer Laboratory. We created a proof of concept for the dissipation-driven drug delivery system. To study the drug release under load, we designed a heat-isolated set-up with a temperature monitoring system installed on a universal compression machine. With our system, we studied the drug release properties of the developed self-heating composite hydrogel system under cyclic mechanical loading with a model drug.

Forth aim (Chapter 5): improving self-heating hydrogels for clinical application: designing biodegradable hydrogels with enhanced mechanical properties.

In this chapter, we modified the structure of self-heating hydrogels to be degradable in the physiological conditions of knee cartilage. In clinical applications, the hydrogel must degrade to allow for the development of a new tissue. Furthermore, we also studied the biocompatibility of hydrogels.

In the last chapter of the thesis (**Chapter 6**), we present a general discussion, limitations of the study, and possible future work.

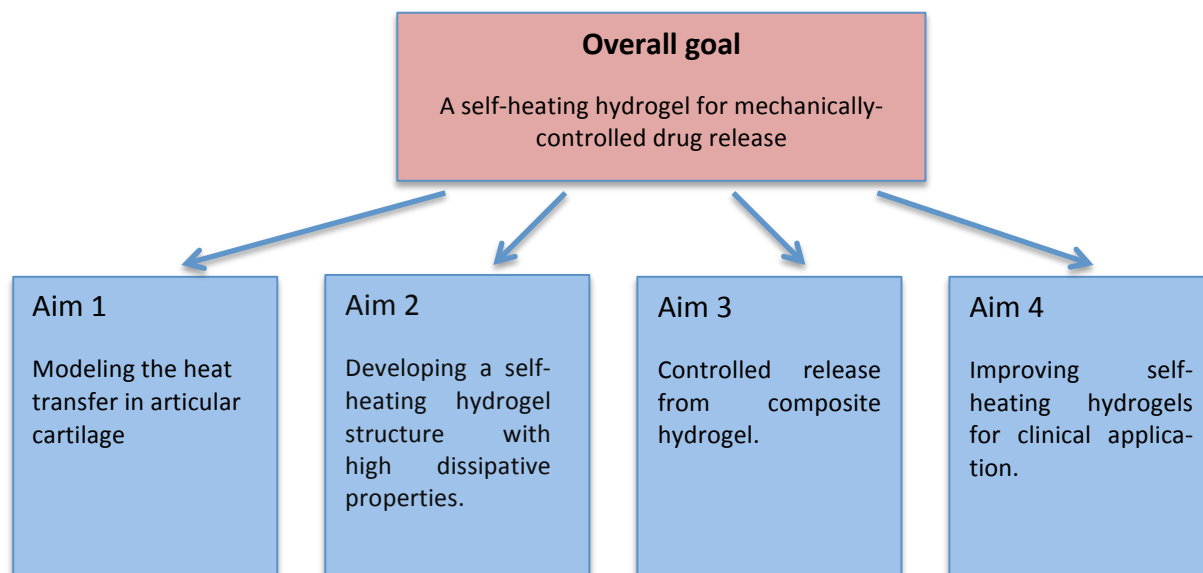


Figure 1.8. Overview of the thesis objectives.

1.4 References

- Alberts B, Bray D, Hopkin K, Johnson A, Lewis J, Raff M, Roberts K, Walter P. 2013. Essential cell biology: Garland Science
- Athanasίου KA, Darling EM, Hu JC. 2009. Articular cartilage tissue engineering. Synthesis Lectures on Tissue Engineering 1, 1-182.
- Atzet S, Curtin S, Trinh P, Bryant S, Ratner B. 2008. Degradable poly (2-hydroxyethyl methacrylate)-co-polycaprolactone hydrogels for tissue engineering scaffolds. Biomacromolecules 9, 3370-7.
- Baker MV, Brown DH, Casadio YS, Chirila TV. 2009. The preparation of poly(2-hydroxyethyl methacrylate) and poly{(2-hydroxyethyl methacrylate)-co-[poly(ethylene glycol) methyl ether methacrylate]} by photoinitiated polymerisation-induced phase separation in water. Polymer 50, 5918-27.
- Bobick BE, Chen FH, Le AM, Tuan RS. 2009. Regulation of the chondrogenic phenotype in culture. Birth Defects Research Part C: Embryo Today: Reviews 87, 351-71.

-
- Bonassar LJ, Grodzinsky AJ, Frank EH, Davila SG, Bhaktav NR, Trippel SB. 2001. The effect of dynamic compression on the response of articular cartilage to insulin-like growth factor-I. *Journal of Orthopaedic Research* 19, 11-7.
- Buscemi L, Ramonet D, Klingberg F, Formey AI, Smith-Clerc J, Meister J-J, Hinz B. 2011. The single-molecule mechanics of the latent TGF- β complex. *Current Biology* 21, 2046-54.
- Cheng GC, Libby P, Grodzinsky AJ, Lee RT. 1996. Induction of DNA synthesis by a single transient mechanical stimulus of human vascular smooth muscle cells: role of fibroblast growth factor-2. *Circulation* 93, 99-105
- Chimal-Monroy Js, Diaz de Leon L. 1999. Expression of N-cadherin, N-CAM, fibronectin and tenascin is stimulated by TGF-beta1, beta2, beta3 and beta5 during the formation of precartilage condensations. *International Journal of Developmental Biology* 43, 59-67.
- Chuckpaiwong B. 2009. Surgical treatments of the lateral ankle sprain. *Siriraj Medical Journal* 61, 104-6.
- Chung C, Burdick JA. 2008. Engineering cartilage tissue. *Advanced Drug Delivery Reviews* 60, 243-62.
- Clark JM. 1990. The organisation of collagen fibrils in the superficial zones of articular cartilage. *Journal of Anatomy* 171, 117-126.
- Cohen NP, Foster RJ, Mow VC. 1998. Composition and dynamics of articular cartilage: structure, function, and maintaining healthy state. *Journal of Orthopaedic & Sports Physical Therapy* 28, 203-15.
- De Jong S, Van Eerdenbrugh B, van Nostrum Cv, Kettenes-Van Den Bosch J, Hennink W. 2001. Physically crosslinked dextran hydrogels by stereocomplex formation of lactic acid oligomers: degradation and protein release behavior. *Journal of Controlled Release* 71, 261-75.
- Edelman ER, Fiorino A, Grodzinsky A, Langer R. 1992. Mechanical deformation of polymer matrix controlled release devices modulates drug release. *Journal of Biomedical Materials Research* 26, 1619-31.
- Elder BD, Athanasiou KA. 2008. Synergistic and additive effects of hydrostatic pressure and growth factors on tissue formation. *PLoS ONE* 3, e2341.
- Getgood A, Brooks R, Fortier L, Rushton N. 2009. Articular cartilage tissue engineering: today's research, tomorrow's practice? *The Journal of Bone and Joint Surgery. British volume* 91, 565-76.
- Gil ES, Hudson SM. 2004. Stimuli-responsive polymers and their bioconjugates. *Progress in Polymer Science* 29, 1173-222.
- Gillogly SD, Voight M, Blackburn T. 1998. Treatment of articular cartilage defects of the knee with autologous chondrocyte implantation. *Journal of Orthopaedic & Sports Physical Therapy* 28, 241-51.

-
- Gomoll AH, Madry H, Knutsen G, van Dijk N, Seil R, Brittberg M, Kon E. 2010. The subchondral bone in articular cartilage repair: current problems in the surgical management. *Knee Surgery, Sports Traumatology, Arthroscopy* 18, 434-47.
- Haddo O, Mahroof S, Higgs D, David L, Pringle J, Bayliss M, Cannon S, Briggs T. 2004. The use of chondroide membrane in autologous chondrocyte implantation. *The Knee* 11, 51-5.
- Han Y, Lee E, Ji B. 2008. Mechanical properties of semi-interpenetrating polymer network hydrogels based on poly(2-hydroxyethyl methacrylate) copolymer and chitosan. *Fibers and Polymers* 9, 393-9.
- Hangody L, Kish G, Karpati Z, Udvarhelyi I, Szigeti I, Bely M. 1998. Mosaicplasty for the treatment of articular cartilage defects: application in clinical practice. *Orthopedics* 21, 751-6.
- Hennink W, Van Nostrum C. 2012. Novel crosslinking methods to design hydrogels. *Advanced Drug Delivery Reviews* 64, 223-36.
- Hiyama A, Mochida J, Iwashina T, Omi H, Watanabe T, Serigano K, Iwabuchi S, Sakai D. 2007. Synergistic effect of low-intensity pulsed ultrasound on growth factor stimulation of nucleus pulposus cells. *Journal of Orthopaedic Research* 25, 1574-81.
- Hoffman AS. 2002. Hydrogels for biomedical applications. *Advanced Drug Delivery Reviews* 54, 3-12.
- Holland TA, Mikos AG. 2003. Advances in drug delivery for articular cartilage. *Journal of Controlled Release* 86, 1-14.
- Hu X, Cheng D, Zhang Y, Jiang F, Yang D, Ding Y. 2008. Low level mechanical strain induces extracellular signal regulated kinase 1/2 activation in alveolar epithelial cells. *Respirology* 13, 781-7.
- Johnson LL. 1986. Arthroscopic abrasion arthroplasty historical and pathologic perspective: present status. *Arthroscopy: The Journal of Arthroscopic & Related Surgery* 2, 54-69.
- Kamath KR, Park K. 1993. Biodegradable hydrogels in drug delivery. *Advanced Drug Delivery Reviews* 11, 59-84.
- Kenawy E-R, Kamoun EA, Mohy Eldin MS, El-Meligy MA. 2014. Physically crosslinked poly(vinyl alcohol)-hydroxyethyl starch blend hydrogel membranes: Synthesis and characterization for biomedical applications. *Arabian Journal of Chemistry* 7, 372-80.
- Klouda L, Mikos AG. 2008. Thermoresponsive hydrogels in biomedical applications. *European Journal of Pharmaceutics and Biopharmaceutics* 68, 34-45.
- Kuo CK, Ma PX. 2001. Ionically crosslinked alginate hydrogels as scaffolds for tissue engineering: part 1. Structure, gelation rate and mechanical properties. *Biomaterials* 22, 511-21.
- Lakes RS. 1999. *Viscoelastic solids*: CRC Press/ Llc
- Lee KY, Peters MC, Anderson KW, Mooney DJ. 2000. Controlled growth factor release from synthetic extracellular matrices. *Nature* 408, 998-1000.

-
- Li Y, Xu M. 2007. Hysteresis loop and energy dissipation of viscoelastic solid models. *Mechanics of Time-Dependent Materials* 11, 1-14.
- Li Z, Kupcsik L, Yao S-J, Alini M, Stoddart MJ. 2010. Mechanical load modulates chondrogenesis of human mesenchymal stem cells through the TGF- β pathway. *Journal of Cellular and Molecular Medicine* 14, 1338-46.
- Lima EG, Bian L, Ng KW, Mauck RL, Byers BA, Tuan RS, Ateshian GA, Hung CT. 2007. The beneficial effect of delayed compressive loading on tissue-engineered cartilage constructs cultured with TGF- β 3. *Osteoarthritis and Cartilage* 15, 1025-33.
- Lin CC, Metters AT. 2006. Hydrogels in controlled release formulations: network design and mathematical modeling. *Advanced Drug Delivery Reviews* 58, 1379-408.
- Magnussen RA, Dunn WR, Carey JL, Spindler KP. 2008. Treatment of focal articular cartilage defects in the knee. *Clinical Orthopaedics and Related Research* 466, 952-62.
- Mansour JM. 2003. Biomechanics of cartilage. *Kinesiology: the mechanics and pathomechanics of human movement*, 66-79.
- Masuda K, An H. 2006. Prevention of disc degeneration with growth factors. *European Spine Journal* 15, 422-32.
- Mauck RL, Nicoll SB, Seyhan SL, Ateshian GA, Hung CT. 2003. Synergistic action of growth factors and dynamic loading for articular cartilage tissue engineering. *Tissue Engineering* 9, 597-611.
- Moffat KL, Marra KG. 2004. Biodegradable poly(ethylene glycol) hydrogels crosslinked with genipin for tissue engineering applications. *Journal of Biomedical Materials Research Part B: Applied Biomaterials* 71B, 181-7.
- Mow VC, Holmes MH, Michael Lai W. 1984. Fluid transport and mechanical properties of articular cartilage: A review. *Journal of Biomechanics* 17, 377-94.
- Neu CP, Khalafi A, Komvopoulos K, Schmid TM, Reddi AH. 2007. Mechanotransduction of bovine articular cartilage superficial zone protein by transforming growth factor β signaling. *Arthritis & Rheumatism* 56, 3706-14.
- Ohno S, Tanaka N, Ueki M, Honda K, Tanimoto K, Yoneno K, Ohno-Nakahara M, Fujimoto K, Kato Y, Tanne K. 2005. Mechanical regulation of terminal chondrocyte differentiation via RGD-CAP/ α 1(I)- β 3 induced by TGF- β . *Connective Tissue Research* 46, 227-34.
- Ossipov DA, Hilborn Jn. 2006. Poly (vinyl alcohol)-based hydrogels formed by "click chemistry". *Macromolecules* 39, 1709-18.
- Park SH, Lim ST, Shin TK, Choi HJ, Jhon MS. 2001. Viscoelasticity of biodegradable polymer blends of poly(3-hydroxybutyrate) and poly(ethylene oxide). *Polymer* 42, 5737-42.
- Peppas N, Bures P, Leobandung W, Ichikawa H. 2000. Hydrogels in pharmaceutical formulations. *European Journal of Pharmaceutics and Biopharmaceutics* 50, 27-46.

-
- Peppas NA, Hilt JZ, Khademhosseini A, Langer R. 2006. Hydrogels in biology and medicine: from molecular principles to bionanotechnology. *Advanced Materials* 18, 1345-60.
- Pridie K, Gordon G. 1959. A method of resurfacing osteoarthritic knee joints. *Journal of Bone and Joint Surgery* 41, 618-19.
- Priya James H, John R, Alex A, Anoop KR. 2014. Smart polymers for the controlled delivery of drugs, a concise overview. *Acta Pharmaceutica Sinica B* 4, 120-7.
- Qiu Y, Park K. 2012. Environment-sensitive hydrogels for drug delivery. *Advanced Drug Delivery Reviews* 64, 49-60.
- Radin EL, Rose RM. 1986. Role of subchondral bone in the initiation and progression of cartilage damage. *Clinical Orthopaedics and Related Research* 213, 34-40.
- Ruckstuhl H, de Bruin ED, Stussi E, Vanwanseele B. 2008. Post-traumatic glenohumeral cartilage lesions: a systematic review. *BMC Musculoskeletal Disorders* 9, 107-14.
- Schmaljohann D. 2006. Thermo- and pH-responsive polymers in drug delivery. *Advanced Drug Delivery Reviews* 58, 1655-70.
- Shu XZ, Ahmad S, Liu Y, Prestwich GD. 2006. Synthesis and evaluation of injectable, in situ crosslinkable synthetic extracellular matrices for tissue engineering. *Journal of Biomedical Materials Research Part A* 79, 902-12.
- Stadelmann VA, Terrier A, Pioletti DP. 2008. Microstimulation at the bone-implant interface upregulates osteoclast activation pathways. *Bone* 42, 358-64.
- Steadman JR, Rodkey WG, Singleton SB, Briggs KK. 1997. Microfracture technique for full-thickness chondral defects: Technique and clinical results. *Operative Techniques in Orthopaedics* 7, 300-4.
- Sun JY, Zhao X, Illeperuma WR, Chaudhuri O, Oh KH, Mooney DJ, Vlassak JJ, Suo Z. 2012. Highly stretchable and tough hydrogels. *Nature* 489, 133-6.
- Syedain ZH, Tranquillo RT. 2011. TGF- β 1 diminishes collagen production during long-term cyclic stretching of engineered connective tissue: Implication of decreased ERK signaling. *Journal of Biomechanics* 44, 848-55.
- Tschumperlin DJ, Dai G, Maly IV, Kikuchi T, Laiho LH, McVittie AK, Haley KJ, Lilly CM, So PTC, Lauffenburger DA, Kamm RD, Drazen JM. 2004. Mechanotransduction through growth-factor shedding into the extracellular space. *Nature* 429, 83-6.
- Van Osch GJVM, Brittberg M, Dennis JE, Bastiaansen Jenniskens YM, Erben RG, Konttinen YT, Luyten FP. 2009. Cartilage repair: past and future lessons for regenerative medicine. *Journal of Cellular and Molecular Medicine* 13, 792-810.

Zhang J, Misra R. 2007. Magnetic drug-targeting carrier encapsulated with thermosensitive smart polymer: Core-shell nanoparticle carrier and drug release response. *Acta Biomaterialia* 3, 838-50.

Chapter 2

Modeling the Heat Transfer in Articular Cartilage

2.1 Impact of Synovial Fluid Flow on Temperature Regulation in Knee Cartilage^{*}

2.1.1 Abstract

Several studies have reported an increase of temperature in cartilage submitted to cyclic sinusoidal loading. The temperature increase is in part due to the viscous behavior of this tissue, which partially dissipates the input mechanical energy into heat. While the synovial fluid flow within the intra-articular gap and inside the porous cartilage is supposed to play an important role in the regulation of the cartilage temperature, no specific study has evaluated this aspect. In the present numerical study, a poroelastic model of the knee cartilage is developed to evaluate first the temperature increase in the cartilage due to dissipation and second the impact of the synovial fluid flow in the cartilage heat transfer phenomenon. Our results showed that, the local temperature is effectively increased in knee cartilage due to its viscous behavior. The synovial fluid flow cannot significantly prevent this phenomenon. We explain this result by the low permeability of cartilage and the moderate fluid exchange at the surface of cartilage under deformation.

Keywords: cartilage, dissipation, synovial fluid, poroelasticity, heat

^{*}

This section has been accepted in "Journal of Biomechanics".

2.1.2 Introduction

Most of the biomechanical studies consider that the temperature of the healthy knee cartilage is constant (Romanovsky, 2007, Tandon and Bali, 1997). However, given that cartilage is avascular and has viscous properties (Hayes and Mockros, 1971, Huang et al., 2003), a local temperature increase in this tissue could result from dissipation following a cyclic mechanical loading (Abdel-Sayed et al., 2014, Bali and Sharma, 2011). While this temperature increase could be moderate, its effect can be important on biochemical reactions. For example it has been shown that the rate of proteoglycan synthesis of chondrocytes increase with slight change in temperature (Brand et al., 1991, Castor and Yaron, 1976). Synthesis rates of hyaluronic acid by synovial cells changes as a function of temperature (Castor and Yaron, 1976). Furthermore, it has been reported that the rate of destruction of articular cartilage collagen fibers by synovial collagenase is 4 times greater at 36°C than at 33°C (Harris and McCroskery, 1974) and affects transport of molecules like polysaccharides and proteins in articular cartilage (Moeini et al., 2012).

An indirect link exists then between the dynamic loading of knee and the cartilage homeostasis through dissipative phenomenon suggesting a possible new mechanobiological pathway in cartilage (Abdel-Sayed et al., 2014).

Beside the dissipative properties of the cartilage, heat transfer is an important parameter in the local temperature regulation (Bali and Sharma, 2011, Martin et al., 2001, Tandon and Bali, 1997). In particular, synovial fluid flow would naturally play a central role in the heat transfer aspect. The performance of human articular joints is indeed strictly connected with the properties of the synovial fluid, which determines load transmission, lubrication, wear inhibition and protection of the articular cartilage from mechanical stresses during joint movements (Bali and Sharma, 2011, Hui et al., 2012). The lubricant properties of synovial fluid are essential in preventing the temperature increase due to friction (Bergmann et al., 2001, Bergmann et al., 2001, Sawyer et al., 2003, Tandon and Bali, 1997). However, how the synovial fluid flow affects the temperature increase due to the intrinsic viscous dissipation of the cartilage has not been described yet.

The goal of this study is to evaluate the impact of the synovial fluid flow on heat transfer in knee cartilage. We specifically focused on the heat generated due to viscous dissipation when the cartilage is deformed sinusoidally to mimic walking.

2.1.3 Methods

2.1.3.1 Model of Heat Transfer in Cartilage

We used the theory of porous media for heat transfer in biological tissues. Since it considers less assumptions, it seems to be the most suitable one for bioheat models (Khaled and 2003). The problem was formulated as a two steps model. In the first step, the velocity field of the synovial fluid in the cartilage under deformation was determined in a poroelastic 3D finite element model. In the second step, the solution of the velocity field was introduced into the thermal diffusion equation. The thermal field within the porous cartilage was then determined.

Comsol Multiphysics 4.4 software (COMSOL Inc., Burlington, MA, USA) was used to develop the poroelastic, heat transfer model. The axisymmetric model consisted of femoral and tibial cartilage layers each with the thickness of 4 millimeters. As the contact area of cartilage (1200 mm^2) comparing to its thickness (max 4 mm) is large enough, to simplify the model the articulation shape of the cartilage was neglected (Liu et al., 2010). The cartilage was considered as a poroelastic material. As 80% percent of the cartilage is composed of fluid, the porosity was set accordingly to 0.8 (Hosoda et al., 2009). Both cartilage layers were attached to their corresponding femoral and tibial bones. Bone was modeled as rigid body. The synovial cavity was modeled as a reservoir for synovial fluid, which allowed the exchange of the fluid at each deformation cycle. The geometry was meshed with triangular elements (Figure 2.1). The simulation consisted of two coupled multiphysics: poroelasticity and heat transfer interfaces.

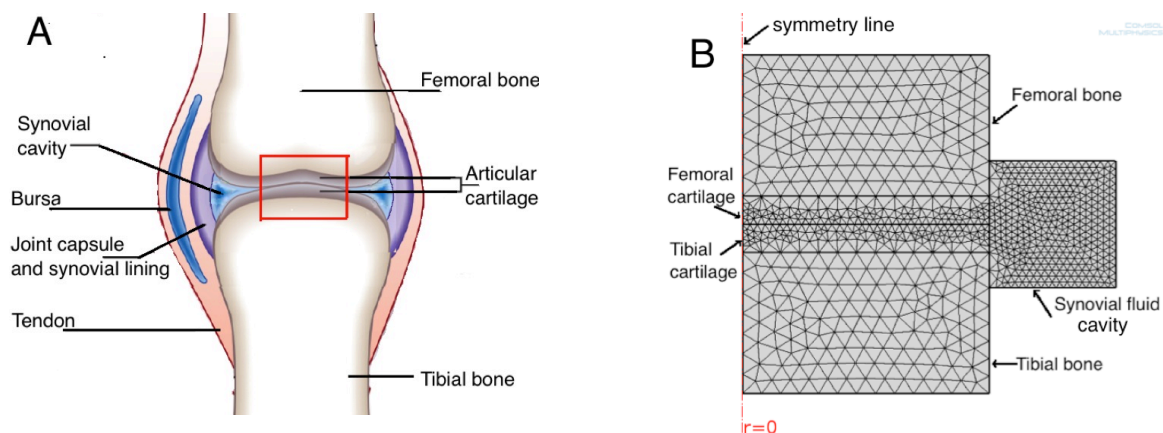


Figure 2.1. (A) We modeled the load bearing part of cartilage (the red rectangle) and synovial cavity. (B) Geometry of the problem. The model consisted of a femoral and a tibial layer of cartilage with their corresponding femoral and tibial bones and synovial cavity as fluid reservoir. The model was axisymmetric and the whole structure was meshed with triangular elements.

Poroelasticity interface: calculation of the velocity field of the synovial fluid. The Biot's theory of poroelasticity was used, relating continuity equation for fluid flow in porous medium (2.1) and Navier's equation (2.2) (Biot, 1962):

$$\rho_l S \frac{\partial p_l}{\partial t} + \nabla \cdot (\rho_l u) = -\rho_l \alpha_B \frac{\partial \epsilon_{vol}}{\partial t} \quad (2.1)$$

$$-\nabla \sigma = 0 \quad (2.2)$$

where u and S are:

$$u = -\frac{k}{\mu} \nabla p_l \quad (2.3)$$

$$S = \epsilon_p \chi_l + \frac{(\alpha_B - \epsilon_p)(1 - \alpha_B)}{K} \quad (2.4)$$

$\partial \epsilon_{vol} / \partial t$ is the rate of change in volumetric strain, p_l is the pressure field, ρ_l is the density of the fluid, and α_B is the Biot-Willis coefficient, which is considered equal to 1 in our situation. The material properties needed for the poroelastic model (equations 2.1-2.4) are listed in Table 2.1. The strain dependent permeability, k was also implemented using the variable void ratio as (Mow, 1976):

$$k = k_0 \left(\frac{1+e}{1+e_0} \right)^M, \quad e = \Theta_l / \Theta_p \quad (2.5)$$

where k_0 is the initial permeability (equal to 10^{-14} m^2), e is void ratio (defined as the ratio of fluid volume fraction Θ_l to solid volume fraction Θ_p), e_0 is the initial void ratio (equal to 4), and M is the permeability coefficient, with the value 1.3 (Prendergast et al., 1996).

This model allows us to quantify the synovial fluid flow inside the cartilage when the cartilage is sinusoidally deformed. Both cartilage layers were deformed at a frequency of 1.5 Hz and a 15% amplitude to simulate gagging when the tibial bone is fully constrained (Liu et al., 2010). A zero pressure boundary condition ($p = 0$) was defined at the contact surface of the two cartilages to let the fluid flows in and out of the porous cartilage from the cartilage surface during deformation. At each time step, the pressure and velocity distribution were calculated.

Table 2.1. Material properties used in the model (Barker and Seedhom, 2001, Mow et al., 1984).

Bulk modulus of cartilage, K	0.36 MPa
Viscosity of synovial fluid, μ	0.6 Pa.s
Porosity of cartilage, ϵ_p	0.8
Compressibility of synovial fluid, χ_l	1e -10 1/Pa
Density of fluid, ρ_l	1000 kg/m ³

Heat transfer interface: calculation of the thermal field. The following form of the heat equation was used to model the heat transfer in cartilage (Incropera et al., 2011):

$$(\rho C_p)_{eq} \frac{\partial T}{\partial t} + \rho_l C_l u \cdot \nabla T = \nabla \cdot (k_{eq} \nabla T) + \dot{Q} \quad (2.6)$$

In this equation u is the fluid velocity (introduced in equation 2.3). At each time step the fluid velocity magnitude was solved from the poroelastic model and was used in equation 2.6 for calculating the temperature distribution. The equivalent conductivity of the solid-fluid system, k_{eq} was related to the conductivity of the solid, k_p and to the conductivity of the fluid, k_l by $k_{eq} = \Theta_p k_p + \Theta_l k_l$. The equivalent volumetric heat capacity of the solid-fluid system was related to the heat capacity of the solid C_p and to the heat capacity of the fluid C_l by $(\rho C_p)_{eq} = \Theta_p \rho_p C_p + \Theta_l \rho_l C_l$. The heat capacity and conductivity of the cartilage as well as of the synovial fluid were measured experimentally (see below).

In equation 2.6, \dot{Q} is the heat source (heat power per volume), which in our model corresponded to the cartilage viscous dissipation. The amount of cartilage dissipation was measured experimentally. To evaluate other possible heat transfer phenomena between the cartilage and the surrounding area, we considered a heat transfer boundary condition at the free boundary of the model by introducing a general heat transfer coefficient (λ) experimentally determined.

2.1.3.2 Experimental Determination of the Model Parameters

Dissipation of cartilage: we applied cyclic compression on human cartilage samples (n=6) at 1.5 Hz and 15% strain amplitude. The dissipation power was calculated from the load-displacement graphs as the integral of the area enclosed by the hysteresis curve. The detailed procedure is explained in a previous study (Abdel-Sayed et al., 2014).

Heat capacity of cartilage and synovial fluid: heat capacity of human cartilage samples (n=6) and synovial fluid (n=3) were determined using a general published differential scanning calorimeter (DSC) method (McHugh et al., 2010). Briefly, the DSC heat flow signal from the sample was recorded between 10°C and 60°C with a heat rate of 10°C/min (MDS-Q100, TA Instruments, New Castle, DE, USA). The DSC signal was compared to the DSC signal of sapphire calibration standard with a known specific heat. Both curves were corrected by a base line correction experiment.

Thermal conductivity of cartilage: as large pieces of cartilage samples were necessary to evaluate their thermal conductivity, for this measurement, cartilage samples (n=6) were punched (20 mm diameter) from bovine femoral head. Hot Disk Thermal Constants Analyzer (TPS-500, Hot Disk, Gothenburg, Sweden) was used to measure the heat conductivity of cartilage. The method is based on the use of a transiently heated plane sensor. The method is based on the use of a transiently heated plane sensor which consist of an electronically pattern in the shape of a double spiral and is etched out of a thin metal Nickel foil. This spiral is sandwiched between two thin sheets of an insulating material. The Hot Disk sensor is used both as a heat source and as a dynamic temperature sensor. The test was also performed on 3 mL of bovine synovial fluid in a 5 mL tube by sinking the Hot Disk sensor directly in the liquid.

Heat transfer coefficient of cartilage: the heat transfer coefficient (λ) was obtained from a Proton Resonance Frequency Shift (PRFS)-based MR thermometry used to monitor the temperature drop of the cartilage when the knee of 4 volunteers was immobilized after a 20 minutes joint activity (Abdel-Sayed et al., 2014). We calculated the heat transfer coefficient (λ) from the following equation:

$$a = \frac{\lambda S}{mc} \quad (2.7)$$

a is the time constant derived from the curve fitting to the temperature drop curve of the cartilage following the 20 minutes joint activity and was detected by MR thermometry method (Abdel-Sayed et al., 2014), S is the surface of each cartilage element in MRI data (1 mm³ cube), m is the mass of each element and c is the heat capacity of the cartilage. Since the heat transfer coefficient (λ) was calculated when the knee was at rest, meaning that no dynamic load was applied on cartilage to cause fluid flow, it includes all heat transfer mechanisms at the knee cartilage except the effect of synovial fluid flow.

2.1.4 Results

2.1.4.1 Experimental Determination of the Model Parameters

Dissipation of cartilage: the dynamic compression test on cartilage induced a dissipation equal to $0.025 \pm 0.009 \text{ mW/mm}^3$. This value was considered as an internal heat source over the whole cartilage geometry.

Heat capacity and thermal conductivity of cartilage and synovial fluid: the obtained experimental values are shown in Table 2.2. These values are used to for the parameters appearing in the equation 2.6 describing the heat transfer model of the cartilage porous media.

Heat transfer coefficient of cartilage: the results of MR thermometry on 4 volunteers give the value of $\lambda = 0.77 \pm 0.32 \text{ J/m}^2\text{s}$. The value of this heat transfer coefficient was considered at all open boundaries of the cartilage model.

Table 2.2. DSC and TPS experimentally obtained values for cartilage and synovial fluid.

Heat capacity of cartilage, C_p	$3200 \pm 130 \text{ J/kg.K}$
Heat capacity of synovial fluid, C_l	$3900 \pm 95 \text{ J/kg.K}$
Conductivity of cartilage, k_p	$0.21 \pm 0.06 \text{ W/m.K}$
Conductivity of synovial fluid, k_l	$0.62 \pm 0.11 \text{ W/m.K}$

2.1.4.2 Model of Heat Transfer in Cartilage

Velocity field of the synovial fluid: to evaluate the pertinence of the calculated synovial fluid flow during cyclic loading in our numerical model, we first looked at the cartilage deformation and fluid flow. Figure 2.2 shows the cartilage deformation between two layers of tibial and femoral bone during one complete cycle of loading and unloading. The black arrows show the fluid velocity in and out of the porous cartilages during exudation and imbibition. During the cartilage compression corresponding to stance phase of gait cycle, fluid is squeezed out of the cartilage to the synovial fluid reservoir cavity. Conversely, during unloading corresponding to the swing phase of gait cycle, cartilage sucks back the fluid. Figure 2.3 provides a closer look at the maximum fluid velocity in cartilage during cyclic compression. The fluid velocity at the area near the cartilage surface

(Zone Z2, Figure 2.3A) is more than 10 times higher than the velocity in deep zones (Zones Z1, Figure 2.3A).

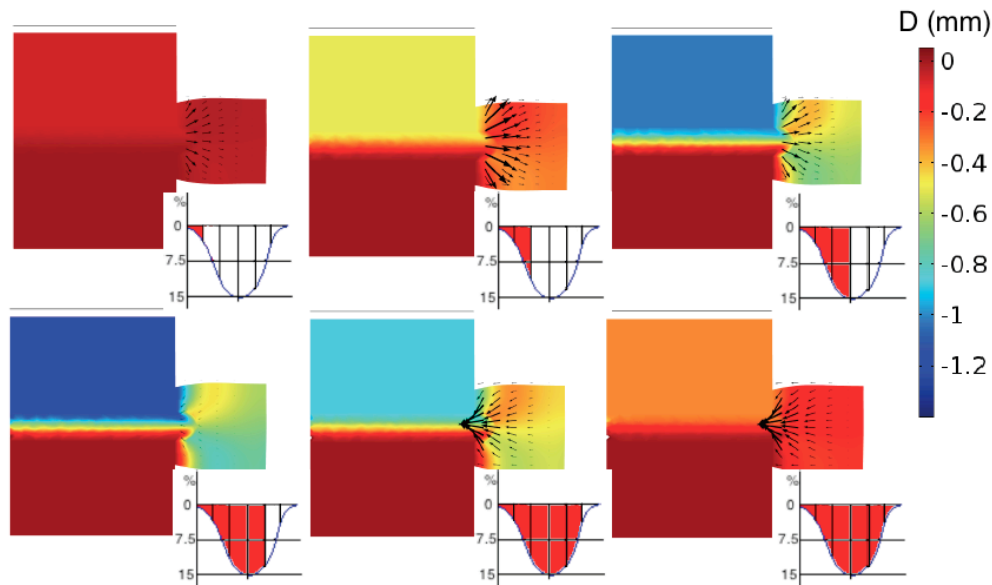


Figure 2.2. Deformation field and synovial fluid flow (arrows) during one complete sinusoidal compression deformation of cartilage. The bottom right graph on each figure shows the stage of deformation during one sinusoidal compression.

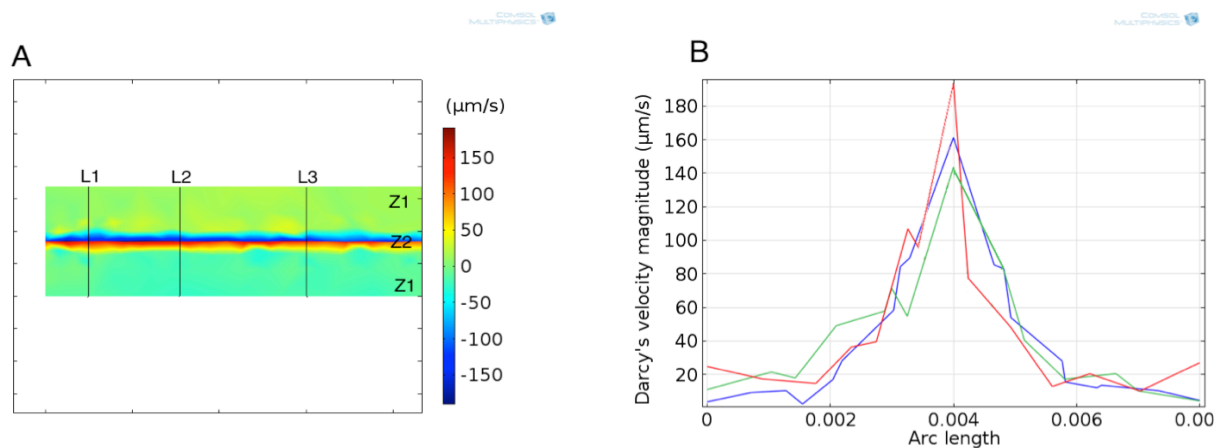


Figure 2.3. (A) Maximum velocity field in cartilage and **(B)** velocity magnitude in 3 areas, green: along the line L1, blue along the line L2 and red along the line L3.

Effect of synovial fluid flow in the regulation of cartilage temperature: Figure 2.4 shows the spatial distribution of knee cartilage temperature due to its viscous dissipation after 10 minutes cyclic loading at 1.5 Hz. Results are presented with or without considering the synovial fluid flow. The flow of fluid has not a significant effect on temperature of cartilage at the contact area. An effect can be observed in the area near the synovial fluid cavity (Zone 2, Figure 2.4) where the fluid can be exchanged faster. Figure 2.5 represents the mean temperature increase of cartilage in the cen-

ter of the cartilage contact surface (Zone 1, in Figure 2.4). The model showed that the dissipation could increase the temperature of knee cartilage up to 1.2°C after 10 minutes loading. This temperature increase without fluid flow was about 1.8°C .

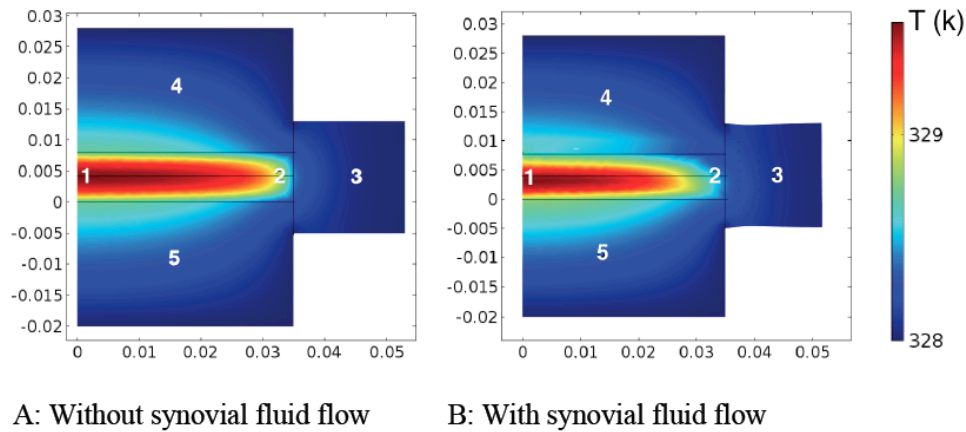


Figure 2.4. Cartilage temperature field after 10 minutes cyclic deformation at 1.5 Hz and 15% deformation amplitude. Zone 1: center of contact area. Zone 2: end of the contact zone. Zone 3: synovial fluid reservoir. Zones 4 and 5: femoral and tibial bones.

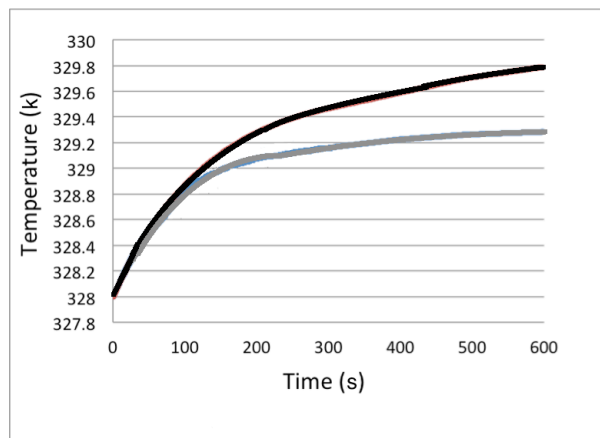


Figure 2.5. Mean temperature in the middle of the cartilage contact zone over time with (gray line) and without (black line) synovial fluid flow.

2.1.5 Discussion

In this study we evaluated the effect of the cartilage dissipation on its temperature distribution and we quantified the importance of the synovial fluid flow in this process.

An original finding was to show that the experimentally determined values of the heat capacity and conductivity of the synovial fluid were much higher than the corresponding values for the car-

tilage tissue. This suggests that the synovial fluid would play an important role in the temperature regulation of the knee cartilage during dynamic loading. However, based on the developed numerical poroelastic model coupled to a thermal diffusion model, we observed that the synovial fluid flow could only partially affect the temperature increase in the cartilage submitted to a dynamic loading. Indeed, a significant temperature increase in the cartilage was observed even when considering the synovial fluid flow. This result allows us to confirm the importance of the dissipation on cartilage temperature increase observed in a previous study where the contribution of the fluid flow could not be included (Abdel-Sayed et al., 2014).

One possible reason to explain the inability of the synovial fluid flow to maintain a constant temperature in the cartilage during its dynamical loading may be related to the cartilage low permeability value (10^{-14} m^2 e.g. (Prendergast et al., 1996)). The low permeability of the cartilage is central to provide enough mechanical properties and shock absorbance (Mow et al., 1984). It also provides a moderate fluid flow to the deep zone of cartilage, enough to transport nutrient and waste in this tissue, where there is no vascularization (O'Hara et al., 1990). At the frequency of activities like walking or running, it seems that such a low permeability does not let the synovial fluid to travel fast enough through the deep zone of cartilage to allow an effective heat exchange at every deformation cycle. Figure 2.3 supports this suggestion as it is reported that the fluid velocity at the area near the cartilage surface is more than 10 times higher than the velocity in deep zones. Within this context, the role of the synovial fluid flow and convectional heat transfer seems not to be significant. Therefore the heat produced due to viscous dissipation at the deep zone of the cartilage can only be transferred through the conductivity of cartilage. On the other hand, the fast exchange of synovial fluid at the thin layer of the cartilage surface observed in our study confirms the role of the synovial fluid for joint lubrication and for removing heat produced by cartilage surface friction (Gleghorn et al., 2009, Schmidt et al., 2007).

In this study we simplified our model considering only the load-bearing part of cartilage where dissipation occurs. An underestimation of heat transfer phenomena may then result by not considering heat produced by muscle activities around the joint or heat transfer through the skin. To overcome this limitation, a general heat transfer coefficient (λ) has been introduced at the boundaries allowing to take into account other heat phenomena not related to dissipation or fluid flow in our model. Another simplification of our description was to model the tibial and femoral bones

as rigid bodies, while bone is usually considered as a poroelastic material. However, the permeability of cartilage is much higher than the permeability of bone (Mow et al., 1984), so the effects of bone poroelasticity on the synovial fluid flow could be neglected.

The results of the developed model can be compared to other previously published models either for the mechanical or for the thermal aspects. Regarding the mechanical aspects, our model shows similar fluid flow profiles compared to previous studies (Barker and Seedhom, 2001, Liu et al., 2010, Mow et al., 1984). However, our model has the advantage to show the velocity magnitude in different zone of cartilage, which to our knowledge has not been yet presented. Based on the calculated velocity at the surface or deep zones of cartilage, we could propose an explanation to better understand the reason why synovial fluid flow had not a significant role in regulating the temperature increase due to dissipation while having a central role in case of frictional heat. Regarding the thermal aspects, in vivo direct measurement of intra-articular knee temperature has shown a temperature increase up to 4°C after an hour of activity (Becher et al., 2008, Trobec et al., 2008). However in these studies it was not possible to access the cartilage temperature, only the intra-articular knee temperature could be measured. Furthermore, in most of the existing numerical/mathematical models, viscous dissipation has not been considered as a heat source, and considerations were given only to friction between the surfaces (Romanovsky, 2007, Tandon and Bali, 1997). Bali and coworkers have reported in their poroelastic model the temperature increase of 1.5°C subsequent to cyclic deformation (Bali and Sharma, 2011, Tandon and Bali, 1997). Nevertheless they did not include the effects of synovial fluid flow in the tissue and related gradients of temperature.

2.1.6 Conclusion

In conclusion, we showed that cartilage viscous dissipation is an important source of heat that can locally increase the cartilage temperature. The synovial fluid cannot significantly prevent this temperature increase when the cartilage is mechanically loaded. As previously mentioned, the resulting increase of temperature may induce profound effects on the metabolism of cartilage.

2.1.7 Acknowledgments

This work was supported by the Swiss National Science Foundation (#406240_126070, PNR 62 program).

2.1.8 References

- Abdel-Sayed P, Darwiche SE, Kettenberger U, Pioletti DP. 2014. The role of energy dissipation of polymeric scaffolds in the mechanobiological modulation of chondrogenic expression. *Biomaterials* 35, 1890-7.
- Abdel-Sayed P, Moghadam MN, Salomir R, Tchernin D, Pioletti DP. 2014. Intrinsic viscoelasticity increases temperature in knee cartilage under physiological loading. *Journal of the Mechanical Behavior of Biomedical Materials* 30, 123-30.
- Bali R, Sharma S. 2011. A Model for Intra-Articular Heat Exchange in a Knee Joint. *Tribology Letters* 41, 379-86.
- Barker M, Seedhom B. 2001. The relationship of the compressive modulus of articular cartilage with its deformation response to cyclic loading: does cartilage optimize its modulus so as to minimize the strains arising in it due to the prevalent loading regime? *Rheumatology* 40, 274-84.
- Becher C, Springer J, Feil S, Cerulli G, Paessler H. 2008. Intra-articular temperatures of the knee in sports, An in-vivo study of jogging and alpine skiing. *BMC Musculoskeletal Disorders* 9, 46-52.
- Bergmann G, Graichen F, Rohlmann A, Verdonschot N, Van Lenthe G. 2001. Frictional heating of total hip implants. Part 2: finite element study. *Journal of Biomechanics* 34, 429-35.
- Biot MA. 1962. Mechanics of deformation and acoustic propagation in porous media. *Journal of Applied Physics* 33, 1482-98.
- Brand HS, De Koning MHMT, Van Kampen GPJ, Van Der Korst JK. 1991. Effect of temperature on the metabolism of proteoglycans in explants of bovine articular cartilage. *Connective Tissue Research* 26, 87-100.
- Castor CW, Yaron M. 1976. Connective tissue activation: VIII. The effects of temperature studied in vitro. *Archives of Physical Medicine and Rehabilitation* 57, 5-9.
- Gleghorn JP, Jones AR, Flannery CR, Bonassar LJ. 2009. Boundary mode lubrication of articular cartilage by recombinant human lubricin. *Journal of orthopaedic research. Orthopaedic Research Society* 27, 771-7.
- Harris ED, McCroskery PA. 1974. The Influence of temperature and fibril stability on degradation of cartilage collagen by rheumatoid synovial collagenase. *New England Journal of Medicine* 290, 1-6.
- Hayes W, Mockros L. 1971. Viscoelastic properties of human articular cartilage. *Journal of Applied Physiol* 31, 562 - 8.
- Hosoda N, Sakai N, Sawae Y, Murakami T. 2009. Finite Element Analysis of articular cartilage model considering the configuration and biphasic property of the tissue. In 13th International Conference on Biomedical Engineeringl, Berlin 1883-7.
- Huang C-Y, Soltz MA, Kopacz M, Mow VC, Ateshian GA. 2003. Experimental verification of the roles of intrinsic matrix viscoelasticity and tension-compression nonlinearity in the biphasic response of cartilage. *Journal of Biomechanical Engineering* 125, 84-93.

-
- Hui AY, McCarty WJ, Masuda K, Firestein GS, Sah RL. 2012. A systems biology approach to synovial joint lubrication in health, injury, and disease. *Wiley Interdisciplinary Reviews: Systems Biology and Medicine* 4, 15-37.
- Incropera FP, Bergman TL, Lavine AS, DeWitt DP. 2011. *Fundamentals of heat and mass transfer*: Wiley
- Khaled A-RA, KV. 2003. The role of porous media in modeling flow and heat transfer in biological tissues. *International Journal of Heat and Mass Transfer* 46, 4989–5003.
- Liu F, Kozanek M, Hosseini A, Van de Velde SK, Gill TJ, Rubash HE, Li G. 2010. In vivo tibiofemoral cartilage deformation during the stance phase of gait. *Journal of Biomechanics* 43, 658-65.
- Martin SS, Spindler KP, Tarter JW, Detwiler K, Petersen HA. 2001. Cryotherapy: an effective modality for decreasing intraarticular temperature after knee arthroscopy. *The American Journal of Sports Medicine* 29, 288-91.
- McHugh J, Fideu P, Herrmann A, Stark W. 2010. Determination and review of specific heat capacity measurements during isothermal cure of an epoxy using TM-DSC and standard DSC techniques. *Polymer Testing* 29, 759-65.
- Moeini M, Lee K-B, Quinn TM. 2012. Temperature affects transport of polysaccharides and proteins in articular cartilage explants. *Journal of Biomechanics* 45, 1916-23.
- Mow JMaV. 1976. The permeability of articular cartilage under compressive strain and at high pressures. *Journal of Bone Joint Surgery* 58, 509-16.
- Mow VC, Holmes MH, Michael Lai W. 1984. Fluid transport and mechanical properties of articular cartilage: A review. *Journal of Biomechanics* 17, 377-94.
- O'Hara B, Urban J, Maroudas A. 1990. Influence of cyclic loading on the nutrition of articular cartilage. *Annals of the Rheumatic Diseases* 49, 536-9.
- Prendergast P, Van Driel W, Kuiper J. 1996. A comparison of finite element codes for the solution of biphasic poroelastic problems. *Proceedings of the Institution of Mechanical Engineers, Part H: Journal of Engineering in Medicine* 210, 131-6.
- Romanovsky AA. 2007. Thermoregulation: Some concepts have changed. *Functional architecture of the thermoregulatory system. American Journal of Physiology - Regulatory Integrative and Comparative Physiology* 292, R37-R46.
- Sawyer W, Hamilton M, Fregly B, Banks S. 2003. Temperature modeling in a total knee joint replacement using patient-specific kinematics. *Tribology Letters* 15, 343-51.
- Schmidt TA, Gastelum NS, Nguyen QT, Schumacher BL, Sah RL. 2007. Boundary lubrication of articular cartilage: role of synovial fluid constituents. *Arthritis and Rheumatism* 56, 882-91.
- Tandon PN, Bali R. 1997. A study on temperature regulation in synovial joints. *Tribology Letters* 3, 209-13.
- Trobec R, Sterk M, AlMawed S, Veselko Mæ. 2008. Computer simulation of topical knee cooling. *Computers in Biology and Medicine* 38, 1076-83.

2.2 Estimation of the Required Heat Power for a Relevant Temperature Increase in Hydrogels to Activate Thermosensitive Nanoparticles

2.2.1 Introduction

To design a self-heating hydrogel structure for our proposed smart drug delivery system (Section 1.3.1), we need to estimate how much heat power is required to be produced by the dissipation of the hydrogel. If we assume our system is adiabatic and the hydrogel is heat isolated, the relation between temperature increase and heat power can be obtained from the heat transfer equation (2.6). In the case of adiabatic condition, the equation (2.6) can be simplified to (Incropera et al, 2011):

$$\rho C \frac{\partial T}{\partial t} = \dot{Q} \quad (2.8)$$

where \dot{Q} , the heat source (heat power per volume), is the hydrogel dissipation, C and ρ are the heat capacity and the density of the hydrogel, respectively.

Considering the cartilage environment and different heat transfer mechanisms at the knee joint, the adiabatic assumption seems to underestimate the required heat power. Therefore, we used our developed FE model of heat transfer in knee cartilage (Section 2.1) to estimate a more realistic heat power required. The objective of the simulation was to optimize the value of the heat power needed to increase the mean temperature by 2°C of a hydrogel placed in the middle of tibial cartilage when the cartilage is deformed sinusoidally.

2.2.2 Methods

The hydrogel was modeled as a poroelastic cylinder (diameter = 8 mm, height = 4 mm) placed in the middle of the tibial cartilage. Since we targeted a material with thermal and mechanical properties similar to the thermal and mechanical properties of articular cartilage when designing our hydrogel system, we considered the heat capacity, conductivity, density, stiffness and the permeability of the hydrogel to be equal to those of cartilage for our simulation. We modeled the heat transfer between this implanted hydrogel and cartilage when both deformed sinusoidally over 10 minutes at 1.5 Hz and 15% deformation. For our simulations, we varied the hydrogel heat power,

\dot{Q} , from 0.07 mW/mm^3 to 0.2 mW/mm^3 . The output of our simulation was the temperature increase after 10 minutes of loading.

2.2.3 Results and Discussion

Figure 2.6A shows the temperature after 10 minutes when $\dot{Q} = 0.1 \text{ mW/mm}^3$. Figure 2.6B is a plot of the mean temperature of the hydrogel for the various heat power values simulated. Our results showed that, to be able to increase the local temperature in the hydrogel under mechanical loading by 2°C (area 1 in Figure 2.6A), the self-heating hydrogel needed to provide 0.1 mW/mm^3 of heat power. This value is about four times higher than the cartilage dissipation. We used this value of heat power as a target when designing our self-heating hydrogels. In the next chapter we developed a hydrogel structure, which was able to dissipate at least 0.1 mW/mm^3 heat under mechanical loading.

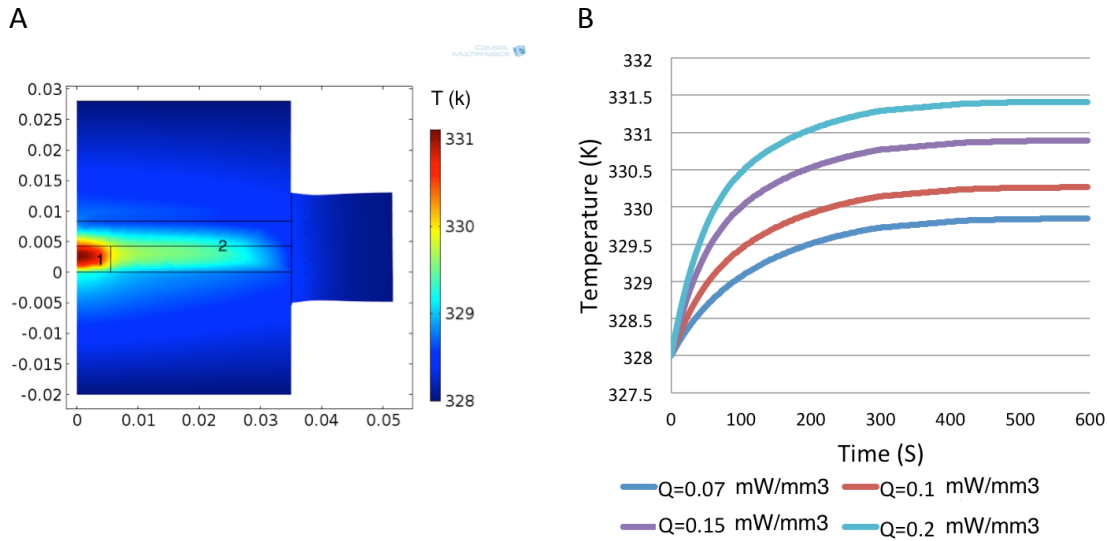


Figure 2.6. Simulated temperature increase of the implanted hydrogel under 10 minutes of mechanical loading. (A) Temperature field (label 1: hydrogel, label 2: cartilage). (B) Mean temperature of the hydrogel over time for the four heat power values simulated. To increase the temperature of the hydrogel by 2°C after 10 minutes of loading, the hydrogel should produce at least 0.1 mW/mm^3 of heat.

2.2.4 References

Incropera FP, Bergman TL, Lavine AS, DeWitt DP. 2011. Fundamentals of heat and mass transfer: Wiley

Chapter 3

Developing a Self-heating Hydrogel Structure with High Dissipative Properties

Paper: Improving hydrogels' toughness by increasing the dissipative
properties of their network^{*}

^{*} This chapter has been published in the "Journal of Mechanical Behavior of Biomedical Materials",
2015; 41: 161-167.

3.1 Abstract

The weak mechanical performance and fragility of hydrogels limit their application as biomaterials for load bearing applications. The origin of this weakness is their low resistance to chain breakage and crack propagation under loading because of insufficient energy dissipation mechanism in the hydrogel structure. The goal of this study is to evaluate the dissipation mechanism in covalently bonded hydrogels so that tougher hydrogels can be developed while keeping for the hydrogel a relatively high mechanical stiffness. By varying parameters such as cross-linker type or concentration as well as water ratio, the dissipative properties of HEMA-based hydrogels were investigated at large deformations. Different mechanisms such as special friction-like phenomena, nanoporosity, and hydrophobicity were proposed to explain the dissipative behavior of the tested hydrogels. Based on this analysis, it was possible to develop hydrogels with increased toughness properties.

Keywords: hydrogels, toughness, viscous dissipation, hydrophobicity

3.2 Introduction

Hydrogel systems are widely used for different biomedical applications. They present however two major drawbacks from a mechanical point of view. First, they usually have a low degree of stiffness and second they show a brittle behavior. While the stiffness and rigidity of hydrogels can be controlled and increased by chemical cross-linking (Anseth et al., 1996, Hennink and van Nostrum, 2012), hydrogels have an inherently low toughness, which does not allow them to sustain large deformations (Abdurrahmanoglu et al., 2009, Sun et al., 2012). As large deformations are common in different musculoskeletal tissues, the use of hydrogels is limited in these tissues.

It has been reported that the poor mechanical performance and brittleness of hydrogels mainly is due to low resistance to crack propagation because of insufficient dissipative properties in the hydrogel structure (Abdurrahmanoglu et al., 2009, Sun et al., 2012). To increase hydrogel dissipative properties, modifications at the molecular level have been suggested including reversible interactions like hydrophobic bilayers in a hydrophilic polymer network (Haque et al., 2011), ionic cross-linking (Sun et al., 2012), and physical interactions instead of covalent cross-linking (Abdurrahmanoglu et al., 2009, Tuncaboylu et al., 2011). The obtained noncovalent cross-linked hydrogels usually present a high degree of toughness. However, the stiffness of noncovalent cross-linked hydrogels is significantly lower than covalent cross-linked ones (Haque et al., 2011, Naficy et al., 2011, Sun et al., 2012). Noncovalent cross-linked hydrogels can then not be used in load bearing biomedical applications, where a high degree of stiffness and toughness are simultaneously needed. So in this study we focus on covalently bonded hydrogels to develop tougher hydrogels while keeping for the hydrogel a relatively high mechanical stiffness.

Among different hydrogel systems being covalently cross-linked, Poly(2-hydroxyethyl methacrylate) (PHEMA) has received considerable attention as a biocompatible hydrogel with tunable mechanical properties (Lou et al., 2004, Moghadam et al., 2014, Traian V, 2001, Voldrich et al., 1975, Young et al., 1998). HEMA monomers have a hydrophilic nature. The primary structure of homogeneous PHEMA hydrogel is a covalently linked three-dimensional network. In conjunction with this covalently bonded structure, PHEMA chains are held together by noncovalent forces in a secondary structure stabilized by hydrophobic bonding (Refojo, 1967). It has been reported that hydrophobic interactions can increase energy dissipation in hydrogels' network under loading when the external load reversibly disengages the adhered hydrophobic chains in the hydrogel structure

(Abdurrahmanoglu et al., 2009, Tuncaboylu et al., 2011). With these special properties, PHEMA hydrogels offer then the possibility to simultaneously increase their stiffness and toughness properties.

The mechanical properties, hydrophobicity, and pore size of HEMA-based hydrogels are tunable by controlling the type and the amount of cross-linkers as well as their water content (Baker et al., 2009, Peppas et al., 1985). In particular, these hydrogels can be produced with nanoscale pore size (Peppas et al., 1985). Nanopores provide a large pore surface area, which generates a unique nanofluidic behavior generating high friction between liquid and solid phase when the fluid flows through the nanopores (Kong and Qiao, 2005, Surani et al., 2005, Zhao et al., 2009).

Previous studies have investigated the effect of cross-linking density on PHEMA swelling, stiffness, and stress relaxation (Baker et al., 2009, Mabilieu et al., 2006, Peppas et al., 1985, Refojo, 1967). These studies showed that the degree of stiffness increases with increasing cross-linker concentration and polymer to water ratio during polymerization (Janacek, 1973). Since dissipation is a measure of toughness (Haque et al., 2011), in the present study, we further evaluate the effect of cross-linker type or concentration as well as water ratio on the dissipative properties of PHEMA hydrogels. We also evaluate the effect of adding hydrophobic HEMA chains in highly hydrophilic fragile hydrogel matrixes. Based on the obtained results, we develop hydrogels presenting high toughness properties while keeping high degree of stiffness allowing them to sustain large deformations.

3.3 Materials and Methods

3.3.1 Materials

2-Hydroxyethyl methacrylate (HEMA, 97%) was purified by basic aluminum oxide column chromatography to remove inhibitor. 2,2-dimethoxy-2-phenylacetophenone (DPAP) (Irgacur-651, 99%) was used as photo initiator and prepared as an ethanolic solution of DPAP (57 mg/mL solution, each mL = 0.2 mmol). Ethylene glycol di-methacrylate (EGDMA, 98%), poly(ethylene glycol di-methacrylate) (PEGDM) 550 and 750, triethylene glycol di-methacrylate (TEGDM), and poly(ethylene glycol methacrylate) (PEGM) 360 were purified with the same method as HEMA. All materials were purchased from Aldrich (Bucks, Switzerland) and were stored at 4°C until use.

3.3.2 Hydrogel Preparation

3.3.2.1 PHEMA hydrogels

PHEMA hydrogels were prepared with different PEGDM ($\text{C}_3\text{H}_5\text{C}(\text{O})(\text{OCH}_2\text{CH}_2)_n \text{OC}(\text{O})\text{C}_3\text{H}_5$) family cross-linkers (EGDMA, TEGDM, PEGDM 550 and 750) as well as with different concentrations of cross-linker (4% and 6% of mol HEMA). These cross-linkers are linear molecules differing with respect to their molecule length. EGDMA is the shortest molecule of the chosen cross-linkers with one ethylene glycol (OCH_2CH_2) functionalized with 2 methacrylate groups. PEGDM 750 is the longest one with 13 ethylene glycols (OCH_2CH_2). By using these cross-linkers, we can then evaluate the effect of cross-linker length on hydrogels dissipation. In parallel, the volumetric ratio of water was varied between 20%, 40%, and 50% of volume of mixture. The different combinations of parameters as well as the material volume ratio used in the preparation of the HEMA-based hydrogel are summarized in Table 1S (supplementary material: APPENDIX 7.1). Specifically for the EGDMA cross-linker, a wider range in concentration of this cross-linker (2%, 4%, and 6%) and water ratio (20%, 40%, 50%, 60%, and 70%) were evaluated. The mixture containing the photo initiator DPAP (0.1% of mol HEMA) was stirred and sonicated for 1 min. It was then transferred to cylindrical wells (8 mm diameter and 4 mm depth), placed under UV lamp (365 nm, 8 watt) positioned 10 cm from the sample and irradiated for 15 min, whilst maintaining the temperature below 25°C. Hydrogels were then carefully removed from the well, washed to remove unreacted material, and immersed in water for one week before mechanical test. Four samples per group were prepared.

3.3.2.2 HEMA-PEGM hydrogels

To investigate how hydrophobic interactions affect the dissipation properties and toughness of fragile hydrophilic hydrogels, PHEMA hydrogels were copolymerized with polyethylene glycol methacrylate (PEGM). PEGM hydrogel has been reported to be very hydrophilic and highly swellable in water (Lei et al., 2013). For this experiment, we used EGDMA as cross-linker and kept cross-linker ratio equal to 6% of total monomers molarity. Forty percent volumetric ratio of water was adjusted for all HEMA-PEGM-EGDMA hydrogels. We prepared hydrogels with different molar ratios of HEMA and PEGM (6.5%, 12.5%, and 25% of mol of HEMA) as well as PEGM without HEMA. The polymerization process was similar as for the HEMA-based hydrogel.

3.3.3 Hydrogel Mechanical Characterization

To characterize elastic and viscoelastic behavior of hydrogels under compressive loading at large deformations, the total input energy and dissipated energy were chosen as measures. These measures, unlike elastic and lost moduli, are valid to quantify material properties at large deformations and in nonlinear regime (Lakes, 1999). We also introduced the damping ratio as the ratio of dissipated work to total input work that the material received during deformation. This ratio represents the viscous behavior of the material over its elastic behavior (Vogel and Pioletti, 2012).

3.3.3.1 Dissipation measurement

The dissipation of PHEMA hydrogels was obtained by integrating the hysteresis force-deformation loop appearing during sinusoidal compressions of the hydrogel (Lakes, 1999, Li and Xu, 2007). The dissipation was normalized to the volume of the sample. The sinusoidal compression was applied on each sample with an Instron E3000 linear mechanical testing machine (Norwood, MA, USA). During the test, samples were immersed in water. A 10% pre-strain was imposed on the sample followed by a sinusoidal 15% compressive strain at 1 Hz for 100 cycles. The dissipation was measured on the last 10 cycles and averaged.

3.3.3.2 Damping ratio measurement

To further compare the dissipative properties of different hydrogels, damping ratio is a useful variable as it quantifies the capacity of a material in dissipating input work, which is the total energy giving to material during loading and unloading. A metric valid in case of large deformations and then relevant for hydrogel characterization is the specific damping capacity, which normalizes the dissipation over total input work (Vogel and Pioletti, 2012):

$$\psi = \frac{\Delta W}{W} \quad (3.1)$$

where ΔW is the energy loss per cycle or hysteresis and W is the total input work during the mechanical loading. Input work is calculated by integrating the surface under the force-deformation curve during mechanical loading. Since the amount of input work is proportional to the material stiffness, the input work is considered as a measure of material stiffness. The damping ratio normalizes the dissipation over the material stiffness. Material with higher damping ratios present

higher viscous properties compared to material with the same stiffness but lower damping ratios (Lakes, 1999, Vogel and Pioletti, 2011).

3.4 Results

Figure 3.1 shows the typical hysteresis loop of hydrogels with different cross-linker types. As it can be qualitatively observed from Figure 3.1, the area of the hysteresis loop reduces with the increase of the cross-linker chain length. By keeping the cross-linker concentration and the deformation magnitude fixed in all tests, it can also be seen on Figure 3.1 that the maximum reached force and the amount of input work (the gray area) do not significantly change between different tested samples. This result suggests that increasing cross-linker length has not an effect on the hydrogels' stiffness as significant as on their dissipative properties.

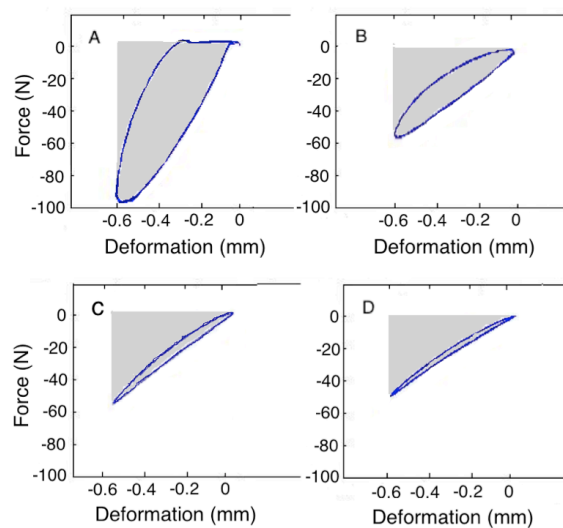


Figure 3.1. Hysteresis loop of HEMA hydrogels and input work (gray area) obtained with different types of cross-linker at 6% and water at 40% (APPENDIX 7.1 table 1S), (A) HEMA-EGDMA (S13), (B) HEMA-TEGDM (S14), (C) HEMA-PEGDM550 (S15), (D) PEGDM750 (S16)).

3.4.1 Effect of Cross-Linker

From a quantitative point of view, the dependency of dissipation and damping ratio of HEMA hydrogels to the type and the concentration of cross-linkers as well as to its water ratio are reported in Figure 3.2 and 3.3. In particular, we can observe from Figure 3.2 that increasing PEGDM cross-linker molecule length decreases dissipation ($p < 0.001$). EGDMA induces the highest dissipation and PEGDM 750 the lowest one. Also for all types of developed hydrogels, increasing cross-linker

concentration increases dissipation magnitude, but on the other hand it slightly decreases the damping ratio ($p < 0.05$) (Figure 3.3). Since the damping ratio represents the damping properties of materials over its elastic behavior, this decrease confirms that increasing the cross-linker concentration increases the elastic properties of hydrogel more than its viscous properties as it is generally reported.

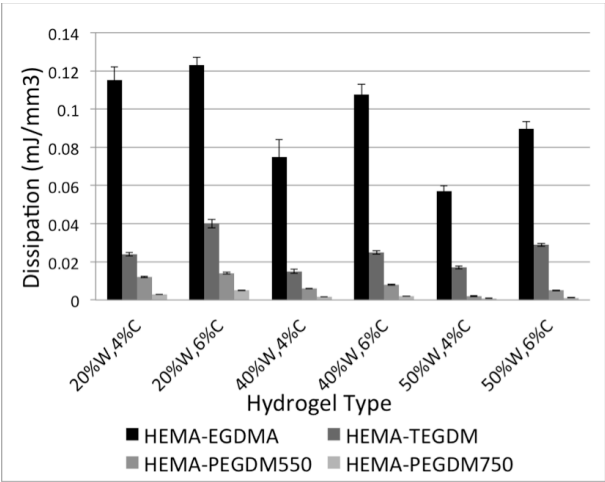


Figure 3.2. Dissipation of HEMA hydrogels: effect of cross-linker type and amount as well as water ratio (W: water, C: cross-linker).

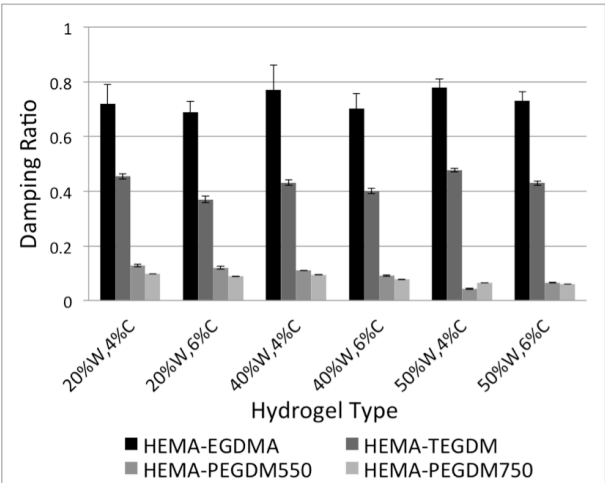


Figure 3.3. Damping ratio of hydrogels: effect of cross-linker type and amount as well as water ratio (W: water, C: cross-linker).

As EGDMA cross-linker induced the highest dissipation between all tested cross-linker, we further characterized its performance. From Figure 3.4 we can observe that even at the lowest cross-linker concentration used, the damping ratio of HEMA-EGDMA remains high (0.72 ± 0.3). Therefore, under high loads and large deformations, HEMA-EGDMA hydrogels damp most part of the input work.

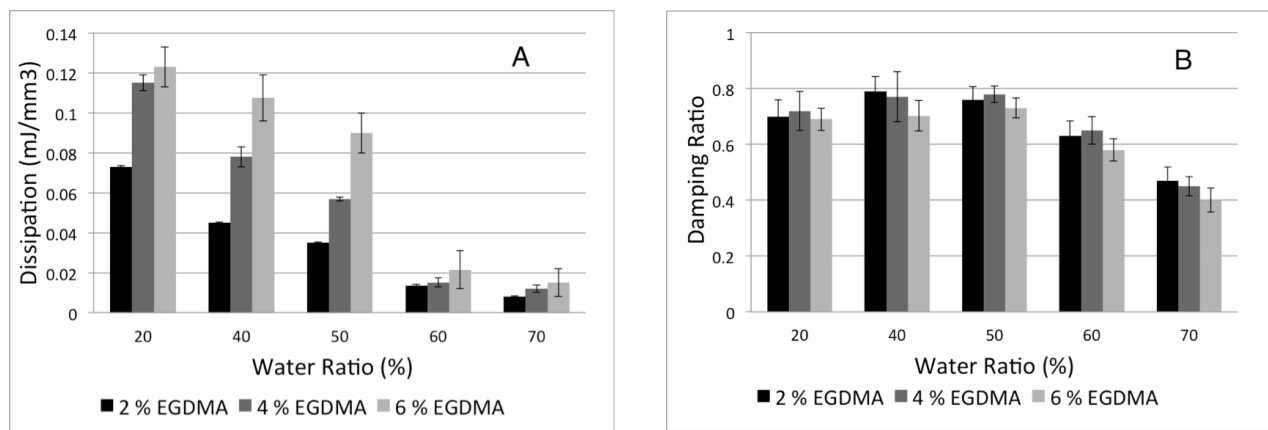


Figure 3.4. HEMA-EGDMA hydrogels: effect of water ratio and cross-linker percentage on (A) dissipation and (B) damping ratio.

3.4.2 Effect of Water Ratio

Figure 3.2 shows that increasing water ratio during polymerization decreases the amount of dissipation ($p < 0.01$). On the other hand, the damping ratio seems not to be sensitive to water concentration ($p > 0.1$) (Figure 3.3). The low sensitivity of the damping ratio on water content suggests that the input work also decreases by increasing water ratio meaning that the hydrogel becomes softer while keeping its dissipative properties. However for EGDMA cross-linker with the water ratio above 60%, the damping ratio also decreases (Figure 3.4B).

3.4.3 Effect of Hydrophobicity

To further confirm the effect of increasing hydrophobicity on the toughness of hydrophilic hydrogels, we studied the effect of adding PHEMA chains to the backbone of highly hydrophilic PEGM hydrogels. In particular, Figure 3.5 shows the effect of adding HEMA on the dissipation of PEGM hydrogels. Having PEGM, even at a low concentration (7.5%), decreased the dissipative properties

of hydrogels significantly ($p < 0.001$) (Figure 3.5A). On the other hand, the swelling of the hydrogels increased (Figure 3.6A). Decreasing the damping ratio by increasing PEGM concentration in hydrogel network, shows that hydrophilic polymers like PEGM increases the elastic properties of hydrogels. PEGM hydrogels were not resistant to large deformations when the percentage of PEGM increased. In some cases after mechanical tests (1 Hz, 1000 cycles of 15% deformation), several cracks were visually apparent (Figure 3.6B). Hydrogels made of PEGM without HEMA were very fragile. They highly swelled in water but could not resist large deformation (Figure 3.6).

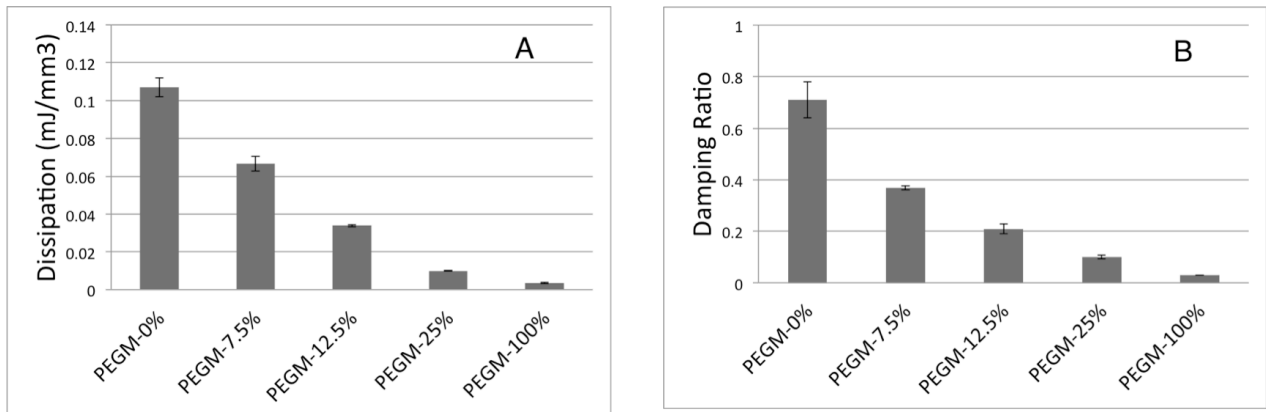


Figure 3.5. Effect of adding hydrophilic elements in hydrogels structure. (A) Effect on dissipation. (B) Effect on damping ratio.

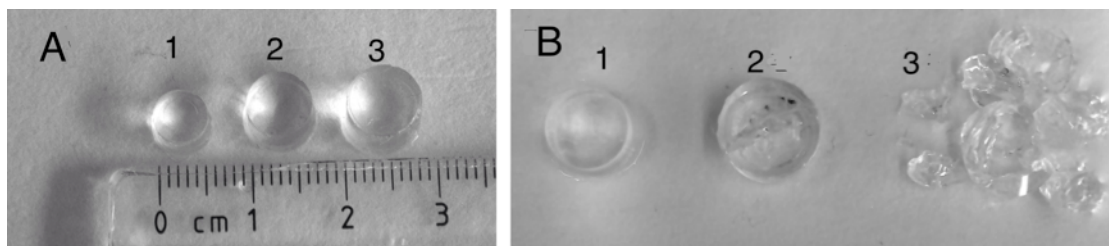


Figure 3.6. HEMA-PEGM hydrogels. (A) Hydrogels after swelling: 1 HEMA, 2 HEMA + 25% PEGM, 3 PEGM. (B) Hydrogels after applying 1000 cyclic deformations (1 Hz, 15% deformation amplitude).

3.5 Discussion

Controlling polymerization conditions can improve the stiffness and rigidity of hydrogels. However, just having a high degree of stiffness is not enough for a biomaterial to be used in load bearing application. The material needs to have enough toughness not to fracture and be destroyed under cyclic load especially at large deformations. To increase toughness of the hydrogel, its dissipative properties should be increased. Our results showed that due to the special structure of HEMA hydrogels, changing cross-linking molecular length and ratio and water ratio could tune their dissipation properties. Due to this dissipation, the stored energy in hydrogel network is then limited reducing the possibility to reach the crack tip energy of these hydrogels. We showed that using short length cross-linkers like EGDMA results in much higher dissipation when we use the same amount of cross-linker. Since for all of cross-linkers that we used in this study, people have already shown a high monomer conversion with UV polymerization (Baker et al., 2009, Dziubla et al., 2001, Li and Lee, 2005), the sol and gel fraction cannot be the case for such a high dissipation difference among these hydrogels. A possible explanation for such high dissipative behavior may reside in the conjunction of two specific properties related to solid-fluid interactions in the developed HEMA-EGDMA hydrogels. The first specific property is related to the nanoporous structure of these hydrogels. The average pore size of HEMA-EGDMA hydrogels was quantified to be less than 5 nm (Table 2S, APPENDIX 7.1). This porosity was the result of using very short molecules like EGDMA as cross-linker. Because of the very large pore surface area of nanoporous materials, high friction can be produced when fluids move through the nanopores as it has been previously reported (Kong and Qiao, 2005). The second specific property is related to the increase of the PHEMA hydrogel hydrophobicity, which has been reported to be induced by EGDMA (Peppas et al., 1985). Indeed, it has been shown that having hydrophobic properties along with nanoporous structure induces a special interaction between hydrogels chains and water composing the hydrogel that can highly increase the dissipation (Kong and Qiao, 2005, Surani et al., 2005, Zhao et al., 2009). For such a material immersed in water or in a nonwetting liquid, previous published studies have shown that when mechanical pressure exceeds a critical threshold, the liquid can be forced to defiltrate or infiltrated the hydrophobic nanopores, which are energetically unfavorable to liquid exchange (Kong and Qiao, 2005, Surani et al., 2005, Zhao et al., 2009). In other words, there will be a defiltration (drainage) and infiltration pressure during loading and unloading that increases interfacial energy. In this situation, the forced in and out motion of the liquid molecules will increase the en-

ergy dissipation via friction-like interaction between solid and liquid phases (Kong and Qiao, 2005, Surani et al., 2005, Zhao et al., 2009).

Beside the two specific properties related to solid-fluid interactions, the high dissipation of HEMA-EGDMA hydrogels could also be related to the sub-molecular structure of these hydrogels. Depending on the length of the cross-linker molecules, an interaction could be induced between HEMA pendant groups in hydrogel network. As Figure 3.7 shows in PHEMA chains structure, there are some pendant groups (Hydroxyethyl groups) dangling from each HEMA unit. These pendant groups make a comb-shape structure connecting with cross-linker molecules. Since the length of these pendant groups is as short as one ethylene glycol, as in EGDMA (Figure 3.7A), using EGDMA as cross-linker lets pendant groups (the teeth of comb-shape structures) to be close enough to touch each other and interact when the material deforms during cyclic load. These interactions might produce a local friction that would then also dissipate energy. When longer cross-linkers are used, it is less likely to obtain these interactions (Figure 3.7B and C). Although we know that polymer chains are not like a rigid rods, but floppy and flexible, because of this particular structure of HEMA-EGDMA hydrogels, the possibility of friction between chains based on what we discussed in most probable comparing to other linear hydrogels without this comb-shape structure. Changing the magnitude of EGDMA cross-linker allows us to tune the stiffness of these hydrogels without affecting their high dissipative properties. With these particular properties, HEMA-EGDMA hydrogels can be considered as tough hydrogels with tunable stiffness.

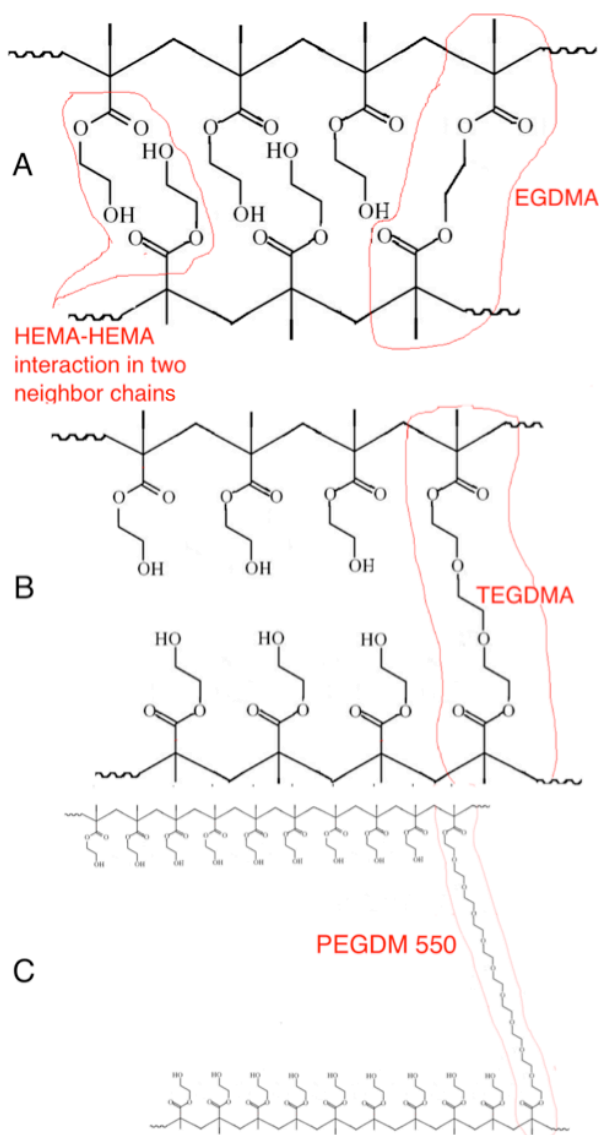


Figure 3.7. Structure of HEMA hydrogel cross-linked with (A) EGDMA, (B) TEGDM and (C) PEGDM 550. Due to the short length of EGDMA, we propose that dissipation due to friction of the pendant groups of two neighbor HEMA chains is increased while the long molecules of TEGDM or PEGDM prevent such an interaction.

Beside cross-linker, water ratio of HEMA hydrogels during polymerization has considerable effect on their mechanical properties. Based on our results, water ratio can regulate the stiffness of hydrogels but doesn't have significant effect on damping properties. This property suggests that with controlling water ratio, we can have hydrogels with wide range of stiffness and high toughness. However, very high water ratio (more than 60%) decreases damping properties as well. This behavior was expected since it has been reported that in PHEMA hydrogels when the water ratio is high (more than 60 %), the network becomes microporous (Baker et al., 2009). We propose that having

such a highly porous structure may decrease the solid-fluid surface and consequently the corresponding friction due to nanoporous liquid-solid interactions. Moreover, when water ratio increases, more water molecules are trapped in the hydrogel network during polymerization and may weaken the hydrophobic interactions.

Furthermore, we showed that copolymerizing HEMA hydrogels with brittle and mechanically poor hydrophilic hydrogel networks improved the toughness and mechanical properties of those hydrogels. Hydrophilic materials show a spring-like behavior due to its high tendency to keep the water molecules (Kong and Qiao, 2005, Surani et al., 2005, Zhao et al., 2009). Under loading the friction-like behavior related to water flow discussed earlier is less likely to happen to dissipate the input work. In such a situation if we apply high forces, the energy stored in the material during loading can reach the crack tip energy, resulting to the fracture of the material (Abdurrahmanoglu et al., 2009). These observations confirm the positive effect of hydrophobicity to increase hydrogel toughness.

3.6 Conclusion

The present study focused on characterizing dissipative properties of HEMA-based hydrogels when polymerization conditions related to cross-linker and water ratios changed. Since the dissipation is a measure of toughness, such a study led us to understand the origin of the toughness of these hydrogels. Based on the obtained results, hydrogels formulation presenting simultaneously high degree of stiffness and dissipative properties could be proposed. Based on our findings, we suggest that to increase the toughness of fragile hydrogels, one has to increase hydrophobicity of the hydrogel network, use short length molecules as cross-linker and add comb-shape molecule chains (like PHEMA) in the backbone of the hydrogel.

3.7 Acknowledgment

This work was supported by the Swiss National Science Foundation (#406240_126070, PNR 62 program) and the Inter-Institutional Center for Translational Biomechanics EPFL-CHUV-DAL.

3.8 References

- Abdurrahmanoglu S, Can V, Okay O. 2009. Design of high-toughness polyacrylamide hydrogels by hydrophobic modification. *Polymer* 50, 5449-55.
- Anseth KS, Bowman CN, Brannon-Peppas L. 1996. Mechanical properties of hydrogels and their experimental determination. *Biomaterials* 17, 1647-57.
- Baker MV, Brown DH, Casadio YS, Chirila TV. 2009. The preparation of poly(2-hydroxyethyl methacrylate) and poly{(2-hydroxyethyl methacrylate)-co-[poly(ethylene glycol) methyl ether methacrylate]} by photoinitiated polymerisation-induced phase separation in water. *Polymer* 50, 5918-27.
- Dziubla TD, Torjman MC, Joseph JI, Murphy-Tatum M, Lowman AM. 2001. Evaluation of porous networks of poly(2-hydroxyethyl methacrylate) as interfacial drug delivery devices. *Biomaterials* 22, 2893-9.
- Haque MA, Kurokawa T, Kamita G, Gong JP. 2011. Lamellar bilayers as reversible sacrificial bonds to toughen hydrogel: hysteresis, self-Recovery, fatigue resistance, and crack blunting. *Macromolecules* 44, 8916-24.
- Hennink WE, van Nostrum CF. 2012. Novel crosslinking methods to design hydrogels. *Advanced Drug Delivery Reviews* 64, 223-36.
- Janacek J. 1973. Mechanical Behavior of Hydroxyalkyl Methacrylate Polymers and Copolymers. *Journal of Macromolecular Science, Part C* 9, 3-47.
- Kong X, Qiao Y. 2005. Improvement of recoverability of a nanoporous energy absorption system by using chemical admixture. *Applied Physics Letters* 86, 1-3.
- Lakes RS. 1999. *Viscoelastic solids*: CRC Press LLC
- Lei J, Mayer C, Freger V, Ulbricht M. 2013. Synthesis and Characterization of Poly(ethylene glycol) Methacrylate Based Hydrogel Networks for Anti-Biofouling Applications. *Macromolecular Materials and Engineering* 298, 967-80.
- Li L, Lee LJ. 2005. Photopolymerization of HEMA/DEGDMA hydrogels in solution. *Polymer* 46, 11540-7.
- Li Y, Xu M. 2007. Hysteresis loop and energy dissipation of viscoelastic solid models. *Mechanics of Time-Dependent Materials* 11, 1-14.
- Lou X, Munro S, Wang S. 2004. Drug release characteristics of phase separation pHEMA sponge materials. *Biomaterials* 25, 5071-80.
- Mabilleau G, Stancu IC, Honore T, Legeay G, Cincu C, Basle MF, Chappard D. 2006. Effects of the length of crosslink chain on poly(2-hydroxyethyl methacrylate) (pHEMA) swelling and biomechanical properties. *Journal of Biomedical Materials Research. Part A* 77, 35-42.
- Moghadam MN, Kolesov V, Vogel A, Klok H-A, Pioletti DP. 2014. Controlled release from a mechanically-stimulated thermosensitive self-heating composite hydrogel. *Biomaterials* 35, 450-5.

-
- Naficy S, Brown HR, Razal JM, Spinks GM, Whitten PG. 2011. Progress toward robust polymer hydrogels. *Australian Journal of Chemistry* 64, 1007-25.
- Peppas NA, Moynihan HJ, Lucht LM. 1985. The structure of highly crosslinked poly(2-hydroxyethyl methacrylate) hydrogels. *Journal of Biomedical Materials Research* 19, 397-411.
- Refojo MF. 1967. Hydrophobic interaction in poly(2-hydroxyethyl methacrylate) homogeneous hydrogel. *Journal of Polymer Science Part A-1: Polymer Chemistry* 5, 3103-13.
- Sun JY, Zhao X, Illeperuma WR, Chaudhuri O, Oh KH, Mooney DJ, Vlassak JJ, Suo Z. 2012. Highly stretchable and tough hydrogels. *Nature* 489, 133-6.
- Surani FB, Kong X, Panchal DB, Qiao Y. 2005. Energy absorption of a nanoporous system subjected to dynamic loadings. *Applied Physics Letters* 87, 1-3.
- Traian V C. 2001. An overview of the development of artificial corneas with porous skirts and the use of PHEMA for such an application. *Biomaterials* 22, 3311-7.
- Tuncaboylu DC, Sari M, Oppermann W, Okay O. 2011. Tough and self-healing hydrogels formed via hydrophobic interactions. *Macromolecules* 44, 4997-5005.
- Vogel A, Pioletti DP. 2011. Thermomechanical hysteresis of biological and synthetic hydrogels: theory, characterisation, and development of a novel deformation calorimeter. PhD thesis, école polytechnique federale de Lausanne
- Vogel A, Pioletti DP. 2012. Damping properties of the nucleus pulposus. *Clinical Biomechanics* 27, 861-5.
- Voldrich Z, Tomanek Z, Vacik J, Kopecek J. 1975. Long-term experience with poly (glycol monomethacrylate) gel in plastic operations of the nose. *Journal of Biomedical Materials Research* 9, 675-85.
- Young C-D, Wu J-R, Tsou T-L. 1998. High-strength, ultra-thin and fiber-reinforced pHEMA artificial skin. *Biomaterials* 19, 1745-52.
- Zhao J, Culligan PJ, Germaine JT, Chen X. 2009. Experimental study on energy dissipation of electrolytes in nanopores. *Langmuir* 25, 12687-96.

Chapter 4

Controlled Release from Composite Hydrogel

Paper: Controlled Release from a Mechanically-Stimulated Thermo-sensitive Self-Heating Composite Hydrogel^{*}

^{*} This chapter has been published in “Biomaterials”, 2014; 35 (1): 450-455.

4.1 Abstract

Temperature has been extensively explored as a trigger to control the delivery of a payload from environment-sensitive polymers. The need for an external heat source only allows limited spatio-temporal control over the delivery process. We propose a new approach by using the dissipative properties of a hydrogel matrix as an internal heat source when the material is mechanically loaded. The system is comprised of a highly dissipative hydrogel matrix and thermo-sensitive nanoparticles that shrink upon an increase in temperature. Exposing the hydrogel to a cyclic mechanical loading for a period of 5 min leads to an increase of temperature of the nanoparticles. The concomitant decrease in the volume of the nanoparticles increases the permeability of the hydrogel network facilitating the release of its payload. As a proof-of-concept, we showed that the payload of the hydrogel is released after 5 to 8 min following the initiation of the mechanical loading. This delivery method would be particularly suited for the release of growth factor as it has been shown that cell receptor to growth factor is activated 5 to 20 min following a mechanical loading.

Keywords: Hydrogel, Controlled release, mechanical loading, viscous dissipation, thermosensitive nanoparticles

4.2 Introduction

Most of the efforts in the field of drug delivery systems have focused on the development of environment-sensitive polymers. Temperature and pH are commonly used environmental variables (Gil and Hudson, 2004, Gupta et al., 2002, Klouda and Mikos, 2008, Qiu and Park, 2012). While pH can be coupled to variations within the body, temperature sensitive polymers are designed to be altered either externally (Hoare et al., 2009, Schmaljohann, 2006, Yavuz et al., 2009) or are in off/on mode almost immediately after being injected in the body (Gong et al., 2013, Jeong et al., 2002, Yu and Ding, 2008).

Temperature-responsive drug delivery systems are usually based on polymer hydrogel with a lower critical solution temperature (LCST) of around 38°C. The drug is released when the tissue surrounding the hydrogel reaches a temperature slightly above normal body temperature (Qiu and Park, 2012, Zhang and Misra, 2007). While these systems work well for a number of applications, they also have some limitations. The need for an external means to cool or heat in many applications only allows limited spatiotemporal control over the delivery process.

As hydrogels have dissipative properties, their temperature may also be altered internally by viscous dissipation during cyclic loading, a process generally referred to as self-heating (Ahearne et al., 2005, Karnaukhov et al., 1975, Schapery, 1964). There are potentially several advantages of using the self-heating property of materials for drug delivery.

First, the drug release is coupled to a mechanical loading. As mechanical loading has been demonstrated to activate some growth factor cell receptors involved in the healing process of different tissues such as cartilage (Discher et al., 2009, Hiyama et al., 2007, Mauck et al., 2003, Neu et al., 2007), the coupling of mechanical loading and drug release could induce some positive synergetic effects. Drug delivery system coupled to mechanical loading has already been developed, the drug being simultaneously released during the mechanical loading (Edelman et al., 1992, Korin et al., 2012, Lee et al., 2000).

However, it is important to realize that cell receptors are not immediately activated following a mechanical loading. A delay of 5 to 20 minutes has been observed between the initiation of the mechanical loading and the activation of the cell receptor (Tschumperlin et al., 2004). To induce a

maximum potency, the release of a drug following a mechanical loading should then also be delayed by several minutes.

As the self-heating property induces a local temperature increase, which is related to the dissipative properties of the material and to the number of loading cycles, a delay can be obtained between the initiation of the mechanical loading and the temperature increase triggering the drug release. The use of dissipative energy generated in hydrogel could then offer a second advantage, which is the unprecedented spatiotemporal control over the delivery process. In particular, the use of self-heating property would be particularly suited for the delivery of growth factors to induce healing in a cartilage defect where the cells are naturally subjected to mechanical loading.

In this study, we establish the proof-of-concept that dissipative properties can be used as a new environmental variable to spatiotemporally control the release of a drug.

4.3 Materials and Methods

4.3.1 Principle of Dissipation Used as an Environmental Variable

To explore the feasibility of using dissipative properties to control delivery from thermosensitive polymer based systems, we developed a unique hydrogel system consisting of two components: i) poly(2-hydroxyethyl methacrylate) (PHEMA)-based hydrogel matrix with highly dissipative properties and ii) poly(N-isopropyl acrylamide) (PNIPAM)-based thermosensitive nanoparticles, which are entrapped in the matrix hydrogel and shrink at temperatures above their LCST.

The principle used to temporally control the delivery of a payload following a mechanical loading is shown in Figure 4.1A. Upon applying a mechanical load, a part of the mechanical energy is transformed into heat due to the dissipative properties of the hydrogel matrix. The heat produced by the hydrogel increases the temperature of the nanoparticles above their LCST and induces their collapse, which subsequently facilitates diffusion of the payload outside the hydrogel. The dissipative properties of the hydrogel can be modulated to link the duration of the cyclic loading with a targeted increase in temperature. Thus, a specific delay between the initiation of the mechanical stimulation and the release of a payload can be obtained.

HEMA is a hydrogel-forming material that is widely used in the biomaterials field (Chirila, 2001, Dziubla et al., 2001). Water content and crosslink density are the key parameters to control the

mechanical and dissipative properties of these hydrogels (Lai and Quinn, 1997, Mabilieu et al., 2006). The hydrogels can be obtained using different cross-linkers in a one-step photopolymerization process (Baker et al., 2009). The PHEMA hydrogels investigated in this study were cross-linked with ethylene glycol di-methacrylate (EGDMA) and contained 40% water.

4.3.2 Materials

2,2-dimethoxy-2-phenylacetophenone (Irgacure 651, 97%), ethylene glycol dimethacrylate (EGDMA, 98%), TWEEN® 80, Span® 80, N,N,N',N'-Tetramethylethylenediamine (TMEDA, 99%), Ammonium persulfate ($\geq 98\%$) and Xylene Cyanole FF were purchased from Aldrich and used as received. 2-Hydroxyethyl methacrylate (HEMA, 97%) and poly(ethylene glycol) di-methacrylate (PEGDMA, average M_n 550) were purchased from Aldrich and purified by basic aluminum oxide column chromatography to remove inhibitor. N-isopropylacrylamide (Aldrich, 97%) was purified by recrystallization from hexane. Spectra/Por 6 dialysis tubing, 10K MWCO was purchased from Spectrum Labs Europe.

4.3.3 Preparation of the Nanoparticles

The organic phase consisted of n-hexane (15 mL) and a mixture of surfactants TWEEN80 (75 mg) and SPAN80 (225 mg). The oxygen dissolved in the organic phase was removed by evacuating the surfactant mixture for 5 min followed by purging with nitrogen for short period (repeated 3 times). Hexane was purged with nitrogen for 10 min. The aqueous phase was prepared as follows: 150 mg of NIPAM were added to the flask along with 10 mg of poly(ethylene glycol)di-methacrylate (PEGDMA). Solid monomer and cross-linker were dissolved in 0.4 mL PBS pH 7.4 and sonicated. Organic phase was added to aqueous phase and the mixture was emulsified by sonicating 30 s. Polymerization was initiated by the addition of 2 drops of tetramethyl ethylenediamine and 25 mg of ammonium persulfate in 0.1 mL PBS pH 7.4 during sonication. Additional drops of TMEDA were added 10 min after; the miniemulsion was stirred for 4 h at room temperature. The reaction was stopped by exposure to air. Hexane was removed on rotary evaporator at 30°C and 5 mbar, wax-like substance was redispersed in ethyl ether and precipitated. Supernatant was removed, and particles were redispersed in ether two more times. After that, the particles were redispersed in water, dialyzed against water for 3 days (MWCO 10000 membrane, water was changed at least

twice a day) and freeze-dried. Purified particles were redispersed in water, and the diameter was analyzed by DLS as the average of 10 measurements.

4.3.4 Preparation of the Composite Hydrogel

2-Hydroxyethyl methacrylate (HEMA) (880 μL), ethylene glycol di-methacrylate (EGDMA) (84 μL , 6%_{mol}), and Xylene Cyanol FF aqueous solution (1 mg/ml, 590 μL) were mixed in a 5 mL eppendorf tube. The Xylene Cyanol FF was used as drug model. The final aqueous ratio of the mixture was 40% of the total mixture volume. For hydrogels containing nanoparticles, the aqueous phase also contained 15 mg/mL nanoparticles, which is equal to 5.5 mg/mL nanoparticles in total reaction mixture. A solution of Irgacur-651 (photo initiator) in ethanol (36 μL of 57 mg/mL solution) was then added to the polymer mixture. The mixture was stirred and sonicated for 1 min, then transferred to the cylindrical wells (8 mm diameter and 4 mm depth), placed under UV lamp (365 nm, 8 Watt) and irradiated for 15 min, whilst maintaining the temperature below 25°C (using a flow of compressed air). The samples were washed and kept in 1 mL water for two days before mechanical tests (Figure 4.1B).

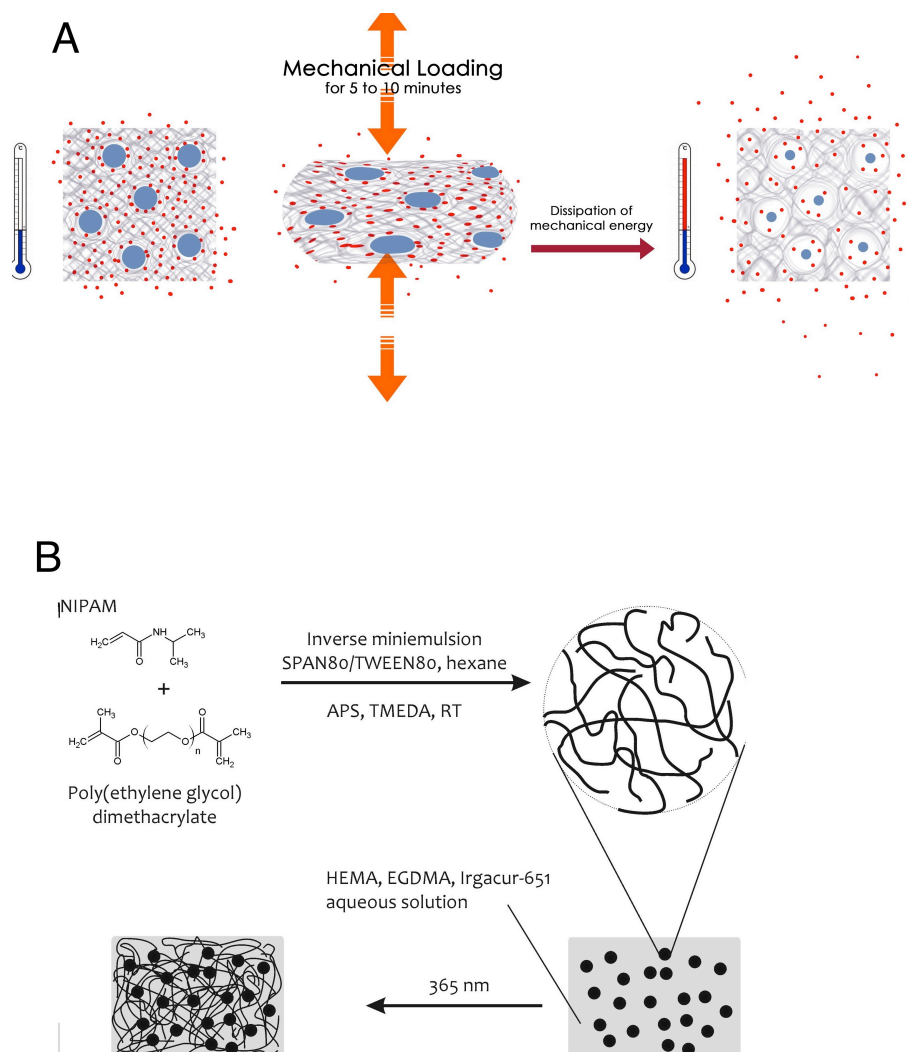


Figure 4.1. (A) Release of a payload from a thermosensitive delivery system using dissipation as an internal heat source. Thermosensitive nanoparticles (blue dots) and payload (red dots) are distributed randomly inside the hydrogel (gray). At temperatures below the LCST of the nanoparticles, only limited amount of payload can be released from the hydrogel. When the hydrogel is under a mechanical loading of 5 to 10 minutes duration, its dissipative properties induce a temperature increase, a process called self-heating. If the temperature rises above the LCST of the nanoparticles, they shrink, which increases the permeability of the hydrogel and facilitates the release of the payload. (B) Synthesis of the composite hydrogel.

4.3.5 Quantification of Xylene Cyanole FF Release

After each test the supernatant water was collected from the test chamber and the amount of released Xylene Cyanole FF was quantified via spectrophotometry at 590 nm. The release amount $c_d(t)$ was reported as $\mu\text{g/mL}$ using the normalized curves we prepared by spectrophotometric analysis of solutions at different concentrations of Xylene Cyanol FF in water.

4.3.6 Mechanical Loading

Mechanical compressive test was performed with an Instron E3000 linear mechanical testing machine (Norwood, MA, USA). To provide a heat-isolated environment, controlling the initial temperature and monitoring the temperature during the test, a specifically designed thermally isolated system was installed on the mechanical testing machine (Figure 1S, APPENDIX 7.2). The temperature of the test chamber was maintained by water circulation around the chamber either at 34°C or at 36°C for different experiments. The hydrogel immersed in 600 µL fresh water was placed in the center of the chamber. The hydrogel temperature was monitored with a thermistor positioned in the center of test chamber (Figure 1S, APPENDIX 7.2). Cyclic compression was applied at 1.5 Hz on displacement control mode. Deformations of 15% amplitude following a 5% prestrain were applied for 5 and 8 min. The temperature was recorded every 10 s during the test.

4.3.7 Effective Diffusion Coefficient Measurement

To calculate the effective diffusion coefficient of the composite hydrogel, we prepared samples in the form of microfilms by injecting the polymer mixture between two glass slides having a 150 µm gap and polymerized them under UV light. After polymerization, films were punched with 8 mm punch and immersed in 600 µL water. Hydrogels with or without nanoparticles were placed either at 34°C or at 39°C (6 samples per group). Xylene Cyanole FF release ($c_d(t)$) was measured every 2 hours for 14 hours from each of the 4 different hydrogel groups (with or without nanoparticles, at 34°C and 39°C). The transient distribution of Xylene Cyanole FF in a cylindrical sample is governed by the following equation (Quinn et al., 2000):

$$\frac{\partial c}{\partial t} = \frac{D_{eff}}{\phi} \left(\frac{1}{r} \frac{\partial}{\partial r} \left(r \frac{\partial c}{\partial r} \right) + \frac{\partial^2 c}{\partial z^2} \right) \quad (4.1)$$

where c is the Xylene Cyanole FF concentration within the sample, D_{eff} is the effective diffusivity and ϕ is the hydrogel water content equal to 40% in our case. Considering the boundary condition $c = 0$ at $r = R$, $z = 0$ and $z = h$ (R and h : sample diameter and height) and the initial condition $c = c_0$ (initial Xylene Cyanole FF concentration inside the hydrogel), we obtained the analytical solution for c . By integrating c over the sample fluid volume and subtracting the result from the total Xylene Cyanole FF release gives the following solution for the Xylene release in the water bath $c_d(t)$:

$$c_d(t) = c_{\max} \left[1 - \sum_{n=1}^{\infty} \sum_{m=1}^{\infty} \frac{16[1 - (-1)^n]}{q_m^2 n^2 \pi^2} \exp\left(-\frac{D_{\text{eff}} \lambda_{nm}^2 t}{\phi}\right) \right] \quad (4.2)$$

$c_d(t)$ is the Xylene Cyanole FF release, c_{\max} is the total Xylene Cyanole FF release from the sample in water if we assume all Xylene in the sample is released in 600 μL (for microfilm samples $c_{\max} = 2.83 \mu\text{g/mL}$), q_m is the m^{th} zero of zero-order Bessel function (J_0) and

$$\lambda_{nm}^2 = \frac{q_m^2}{R^2} + \frac{n^2 \pi^2}{h^2} \quad (4.3)$$

All parameters in Equation (4.2) except D_{eff} were known or measured independently. D_{eff} was calculated by fitting Equation (4.2) to the experimental data from desorption bath (Figure 2S, APPENDIX 7.2).

4.4 Results

4.4.1 Temperature Response of Nanoparticles

The nanoparticles had a diameter of 340 nm as determined by Dynamic Light Scattering (DLS) at room temperature and showed a lower critical solution temperature of 37°C (Figure 4.2). At 37°C, the PNIPAM nanoparticles collapsed and had an average diameter of 255 nm. The resulting decrease in volume corresponds to about 50%.

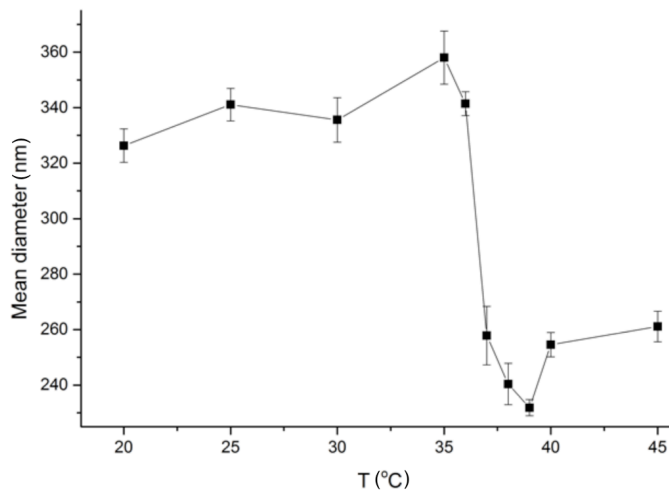


Figure 4.2. The effect of temperature on the size of the PNIPAM nanoparticles. The temperature leading to decrease in nanoparticle size is referred to as LCST and is comprised between 36 and 37°C. The diameter of the nanoparticles was analyzed by DLS as the average of 10 measurements.

4.4.2 Composite Hydrogels

The final formulation of the composite hydrogel consists of an EGMDA cross-linked PHEMA-based hydrogel containing 40% aqueous phase with dispersed nanoparticles and Xylene Cyanole FF, which was used as model drug. Figure 4.3 shows the dispersion of nanoparticles in hydrogels with different concentrations of nanoparticles. For the final formulation we had 5.5 mg nanoparticles per 1000 μL of reaction mixture.

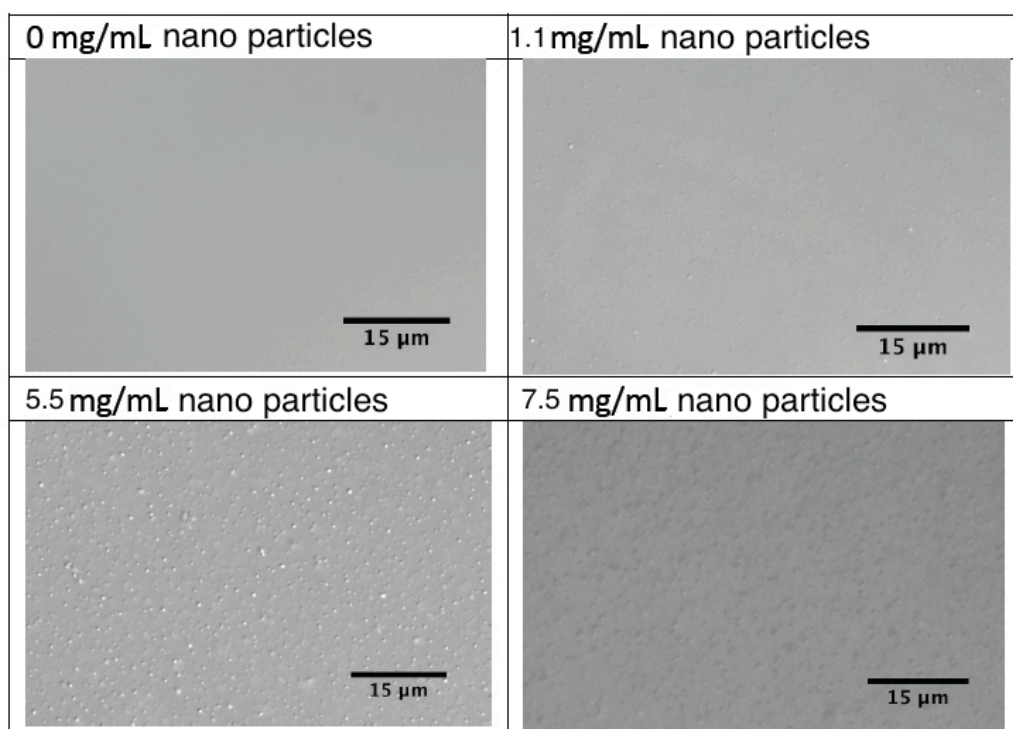


Figure 4.3. Light microscopy images of HEMA hydrogels with different concentrations of nanoparticles. The distribution of nanoparticles is shown for 0 mg/mL, 1.1 mg/mL, 5.5 mg/mL, and 7.5 mg/mL of nanoparticles concentration in the reaction mixture before polymerization. The 5.5 mg/mL nanoparticles concentration was used for the experiments.

4.4.3 Self-Heating of Hydrogels Due to Dissipation

The self-heating property of the composite hydrogels were investigated using a custom-designed thermally isolated system, which was coupled to a mechanical testing machine (Figure 1S, APPENDIX 7.2). To simulate human body environment, the initial temperature of the thermally isolated system was set to 36°C. It was verified that after 5 min of loading (5% of prestrain followed by a 15% deformation amplitude at 1.5 Hz) the temperature of the hydrogel reached

37°C (Figure 4.4A). In another experiment, we set the environment temperature to 34°C and after 5 min loading the temperature reached 34.7°C (Figure 4.4B).

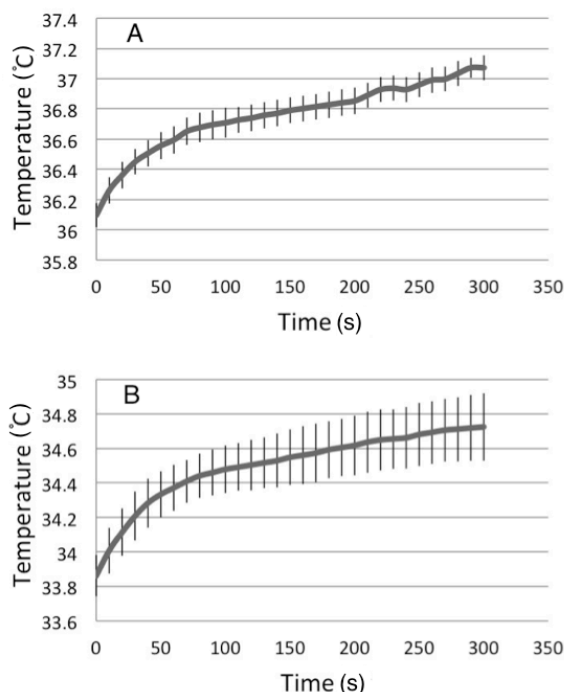


Figure 4.4. Self-heating of the hydrogel following cyclic compressive load. The initial temperature was set in the test chamber (Figure 1S, APPENDIX 7.2) and increased due to the dissipated heat. (A) The initial temperature was set to 36°C and increased to 37°C after 5 min of loading. (B) The initial temperature was set to 34°C and increase to 34.7°C after 5 min of loading.

4.4.4 Drug Release Due to Dissipation

Under mechanical loading, when environmental temperature was fixed to 36°C, a statistically significant increase (133%) in Xylene Cyanole FF release was observed between the 5 and 8 min loading demonstrating the delayed release of the dye following a mechanical loading (Figure 4.5A). To rule out the possibility that the mechanical loading directly induced the expulsion of the Xylene Cyanole FF out of the hydrogel, we repeated the experiment but setting the initial temperature of the thermally isolated system to 34°C. In this test, the temperature of the hydrogel following the mechanical stimulation stayed below the LCST of nanoparticles (Figure 4.4B). It can be observed from Figure 4.5A, that when the hydrogel temperature is below the LCST of nanoparticles, there was no significant difference in Xylene release between a 5 or a 8 min loading. Finally to confirm the role of the nanoparticles in the observed phenomenon and to exclude that the observed

effects were due to a direct thermal effect on the hydrogel, the tests at 34°C and 36°C were repeated with hydrogels that did not contain the thermosensitive nanoparticles. Results in Figure 4.5B showed that only the combination of nanoparticles in hydrogels and mechanical loading inducing a temperature increase of the hydrogel above 37°C allowed a statistical significant increase of the release of Xylene Cyanole FF.

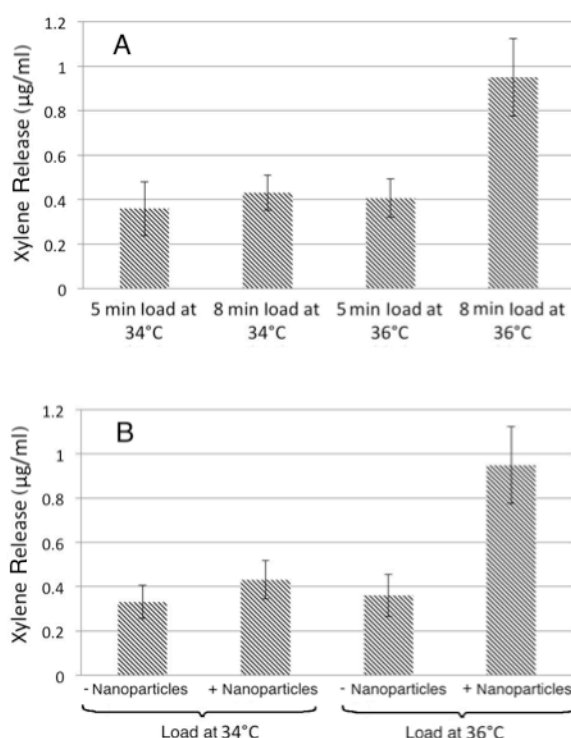


Figure 4.5. (A) Temporal control of Xylene Cyanole FF release triggered by dissipation properties of the composite hydrogel. The release of the Xylene Cyanole FF from hydrogels containing nanoparticles was quantified after 5 and 8 min of cyclic mechanical loading. When the initial temperature was set at 34°C, no statistical difference was observed for the Xylene release between 5 or 8 min. When the initial temperature was set to 36°C, a statistical significant increase (133%) in Xylene Cyanole FF release was measured between the 5 and 8 min loading ($p = 0.026$). **(B) Effect of nanoparticles on Xylene Cyanole FF release during mechanical loading.** Mechanical load was applied on hydrogels with and without nanoparticles for 8 min at the initial temperature of 34°C and 36°C. No statistical significant increase in Xylene release was observed at 36°C for hydrogels without nanoparticles. A statistical significant increase (125%) of dye release was measured when the load was applied on hydrogels containing nanoparticles and initially thermostated to 36°C ($p = 0.031$).

4.4.5 Effective Diffusion Coefficient

When nanoparticles are incorporated in the hydrogels and hydrogel temperature is above the LCST of the nanoparticles, the effective diffusivity of the hydrogel increases by a factor 3 (Figure

4.6). When the hydrogel contained no nanoparticles, the effective diffusivity of the hydrogel was not affected by the temperature increase.

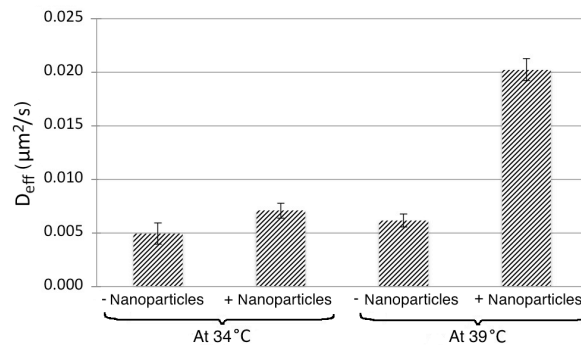


Figure 4.6. Effective diffusion coefficient (D_{eff}). D_{eff} was calculated by curve fitting of the mathematical model for Xylene Cyanole FF release from microfilm hydrogel with or without nanoparticles at temperature above and below the LCST of the nanoparticles.

4.5 Discussion

Mechanical loading has been demonstrated to activate growth factor receptors of cells involved in the healing process of different tissues (Discher et al., 2009, Neu et al., 2007). However, a delay is necessary for the activation of cell receptors following the initiation of a mechanical stimulation (Tschumperlin et al., 2004). A synergetic effect combining the delivery of a drug and the mechanically induced activation of the corresponding receptor could be maximized if drug release is delayed by several minutes following the initiation of the mechanical stimulation. In this study we proposed to use the dissipative property of a hydrogel as a new environmental variable allowing to spatially and temporally controlled the release of a drug. The proposed delivery system could then not only provide unparalleled spatiotemporal control over the release process, but also allows the delivery to be synchronized with the mechanical stimulus favoring the healing of the damaged tissue. The dissipative properties of the hydrogel can be modulated to link the duration of the cyclic loading with a targeted increase in temperature. Thus, a specific delay between the initiation of the mechanical stimulation and the release of a payload can be obtained.

The most probable effect which can explain the results presented in Figure 4.5A and 4.5B is to consider that the temperature-induced shrinkage of nanoparticles due to the dissipation properties of the hydrogel changed the permeability of the hydrogel. To verify this claim, the effective diffusion coefficient was calculated from Xylene Cyanole FF release experiments performed

on thin layer hydrogel film. The obtained result confirmed that the augmentation of the hydrogel temperature affects its permeability. By itself, the observation that a cyclic mechanical loading can affect its permeability is an original result not previously reported. As the change in permeability is obtained following the temperature increase, which in turn is due to the mechanical loading, a time delay is obtained between the initiation of the mechanical loading and the release of the payload. The value of this time delay can be tuned by varying the LCST of nanoparticles (Feil et al., 1993) and/or the dissipative properties of the hydrogel as well as the loading amplitude and frequency.

As previously mentioned, different systems have been developed to couple mechanical loading and drug release (Edelman et al., 1992, Korin et al., 2012, Lee et al., 2000). However, most of these systems could be considered as a sponge containing a payload so that no specific correlation between mechanical loading and drug release could be controlled. Another advantage of the proposed system is that it considerably reduced undesirable passive drug release. If we measure the amount of passive release over days from the composite hydrogel (Figure 3S, APPENDIX 7.2), we observe that after 5 days its value represents 9% of total loaded payload if the temperature is above the LCST and less than 4% of total loaded Xylene if the temperature is lower the LCST. In comparison, the release due to mechanical load was about 1.2% of total Xylene after 8 min. The reluctance of the system to passive release is most probably due to the hydrophobic properties of HEMA base hydrogels. In spite of hydrophilic nature of HEMA monomers, it is postulated that PHEMA hydrogel has, in addition to its covalently linked network structure, a secondary structure stabilized by hydrophobic bonding (Refojo, 1967). It has been showed that for a hydrophobic porous material, because of an defiltration (drainage) and infiltration pressure, force is required to move liquid in and out of the material pores (Zhao et al., 2009). Without mechanical loading the structure is reluctant to exchange fluid and facilitate the payload release. Therefore the amount of passive release is highly decreased with the developed composite hydrogel.

High dissipation properties of HEMA hydrogels also increase its toughness, which is important if the composite hydrogel is used at load bearing sites like in cartilage. In general because hydrogels have poor mechanical properties and are very brittle, their use is limited for load bearing applications. It has been shown that the poor mechanical performance and fragility of hydrogels mainly originate from their low resistance to crack propagation which is due to the lack of an efficient energy dissipation mechanism in the gel Structure (Abdurrahmanoglu et al., 2009, Tuncaboğlu et

al., 2011). The high dissipation property of the developed composite hydrogel is then a particular advantage also for its mechanical behavior.

4.6 Conclusion

Temporal control over the delivery process induced by a mechanical loading is proposed in this study and is an innovative way to deliver a payload. Dissipation properties of materials can be considered as a new environmental variable to trigger the release from thermosensitive, polymer based delivery systems. A synergetic effect between loading and delayed payload delivery could be obtained with the use of dissipative phenomenon, which is not possible with other delivery systems

4.7 Acknowledgments

This work was supported by the Swiss National Science Foundation (#406240_126070, PNR 62 program) and the Inter-Institutional Center for Translational Biomechanics EPFL-CHUV-DAL. We thank Marion Brun from the CHUV-Lausanne for the drawing of Figure 4.1A.

4.8 References

- Abdurrahmanoglu S, Can V, Okay O. 2009. Design of high-toughness polyacrylamide hydrogels by hydrophobic modification. *Polymer* 50, 5449-55.
- Ahearne M, Yang Y, El Haj AJ, Then KY, Liu KK. 2005. Characterizing the viscoelastic properties of thin hydrogel-based constructs for tissue engineering applications. *Journal of the Royal Society Interface* 2, 455-63.
- Baker MV, Brown DH, Casadio YS, Chirila TV. 2009. The preparation of poly(2-hydroxyethyl methacrylate) and poly {(2-hydroxyethyl methacrylate)-co-[poly(ethylene glycol) methyl ether methacrylate]} by photoinitiated polymerisation-induced phase separation in water. *Polymer* 50, 5918-27.
- Chirila TV. 2001. An overview of the development of artificial corneas with porous skirts and the use of PHEMA for such an application. *Biomaterials* 22, 3311-7.
- Discher DE, Mooney DJ, Zandstra PW. 2009. Growth factors, matrices, and forces combine and control stem cells. *Science* 324, 1673-7.
- Dziubla TD, Torjman MC, Joseph JJ, Murphy-Tatum M, Lowman AM. 2001. Evaluation of porous networks of poly(2-hydroxyethyl methacrylate) as interfacial drug delivery devices. *Biomaterials* 22, 2893-9.

-
- Edelman ER, Fiorino A, Grodzinsky A, Langer R. 1992. Mechanical deformation of polymer matrix controlled release devices modulates drug release. *Journal of Biomedical Materials Research* 26, 1619-31.
- Feil H, Bae YH, Feijen J, Kim SW. 1993. Effect of comonomer hydrophilicity and ionization on the lower critical solution temperature of N-isopropylacrylamide copolymers. *Macromolecules* 26, 2496-500.
- Gil ES, Hudson SM. 2004. Stimuli-responsive polymers and their bioconjugates. *Progress in Polymer Science* 29, 1173-222.
- Gong C, Qi T, Wei X, Qu Y, Wu Q, Luo F, Qian Z. 2013. Thermosensitive polymeric hydrogels as drug delivery systems. *Current Medicinal Chemistry* 20, 79-94.
- Gupta P, Vermani K, Garg S. 2002. Hydrogels: from controlled release to pH-responsive drug delivery. *Drug Discovery Today* 7, 569-79.
- Hiyama A, Mochida J, Iwashina T, Omi H, Watanabe T, Serigano K, Iwabuchi S, Sakai D. 2007. Synergistic effect of low-intensity pulsed ultrasound on growth factor stimulation of nucleus pulposus cells. *Journal of Orthopedic Research* 25, 1574-81.
- Hoare T, Santamaria J, Goya GF, Irusta S, Lin D, Lau S, Padera R, Langer R, Kohane DS. 2009. A magnetically triggered composite membrane for on-demand drug delivery. *Nano Letters* 9, 3651-7.
- Jeong B, Kim SW, Bae YH. 2002. Thermosensitive sol-gel reversible hydrogels. *Advanced Drug Delivery Reviews* 54, 37-51.
- Karnaikhov VG, Yakovlev GA, Goncharov LP. 1975. Self-heating of viscoelastic materials under cyclic loads. *Strength of Materials* 7, 164-8.
- Klouda L, Mikos AG. 2008. Thermoresponsive hydrogels in biomedical applications. *European Journal of Pharmaceutics and Biopharmaceutics* 68, 34-45.
- Korin N, Kanapathipillai M, Matthews BD, Crescente M, Brill A, Mammoto T, Ghosh K, Jurek S, Bencherif SA, Bhatta D. 2012. Shear-activated nanotherapeutics for drug targeting to obstructed blood vessels. *Science* 337, 738-42.
- Lai YC, Quinn ET. 1997. The effects of initiator and diluent on the photopolymerization of 2-hydroxyethyl methacrylate and on properties of hydrogels obtained. *Photopolymerization* 673, 35-50.
- Lee KY, Peters MC, Anderson KW, Mooney DJ. 2000. Controlled growth factor release from synthetic extracellular matrices. *Nature* 408, 998-1000.
- Mabilleau G, Stancu IC, Honore T, Legeay G, Cincu C, Basle MF, Chappard D. 2006. Effects of the length of crosslink chain on poly(2-hydroxyethyl methacrylate) (pHEMA) swelling and biomechanical properties. *Journal of Biomedical Materials Research Part A* 77, 35-42.
- Mauck RL, Nicoll SB, Seyhan SL, Ateshian GA, Hung CT. 2003. Synergistic action of growth factors and dynamic loading for articular cartilage tissue engineering. *Tissue Engineering* 9, 597-611.

-
- Neu CP, Khalafi A, Komvopoulos K, Schmid TM, Reddi AH. 2007. Mechanotransduction of bovine articular cartilage superficial zone protein by transforming growth factor β signaling. *Arthritis & Rheumatism* 56, 3706-14.
- Qiu Y, Park K. 2012. Environment-sensitive hydrogels for drug delivery. *Advanced Drug Delivery Reviews* 64, 49-60.
- Quinn TM, Kocian P, Meister J-J. 2000. Static compression is associated with decreased diffusivity of dextrans in cartilage explants. *Archives of Biochemistry and Biophysics* 384, 327-34.
- Refojo MF. 1967. Hydrophobic interaction in poly(2-hydroxyethyl methacrylate) homogeneous hydrogel. *Journal of Polymer Science Part A-1: Polymer Chemistry* 5, 3103-13.
- Schapery RA. 1964. Effect of cyclic loading on the temperature in viscoelastic media with variable properties. *Aiaa Journal* 2, 827-35.
- Schmaljohann D. 2006. Thermo- and pH-responsive polymers in drug delivery. *Advanced Drug Delivery Reviews* 58, 1655-70.
- Tschumperlin DJ, Dai G, Maly IV, Kikuchi T, Laiho LH, McVittie AK, Haley KJ, Lilly CM, So PT, Lauffenburger DA, Kamm RD, Drazen JM. 2004. Mechanotransduction through growth-factor shedding into the extracellular space. *Nature* 429, 83-6.
- Tuncaboylu DC, Sari M, Oppermann W, Okay O. 2011. Tough and self-healing hydrogels formed via hydrophobic interactions. *Macromolecules* 44, 4997-5005.
- Yavuz MS, Cheng YY, Chen JY, Cogley CM, Zhang Q, Rycenga M, Xie JW, Kim C, Song KH, Schwartz AG, Wang LHV, Xia YN. 2009. Gold nanocages covered by smart polymers for controlled release with near-infrared light. *Nature Materials* 8, 935-9.
- Yu L, Ding JD. 2008. Injectable hydrogels as unique biomedical materials. *Chemical Society Reviews* 37, 1473-81.
- Zhang J, Misra RDK. 2007. Magnetic drug-targeting carrier encapsulated with thermosensitive smart polymer: Core-shell nanoparticle carrier and drug release response. *Acta Biomaterialia* 3, 838-50.
- Zhao J, Culligan PJ, Germaine JT, Chen X. 2009. Experimental study on energy dissipation of electrolytes in nanopores. *Langmuir* 25, 12687-96.

Chapter 5

Improving Self-Heating Hydrogels for Clinical Application

Paper: Biodegradable HEMA-Based Hydrogels with Enhanced Mechanical
Properties^{*}

^{*} This chapter is submitted to the "Acta Biomaterialia" Journal.

5.1 Abstract

Hydrogels are widely used in the biomedical field. Their main purposes are either to deliver biological active agents or more recently to temporarily fill a defect until they degrade and are followed by new host tissue formation. However for this latter application, biodegradable hydrogels are usually not capable to sustain any significant load. The development of biodegradable hydrogels presenting load-bearing capabilities would open new possibilities to utilize this class of material in the biomedical field. In this work, an original formulation of biodegradable photo-crosslinked hydrogels based on hydroxyethyl methacrylate (HEMA) is presented. The hydrogels consist of short-length PHEMA chains in a star shape structure, obtained by introducing a tetra-functional chain transfer agent in the backbone of the hydrogels. They are cross-linked with a biodegradable N,O-dimethacryloyl hydroxylamine (DMHA) molecule sensitive to hydrolytic cleavage. We characterized the degradation properties of these hydrogels submitted to mechanical loadings. We showed that the developed hydrogels undergo long-term degradation and specially meet the two essential requirements of a biodegradable hydrogel suitable for load bearing applications: mechanical strength and low molecular weight degradation products.

Keywords: HEMA-based hydrogels, biodegradable hydrogels, mechanical strength

5.2 Introduction

Hydrogels are widely used in biomedical applications either as vehicles to deliver a biological agent or as scaffolds to fill a defect. In particular, the biodegradable version of hydrogels is of great interest since upon their degradation, formation of neo-tissues can be obtained in the defect (Drury and Mooney, 2003, Kamath and Park, 1993, Peppas et al., 2006). However, due to the weak mechanical properties of biodegradable hydrogels, their application is very limited in tissues functioning under load situations (Moffat and Marra, 2004, Van Dijk-Wolthuis et al., 1997, Gunatillake and Adhikari, 2003). Therefore, there is a clear need for developing biodegradable hydrogels with an enhanced load bearing capability.

Biodegradable hydrogels may be produced based on the cleavage of hydrolytically or enzymatically labile bonds (Atzet et al., 2008, Gunatillake and Adhikari, 2003, Moffat and Marra, 2004, van Dijk-Wolthuis et al., 1997) or dissolution of physical cross-links formed via hydrophobic, electrostatic, or hydrogen-bonding forces (Bae et al., 2013, De Jong et al., 2001). Due to these weak cross-linking mechanisms, most of the developed biodegradable hydrogels exhibit poor mechanical properties (Hennink and Van Nostrum, 2012, Sun et al., 2012). In contrast, synthetic chemically cross-linked hydrogels with strong covalent bonds present an enhanced mechanical strength (Anseth et al., 1996, Hennink and Van Nostrum, 2012, Naficy et al., 2011). However the strong covalent bonds limit the degradation of these hydrogels (Anseth et al., 1996, Hennink and Van Nostrum, 2012).

In order to develop a hydrogel with simultaneously strong mechanical properties and degradation capabilities, we focused our attention on methacrylate polymers such as poly(2-hydroxyethyl methacrylate) (HEMA). Hydrogels made of these polymers were shown to be biocompatible, to have tunable mechanical properties, and they can be fabricated in different architectures (Baker et al., 2009, Homsy, 1970, Peppas et al., 1985). We recently showed that HEMA-based hydrogels present very high load tolerance and especially resistance to crack propagation when we increased their dissipation properties (Chapter 3). However, because of its high biostability (Peppas et al., 1985), PHEMA has not been successfully used as a biodegradable hydrogel yet, despite several studies have focused on this aspect (Atzet et al., 2008, Baker et al., 2009, Bayramoğlu and Arica, 2003, Cadee et al., 1999, Casadio et al., 2010, Verestiuc et al., 2006). Although some of the proposed structures presented degradation capabilities to some extent, the resulting hydrogels had

two major deficiencies. First, as expected they showed very poor mechanical properties due to the structure of the cross-linker used (Hennink and Van Nostrum, 2012, Verestiuc et al., 2006) or to the mechanism of cross-linking (Han et al., 2008, Ng and Swami, 2005). Second, their degradation products consisted of very long PHEMA chains (Atzet et al., 2008). Indeed, the structure of HEMA-based hydrogels is composed of long PHEMA chains interconnected with cross-linker molecules. It has been reported that under physiological conditions, PHEMA can be hydrolyzed to poly(Methyl Methacrylate) (Chiellini et al., 2002). However, if the degradation occurs just via dissolution of the cross-linkers, the resulting degradation product consists of very long chains of coiled PHEMA fragments, which cannot be cleared out of the body (Atzet et al., 2008, Huang et al., 2013, Jiang et al., 2007).

To overcome these two drawbacks, we developed an original formulation of biodegradable HEMA-based hydrogels, which present enhanced mechanical properties and degradation products with low molecular weight. These hydrogels were developed based on HEMA cross-linked with a short hydrolysable molecule N,O-dimethacryloyl hydroxylamine (DMHA) and employing a tetra-functional chain transfer agent in the backbone of these hydrogels. DMHA provides high initial mechanical properties and the tetra-functional molecule breaks down the PHEMA long backbone chains to small star-like molecules.

5.3 Materials and Methods

5.3.1 Materials

All materials were purchased from Aldrich (Bucks, Switzerland) and were stored at 4°C until use unless otherwise specified. Hydroxylamine hydrochloride, methacryloyl chloride (-20°C), pyridine, chloroform, and hydrochloric acid were all used for synthesizing N,O-dimethacryloyl hydroxylamine. 2-2-hydroxyethyl methacrylate (HEMA, 97%) was purified using basic aluminum oxide column chromatography to remove inhibitors. 2,2-dimethoxy-2-phenylacetophenone (DPAP) (Irgacure-651, 99%) was used as photo initiator and prepared as an ethanolic solution of DPAP (57 mg/ml solution, each ml = 0.2 mM). Pentaerythritol tetrakis(3-mercaptopropionate) was used as received.

Cell culture media contained 10 ml Dulbecco's Modified Eagle Medium (DMEM) with 25 mM dextrose and 1 mM sodium pyruvate (Life Technologies Ltd, Paisley, UK), 5.97 mM L-Glutamine (Life

Technologies Ltd), 10% fetal bovine serum (Sigma, St. Louis, MO, USA). Giemsa's azur eosin methylene blue solution for microscopy (Merck, Darmstadt, Germany) and CellTiter (G3580 Promega, Fitchburg, WI, USA) were used for the cell study.

5.3.2 DMHA Synthesis

N,O-Dimethacryloyl hydroxylamine (DMHA) was synthesized following a slightly modified protocol initially proposed by South *et al.* (South and Lyon, 2010). Ten grams of hydroxylamine hydrochloride (0.145 mol) was added in a 500 ml round-bottom flask and put under N₂ gas for approximately 30 min to remove moisture. Fifty ml pyridine was added by syringe and stirred with the hydroxylamine hydrochloride until complete dissolution. The solution was maintained under N₂ and in an ice bath to keep the temperature of the reaction mixture below 20°C. Methacryloyl chloride, 29 ml (0.3 mol), was added dropwise. We reduced the system's exposure to light as much as possible by covering the flask with an aluminum foil. The reaction was then stirred for an additional 5 hours. After complete conversion, 100 ml of chloroform was added, and the solution became a transparent yellow-brown liquid. Afterward, 100 ml of hydrochloric acid (1.5 molar) was added dropwise, while the solution was maintained in the ice bath and under aluminum foil. The mixture turned turbid. The solution was poured into a separatory funnel and was washed with 100 ml of deionized water until the aqueous layer became clear (four washes). The organic layer was then dried over magnesium sulfate and filtered. We removed chloroform by rotary evaporation in a dark 200 ml round bottom flask and then, the yellow oily product was dried overnight on a Schlenk line. The product was a yellow highly viscous liquid. Experimental yield was approximately 30%. The chemical composition of DMHA was verified with ¹H NMR using a Varian Unity 300 MHz NMR spectrometer (Fitchburg, MI, USA). For ¹H NMR test, sample (10 µl) was dissolved in DMSO-d₆. The following chemical shifts (δ) were observed in NMR signal: 1.83 [s, 3H, N-CO-C(CH₃)=CH₂], 1.97 [s, 3H, -CO-C(CH₃)=CH₂], 5.48, 5.73 [s, 2H, -N-CO-C(CH₃)=CH₂], 5.85, 6.28 [s, 2H, -O-CO-C(CH₃)=CH₂].

5.3.3 Hydrogels Synthesis

PHEMA hydrogels were prepared with N,O-dimethacryloyl hydroxylamine (DMHA) as cross-linker (1% and 10% of mol) and water (65% and 40% of total mixture volume). In another group of hydrogels we added a four functional group molecule, pentaerythritol tetrakis(3-mercaptopropionate) (0.25% of mol). The term "Tetrakis" will be used for this material in the fol-

lowing sections. Material compositions for all four groups of samples are summarized in Table 5.1 (S1, S2, S3 and S4). The mixture containing the photo initiator DPAP (0.1% of mol) was stirred and sonicated for 1 min. It was then transferred to cylindrical wells (6 mm diameter and 3 mm depth), placed under UV lamp (365 nm, 8 watt) (Upland, CA, USA) positioned 10 cm from the samples and irradiated for 15 min. The system was maintained below 25°C during polymerization by air circulation. Hydrogels were then carefully removed from the wells, washed to remove unreacted materials, and immersed in water for one week. Figure 5.1 shows the expected structure of the hydrogels with and without Tetrakis. In the presence of Tetrakis, hydrogels should have a star structure in which four short PHEMA chains are linked by ester bonds to a tetra-functional Tetrakis molecule. The branches of HEMA in the ideal case contain an average number of units equal to $1/(\text{number of SH groups} \times \text{Tetrakis to HEMA molar ratio})$. The number of SH groups on each Tetrakis is four (Chiellini et al., 2002). The PHEMA branches are connected together with DMHA cross-linkers. Without Tetrakis hydrogels contain long chains of HEMA molecules coiled together and cross-linked with DMHA.

Table 5.1. Hydrogel composition.

Sample Name	HEMA (% mol)	DMHA (% mol)	Tetrakis (% mol)	Water (% total volume)
S1	100	10	0	40
S2	100	10	0.25	40
S3	100	1	0	65
S4	100	1	0.25	65

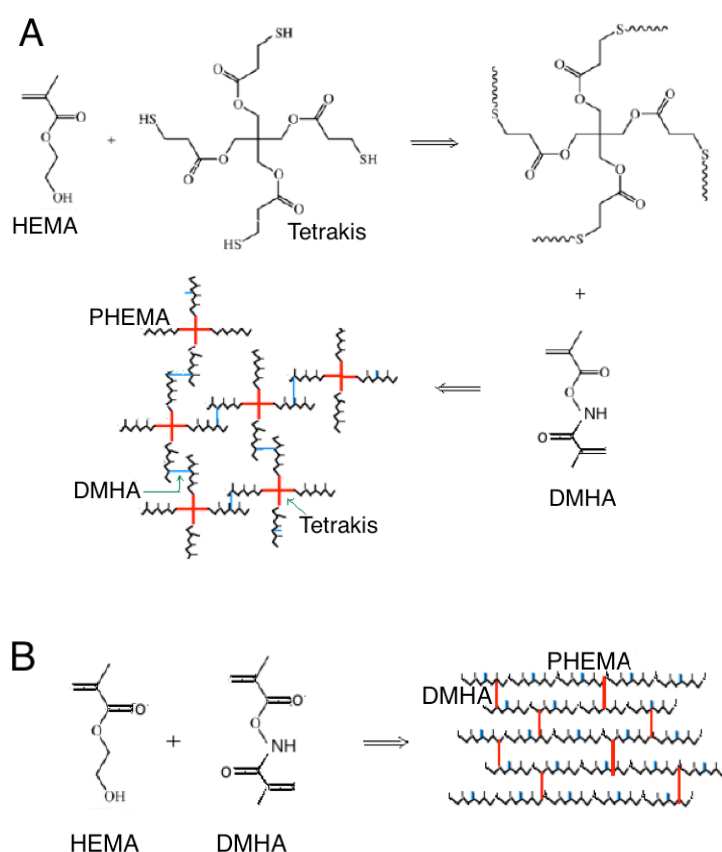


Figure 5.1. Structure of HEMA hydrogels. (A) HEMA-DMHA-Tetrakis hydrogels. In the presence of Tetrakis, hydrogels should have a star structure in which four short PHEMA chains are linked to a Tetrakis molecule. The PHEMA branches are connected together with DMHA cross-linkers. **(B) HEMA-DMHA hydrogels.** Without Tetrakis, hydrogels contain long chains of HEMA molecules cross-linked with DMHA.

5.3.4 Swelling and Mechanical Evaluation of Hydrogels

We studied the swelling behavior of hydrogels by measuring the equilibrium water content at swollen state after one week of swelling in PBS. We prepared six samples for each of the four hydrogel groups. The equilibrium water content was measured as the ratio of the swelling weight of the hydrogels minus their dried weight, over their dried weight. To dry hydrogels, each sample was first flash frozen in liquid nitrogen and then dried under vacuum (Dynavac FD2, Boronia, Australia) over 3 days. We also measured the initial water content as the ratio of the hydrogels' weight immediately after polymerization minus the dried weight, over the dried weight.

The elastic and viscous properties of the swollen samples were characterized by measuring the elastic modulus and the damping ratio of the hydrogels. For the elastic modulus, a single compressive load up to 10% deformation at the rate of 1% per second was applied with an Instron E3000

linear mechanical testing machine (Instron, Norwood, MA, USA). In this range of deformation, each hydrogel had a linear stress-strain curve. The elastic modulus was calculated from the slope of the stress-strain curve of each sample. For quantifying the damping ratio, cyclic compression test at 1 Hz and 15% deformation amplitude was applied on samples for 60 seconds with the Instron machine. The damping ratio was calculated as the ratio of the dissipated work (the area of the hysteresis curve in the force-displacement graph) over the total input work given to the material (the area under the compression curve in the force-displacement graph) during one cyclic deformation (Vogel and Pioletti, 2011). We considered the mean value of damping ratio for the last ten cycles.

5.3.5 Accelerated Degradation Study

It has been shown that basic environment expedites the hydrolysis of DMHA (Ulbrich et al., 1993). In order to compare the degradation capacity of the produced hydrogels and evaluate the effect of different parameters like the cross-linker ratio, water content, and the presence of the Tetrakis molecules, we measured the mass lost of thin films of hydrogels during 30 days, when they were incubated in highly basic environment. The hydrogel thin films were prepared by cutting the hydrogel samples from each group of S1, S2, S3 and S4 with a Vibratome machine (Leica VT1200S, Muttentz, Switzerland) in 300 μ m films (4 mm \times 8 mm). Prior to the degradation test, the initial (time zero) dry mass was measured after drying the samples. Then they were moved to multi-plates containers and 3 ml of NaOH 0.01 molar (pH = 12.3) was added to each sample and incubated at 37°C. The NaOH was changed every week. At days 2, 4, 7, 14, and 28, we took four samples per each hydrogel group, dried and weighed them with the same procedure as for time zero.

5.3.6 Mechanical Stiffness and Weight Lost of Hydrogels Under Cyclic Loading

Since we developed these HEMA-based hydrogels for load bearing applications, in order to study the degradation in this situation, we evaluated the mechanical stiffness and weight lost of hydrogels under cyclic loading. We considered two groups of hydrogels. In the first group, a 1000 cyclic compression load was applied every week while no load was applied in the second group. The cyclic compression consisted of a 15% deformation amplitude at 1 Hz. We used a multi-piston set up, previously designed in our group (Abdel-Sayed et al., 2014) to be able to apply load simultaneously on multiple samples. In both groups, hydrogels were incubated at 37°C and immersed in 3 ml PBS

(pH = 7.4). We changed the PBS every 2 weeks. We monitored the elastic modulus (six samples for each of the four hydrogel groups) and weight lost (four samples for each of the four hydrogel groups) every month during nine months following the same procedures as described under the sections 2.4.

5.3.7 Molecular Weight of Degradation Products

We extracted the degradation products from the PBS media in which the samples were incubated during the degradation study made under the mechanical loading (section 2.6). PBS was collected from each of the four hydrogel groups every month after four months of starting the degradation study and was freeze-dried. After freeze-drying, we obtained the degradation products as white powders. The powders were analyzed with Gel Permeation Chromatography (GPC) facility (GPC 50 Agilent, Santa Clara, CA, USA) to quantify the molecular weight of the degradation products (Gellerstedt, 1992, Striegel et al., 2009). The Eluent for GPC consisted of Milli-Q water and 10% MeOH. A conventional calibration was performed with RI (Nicolet Magna-ir 560, Ontario, Canada) and viscometer (Alpha L, Barcelona, Spain). The standards range was 1010 to 278100 Da.

5.3.8 Structure of Hydrogels Obtained by SEM

The structure of the hydrogels was obtained using a Scanning Electron Microscope (SEM). Cross-sections of the hydrogels were obtained by cracking frozen gels. We prepared a set of swollen new samples of S1, S2, S3 and S4 and a set of samples partially degraded after six months under weekly cyclic loading. Samples were dried by freeze-drying, stuck on SEM pads and were imaged using an electron microscope (Zeiss Merlin, Oberkochen, Germany) at an accelerating voltage of 0.8 kV and 2.5 Kx magnification, with an aperture of 5 mm and working distance of 6 mm.

5.3.9 Biocompatibility of Hydrogels and Degradation Products

The biocompatibility of the developed hydrogels was evaluated by a direct contact test. Cylindrical hydrogels (three samples for each of the four hydrogel groups) were placed separately in the middle of a 60 mm diameter petri dish and primary human chondrocyte cells isolated and characterized in our group (Darwiche et al., 2012) were seeded around the samples (3000 cell/cm²). Five ml of cell culture medium was added to each petri dish. After one week, cells were fixed by adding 1 ml methanol to each plate for 30 seconds following by 1 ml diluted Giemsa solution to color the

cells. Microscopy was performed in order to visualize fixed, colored cells (ZEISS Axiovert 100, Germany).

In a second test, we evaluated the cytotoxicity of the degradation products. The degradation products were collected at random time points from HEMA-DMHA hydrogels (S1 and S3) or HEMA-DMHA-Tetrakis hydrogels (S2 and S4) obtained in section 2.7. Different concentrations of degradation products (0 mg/ml, 0.1 mg/ml, 0.5 mg/ml, 3 mg/ml) were added in the cell culture medium. The cells' proliferation exposed to the different concentrations was evaluated using a CellTiter assay following the standard manufacturer protocol (CellTiter 96® Aqueous, Promega, Fitchburg, WI, USA) and an absorbance reading at 490 nm with a spectrophotometer (Wallac Victor2, 1420, Turku, Finland). The CellTiter assay was performed every day for three days.

5.3.10 Statistical Test

We used an ANOVA test to determine if a significant difference (p -value < 0.05) is present between each of the four hydrogel groups regarding different parameters like cross-linker, water ratio, presence of Tetrakis, and weekly mechanical load. In conjunction with ANOVA we did a Tukey-Kramer post-hoc test to find means that are significantly different from each other.

5.4 Results

5.4.1 Swelling and Mechanical Evaluation of Hydrogels

The equilibrium and initial water contents of the hydrogels are reported in Table 5.2. There was a significant difference between the equilibrium and initial water contents in each group of hydrogels ($p < 0.001$). However, the hydrogels with 1% cross-linker and 65% water ratios (S3 and S4) had higher water content at the equilibrium state compared to the hydrogels with 10% cross-linker and 40% water (S1 and S2) ($p < 0.001$). This confirms that decreasing the amount of cross-linker and increasing the water ratio increase the swelling of the hydrogels. The hydrogels containing Tetrakis (S2 and S4) had slightly higher equilibrium water content compared to the hydrogels without Tetrakis (S1 and S3) ($p < 0.04$). However, the effect of the cross-linker and the water ratios on the swelling of the hydrogels was more significant than the effect of Tetrakis ($p < 0.001$).

Mechanical characterization of the hydrogels highlights that the stiffness highly depends on cross-linker and water ratios. Figure 5.2A shows that the elastic modulus was 10 times lower in hydro-

gels with less cross-linker and more water ratios (S1: 2.5 ± 0.21 MPa vs S3: 0.23 ± 0.019 MPa) ($p < 0.001$). The addition of Tetrakis decreased the elastic modulus of the hydrogels to more than half of its original value (S2: 0.85 ± 0.026 MPa vs S1: 2.5 ± 0.21 MPa and S4: 0.094 ± 0.009 MPa vs S3: 0.23 ± 0.019 MPa) ($p < 0.001$). However, all hydrogels showed high viscous properties (damping ratio greater than 0.6, Figure 5.2B). While the addition of Tetrakis slightly increased the damping ratio, there was no significant difference between the damping ratios of the different groups ($p > 0.3$).

Table 5.2. Initial and equilibrium water contents. Significant differences were observed between the equilibrium and the initial water contents in each group ($p < 0.001$). The addition of Tetrakis, a decrease in cross-linker ratio or an increase in water ratio significantly increased the equilibrium water content ($p < 0.04$).

Hydrogel Type	Equilibrium Water Content (%)	Initial Water Content (%)
S1	51.51 ± 1.97	41.39 ± 2.03
S2	59.66 ± 8.99	39.57 ± 1.32
S3	133.20 ± 7.32	63.07 ± 4.34
S4	149.36 ± 11.37	59.25 ± 5.45

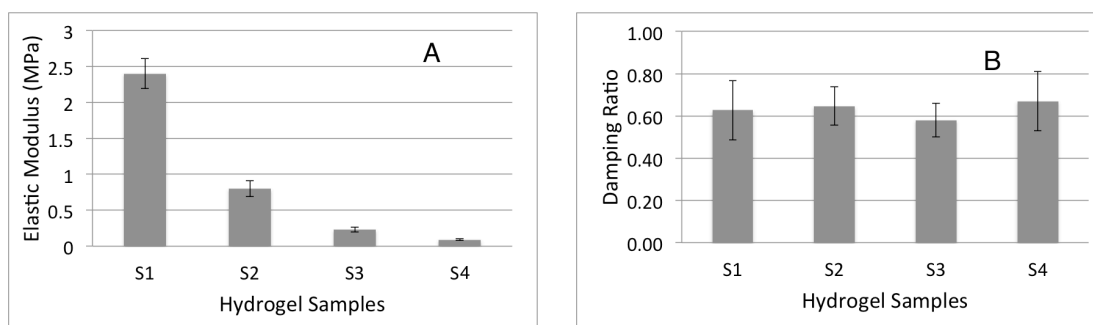


Figure 5.2. (A) The elastic modulus of the four groups of hydrogels. Hydrogels with 1% cross-linker ratio and 65% water content (S3 and S4) had smaller elastic modulus than the ones with 10% cross-linker ratio and 40% water content (S1 and S2) ($p < 0.001$). Hydrogels containing Tetrakis (S2 and S4) had lower elastic modulus compared to those without Tetrakis (S1 and S3) ($p < 0.001$). (B) The damping ratios of the four groups of hydrogels. There was no significant difference between the damping ratios of the different groups ($p > 0.3$).

5.4.2 Accelerated Degradation Study

Figure 5.3 shows the weight lost by the hydrogel films incubated in NaOH 0.01 molar ($pH = 12.3$) over four weeks. Based on our results, adding Tetrakis significantly increased the amount of weight lost at each time point ($p < 0.001$). Also, the weight lost by hydrogels with 1% cross-linker

and 65% water ratios (S3 and S4) was higher than the other two groups (S1 and S2) ($p < 0.001$). However, the effect of adding Tetrakis was more significant than the effect of cross-linker and water ratios on the weight lost ($p < 0.001$). Hydrogels containing Tetrakis, 1% cross-linker and 65% water (S4) completely degraded in one week.

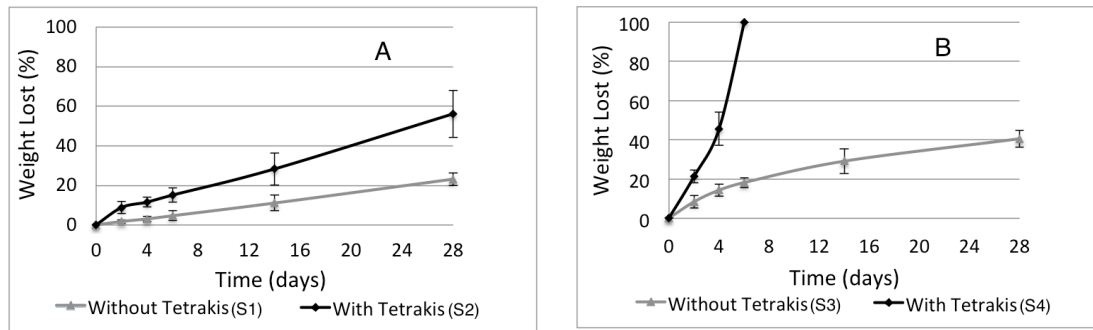


Figure 5.3. The amount of weight lost by hydrogels in an accelerated degradation study. (A) Hydrogels with 10% cross-linker ratio and 40% water content (S1 and S2), (B) Hydrogels with 1% cross-linker ratio and 65% water content (S3 and S4). The addition of Tetrakis significantly increased the amount of weight lost at each time point ($p < 0.001$). Hydrogels with a lower cross-linker ratio and a higher water content (S3 and S4) lost weight faster than the other groups (S1 and S2) ($p < 0.001$). Hydrogels in group S4 completely degraded after one week.

5.4.3 Mechanical Stiffness and Weight Lost by Hydrogels under Cyclic Loading

Figure 5.4 shows the changes in the elastic modulus of all hydrogel groups (S1, S2, S3, and S4) over nine months degradation in PBS, with or without weekly cyclic mechanical loading. The elastic modulus decreased over time, in some cases, by more than 90%. For each group, applying a mechanical load induced a significant decrease in the elastic modulus value at each time point ($p < 0.001$). However, changing the cross-linker and water ratios and adding Tetrakis had no significant influence on the final percentage of elastic modulus lost after nine months ($p > 0.1$). Furthermore, we observed that the rate of loss of elastic modulus (the slope of the curve) was higher during the first two months of degradation for all hydrogels.

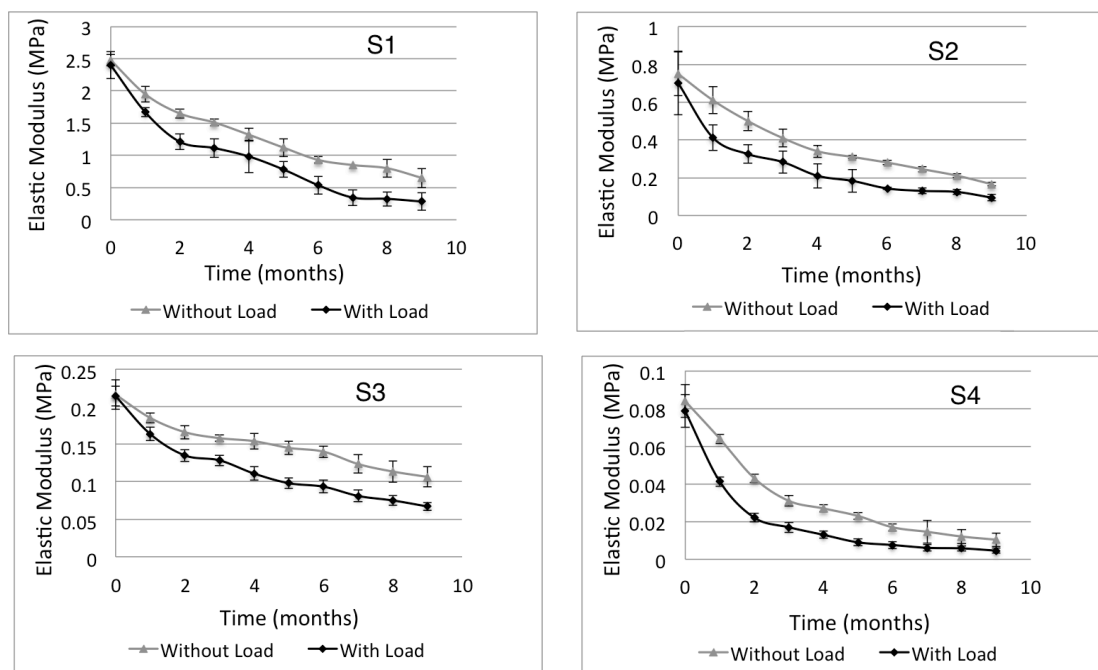


Figure 5.4. Evolution of the elastic modulus of the hydrogels (S1, S2, S3, and S4) during degradation in PBS, with and without applying weekly cyclic loading. For each group, applying a mechanical load induced a decrease in the elastic modulus value at each time point ($p < 0.001$). Changing the cross-linker and water ratios and adding Tetrakis had no significant influence on the final percentage of elastic modulus lost after nine months ($p > 0.1$). The final percentage of elastic modulus lost after nine months was S1: $88.23 \pm 7.54\%$, S2: $86.57 \pm 5.35\%$, S3: $78.96 \pm 8.32\%$ and S4: $94.15 \pm 8.76\%$.

In Figure 5.5, the weight lost by all hydrogel groups during the nine months of degradation, with or without weekly cyclic loading, is reported. For hydrogels S1, S2, and S4, applying mechanical load resulted to a significant increase in the amount of weight lost at each time point ($p < 0.001$). However for the group S3, this effect was observed only after five months. The addition of Tetrakis significantly increased the amount of weight lost in all hydrogel groups over the entire degradation period ($p < 0.001$). A correlation was found between applying mechanical loading and adding Tetrakis ($p < 0.01$), suggesting that having both parameters highly increases the degradation. However, from our results, the effect of cross-linker and water ratios on the amount of weight lost was not clear. While for hydrogels containing Tetrakis the amount of weight lost after nine months was greater for hydrogels with 1% cross-linker ratio and 65% water content (S4) compared to hydrogels with 10% cross-linker ratio and 40% water content (S2), we observed an opposite phenomenon in hydrogels without Tetrakis (S3 and S1). Furthermore, we observed that for hydrogels containing Tetrakis the slope of the weight lost curves increased in the later months of degradation, while for the hydrogels without Tetrakis the slope of the curves decreased. This suggests that

the degradation of hydrogels containing Tetrakis increases in the later months, while this is less likely to happen in hydrogels without Tetrakis.

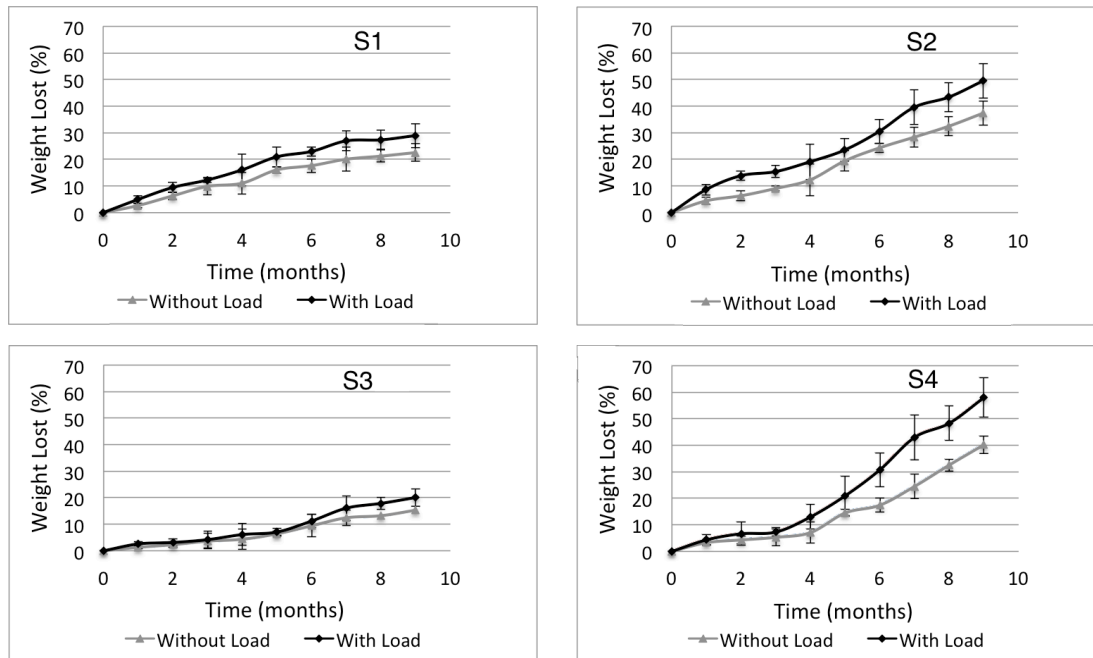


Figure 5.5. The amount of weight lost by the hydrogels (S1, S2, S3, and S4) during degradation in PBS, with and without applying weekly cyclic loading. For each group, applying a mechanical load increased the amount of weight lost at each time point ($p < 0.001$) except the first 5 months of the group S3. Also, the groups with Tetrakis (S2 and S4) showed a greater weight lost compared to the groups without Tetrakis (S1 and S3) ($p < 0.001$). Changing the cross-linker and water ratios had no significant influence on the amount of weight lost ($p > 0.5$).

5.4.4 Molecular Weight of Degradation Products

The results of GPC test showed that there was no significant difference in the molecular weight of degradation products between the hydrogels with 10% cross-linker (S1 and S2) and those with 1% cross-linker ratio (S3 and S4) ($p > 0.5$). Therefore, we considered highly cross-linked and little cross-linked groups together and we only separated groups by whether or not they contained Tetrakis. All the samples without Tetrakis had a peak in the GPC graph ranging between 7000 and 9000 kDa (7668 ± 816 kDa). However two samples had also a second peak, one at 4683 kDa, and the other at 2966 kDa. For samples with Tetrakis we detected two peaks for all samples, one peak between 4500 and 7500 kDa (6096 ± 1544 kDa), and another peak between 2500 and 3200 kDa (2820 ± 351 kDa).

5.4.5 Structure of Hydrogels Obtained by SEM

The morphology and porosity of the hydrogels were examined by SEM (Figure 5.6). We could not observe the porous structure of highly cross-linked hydrogels (S1 and S2) since the structure was too dense to be observed with SEM at the voltage of 0.8 kV and increasing the voltage ruined the samples. In contrast, we were able to see the porous structure of hydrogels with 1% cross-linker and 65% water containing or not Tetrakis (S3 and S4). As Figure 5.6 shows, in the presence of Tetrakis, the hydrogel has larger and rounder pores, which seem to be less interconnected to each other (Figure 5.6A and 5.6B). We also examined these hydrogels after six months of degradation under weekly cyclic load. The structure of the partly degraded hydrogels was highly porous and interestingly we could visually detect the particles of the degradation product on the wall of the pores (Figure 5.6C and 5.6D).

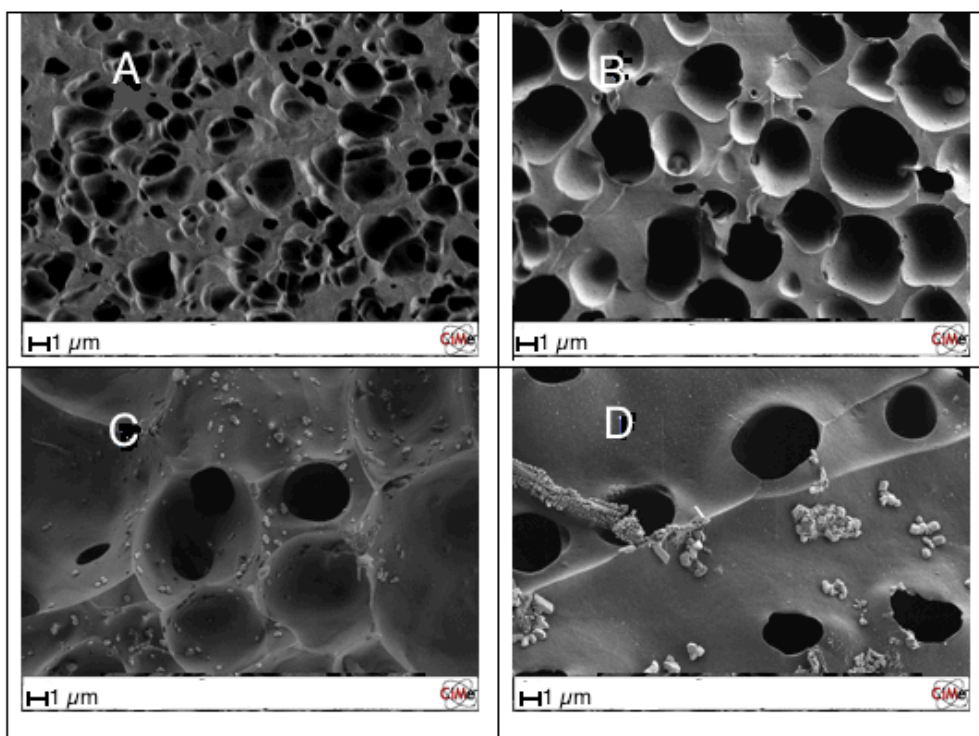


Figure 5.6. Scanning Electron Microscopy pictures of the hydrogels. (A) S3 at zero time point. (B) S4 at zero time point. (C) S3 after six months of degradation under cyclic loading. (D) S4 after six months of degradation under cyclic loading.

5.4.6 Biocompatibility of Hydrogels and Degradation Products

The morphology and proliferation of the cells in contact with the hydrogel samples were similar to those seeded on standard cell culture plates. Figure 5.7 shows a typical Giemsa staining for hydrogel S2. The microscopic picture of the colored cells demonstrated that their density and shape in contact with the hydrogel (Zone 1) were similar to the areas far from the hydrogel (Zone 2) on the cell culture plate.

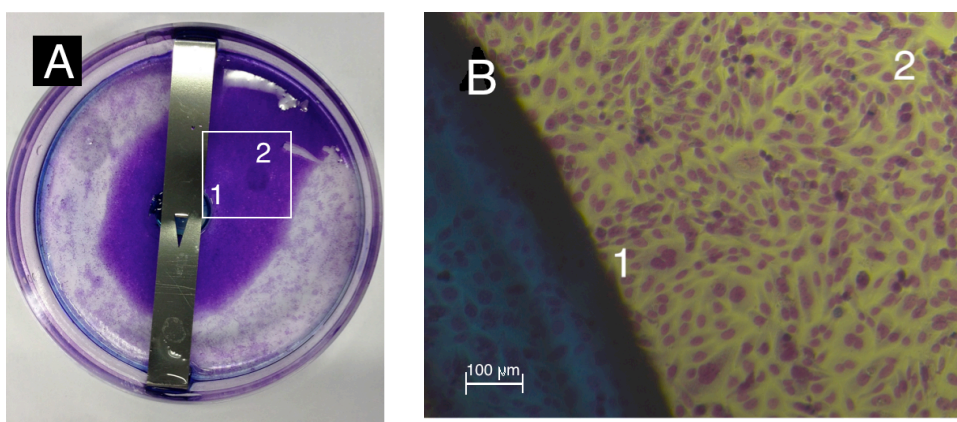


Figure 5.7. Giemsa staining of the sample S2 to visualize cells' distribution around the hydrogel. (A) An overview of the area of interest (white rectangle). (B) Microscopic picture of the area of interest. In each image, the label (1) corresponds to the cells near the hydrogel and the label (2) corresponds to the cells on cell culture plate far from the hydrogel.

The evaluation of the cytotoxicity of the degradation products over three days confirmed that these products did not affect the cells proliferation. In Figure 5.8 we can observe that, at each day, there was no significant difference between the absorbance signal of cells cultured in mediums containing different concentrations of degradation products and the control group, which contains no degradation product ($p > 0.25$).

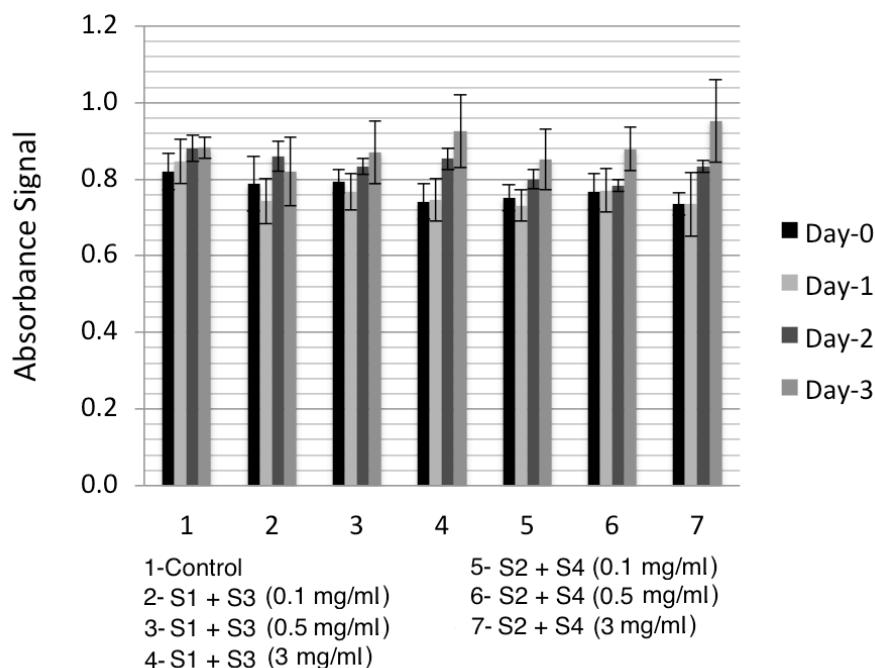


Figure 5.8. Spectrophotometry absorbance signal for CellTiter test, when different concentrations of degradation products from HEMA-DMHA hydrogels (S1 and S3) or HEMA-DMHA-Tetrakis hydrogels (S2 and S4) were exposed to cells for three days. No significant difference could be found between the mean values of the absorbance signal of each group containing the degradation products and the mean values of the control groups at each day ($p > 0.25$).

5.5 Discussion

We developed a biodegradable photo-crosslinked hydrogel based on HEMA with high mechanical properties for load-bearing applications. Our original formulation consisted of HEMA cross-linked with a biodegradable N, O-dimethacryloyl hydroxylamine (DMHA) molecule and a tetra-functional chain transfer agent pentaerythritol tetrakis in the backbone of the hydrogel. We studied the degradation under cyclic mechanical loading, which provides a more realistic environment to evaluate the degradation of hydrogels in load bearing conditions. Mechanical loading can increase water circulation inside the porous structure of hydrogels, which favors hydrolysis and helps to remove the degradation products.

The obtained HEMA-DMHA-Tetrakis hydrogels degraded in low molecular weight products over a prolonged time period. With respect to its mechanical properties, the hydrogels lost their stiffness at the initial stage of the degradation process. Since the stiffness of hydrogels is proportional to their cross-linker ratio (Hennink and van Nostrum, 2012), we concluded that the stiffness lost during the early months of degradation was related to the hydrolysis of the DMHA cross-linker. The

increase of the weight lost rate after several months for the hydrogels containing Tetrakis confirmed that in these hydrogels, their backbone started to break apart during a second stage of degradation. At this stage, the hydrogels began to lose their mechanical integrity. If the hydrogels did not contain any Tetrakis, the degradation could not be completed as in this situation, after the hydrolysis of the cross-linker, the structure of the hydrogels consisted of long non-degradable PHEMA chains which could coil and keep their integrity via some hydrophobic interactions (Refojo, 1967). The presence of Tetrakis allowed the long PHEMA chains to be broken into shorter-length molecules presenting a star structure. This effect has already been described by Chiellini *et al* (Chiellini et al., 2002). Having low molecular weight degradation products is one of the most important aspects when developing biodegradable hydrogels. Since the degradation products of our hydrogels were less than 10 kDa, they could be cleared out of body (Atzet et al., 2008, Jiang et al., 2007).

It should be noticed however that we did not observe a complete degradation of the hydrogels over the nine months degradation study. Slow degradation rate of our hydrogels and their high mechanical properties could anyway be desirable for scaffolding in load bearing applications. Long-term degradation mirrors the rate of tissue development in load-bearing tissues like cartilage and nucleus pulposus where the healing process is slow (A. Getgood et al., 2009, Chung and Burdick, 2008, Moghadam et al., 2014). In parallel, the high damping properties observed in the develop hydrogels provided load and crack resistance under the loading conditions of such tissues (Chapter 3, (Sun et al., 2012)).

It has been already shown that HEMA-based hydrogels can partially degrade when they are cross-linked to some natural polysaccharides molecules such as chitosan (Verestiuc et al., 2006), dextran-based molecules (van Dijk-Wolthuis et al., 1997, Van Tomme et al., 2006), hyaluronic acid and poly(lactic acid) PLA (Hennink and van Nostrum, 2012). Due to the complexity of the functionalization of most of these molecules, their high molecular weight, and their mechanism of cross-linking, resulting hydrogels usually have very poor mechanical properties and cannot be used for load bearing applications. Furthermore, in most cases, the high molecular weight of the resulting degradation products has been reported to be an issue. For example, Atzet *et al.* has developed a biodegradable PHEMA gels cross-linked with polycaprolactone (PCL) which presented high and tunable mechanical properties, but also had degradation products with high molecular weight (Atzet et al., 2008). The degradation properties of DMHA, which we used, have been already characterized

in the literature (Smith et al., 2009, South and Lyon, 2010, Ulbrich et al., 1993). We chose this molecule because it is a hydrolysable short-length molecule similar in size to HEMA monomers. We have previously shown that using cross-linkers similar in size to the HEMA monomers increased the viscous properties of the HEMA-based hydrogels, which favored then their crack resistance (Chapter 3). DMHA undergoes base catalyzed hydrolysis at pH values above 5, thus it is a useful cross-linker which can be cleaved at a physiological pH of 7.4 (South and Lyon, 2010, Ulbrich et al., 1993). Huang *et al.* reported partial weight and stiffness loss in hydrogels made of PHEMA cross-linked by DMHA (Huang et al., 2013). Indeed, these authors showed that the weight lost reached a constant value (20%) after several months. Our results presented the same degradation profile for HEMA-DMHA hydrogels containing no Tetrakis. As mentioned before, this is due to the long interconnected PHEMA chains in the backbone of hydrogels. Based on the results of this study, using Tetrakis in the backbone of hydrogels solved this issue. Chiellini *et al.* has already used Tetrakis molecules to increase the degradation properties of PHEMA hydrogels (Chiellini et al., 2002). However, in their study, they used poly(ethylene glycol di-methacrylate) (PEGDM) as a cross-linker, which is non-degradable. To the best of our knowledge, no other study has tried to use the advantage of Tetrakis molecules in PHEMA hydrogels.

There are some limitations in our study. We evaluated the degradation properties of two HEMA-DMHA-Tetrakis hydrogels as a model system. The first hydrogel was obtained with a low cross-linker ratio and high water content, which can mimic soft-tissues like nucleus pulposus. The second one was made with a high cross-linker ratio and low water content, with resulting mechanical properties similar to articular cartilage. We did not study the effects of these two parameters (cross-linker ratio and water content) separately on the degradation and the mechanical properties of the hydrogels. The effects of these two parameters on the mechanical properties of HEMA-based hydrogels have already been studied for similar geometry cross-linkers like ethylene glycol di-methacrylate (EGDMA) (Chapter 3) (Baker et al., 2009, Peppas et al., 1985, Peppas et al., 2006). Another limitation is related to the GPC method used to measure the molecular weight of the degradation products. This method can only identify the different molecular weights of material composing the hydrogels, but it cannot bring any information on their respective distribution. Nevertheless, the presence of peaks at lower molecular weights in the GPC signal of hydrogels containing Tetrakis strongly suggests that using this molecule decreases the molecular weight of the degradation products. Furthermore, we were still able to show that the molecular weight of all degra-

dation products even from hydrogels without Tetrakis was smaller than the required limit for being cleaned out of the body.

5.6 Conclusion

In conclusion, the new formulation of the HEMA-DMHA-Tetrakis hydrogels allows us to obtain a promising slow degrading biomaterial presenting low molecular weight degradation products, along with tunable mechanical properties. With such properties, the obtained hydrogels could overcome the existing limitations in the application of HEMA-based hydrogels in tissue engineering and drug delivery, especially for load bearing applications.

5.7 Acknowledgments

This work was supported by the Swiss National Science Foundation (#406240_126070, PNR 62 program).

5.8 References

- Getgood A, Brooks R, Fortier L, Rushton N. 2009. Articular cartilage tissue engineering, today's research, tomorrow practice. *Journal of Bone Joint Surgery [Br]* 91, 565-76.
- Abdel-Sayed P, Darwiche SE, Kettenberger U, Pioletti DP. 2014. The role of energy dissipation of polymeric scaffolds in the mechanobiological modulation of chondrogenic expression. *Biomaterials* 35, 1890-7.
- Anseth KS, Bowman CN, Brannon-Peppas L. 1996. Mechanical properties of hydrogels and their experimental determination. *Biomaterials* 17, 1647-57.
- Atzet S, Curtin S, Trinh P, Bryant S, Ratner B. 2008. Degradable poly (2-hydroxyethyl methacrylate)-co-polycaprolactone hydrogels for tissue engineering scaffolds. *Biomacromolecules* 9, 3370-7.
- Bae KH, Wang L-S, Kurisawa M. 2013. Injectable biodegradable hydrogels: progress and challenges. *Journal of Materials Chemistry B* 1, 5371-88.
- Baker MV, Brown DH, Casadio YS, Chirila TV. 2009. The preparation of poly(2-hydroxyethyl methacrylate) and poly{(2-hydroxyethyl methacrylate)-co-[poly(ethylene glycol) methyl ether methacrylate]} by photoinitiated polymerisation-induced phase separation in water. *Polymer* 50, 5918-27.
- Bayramoğlu G, Arica MY. 2003. A novel pH sensitive porous membrane carrier for various biomedical applications based on pHEMA/chitosan: preparation and its drug release characteristics. *Macromolecular Symposia* 203, 213-8.

-
- Cadee JA, De Kerf M, De Groot CJ, Den Otter W, Hennink WE. 1999. Synthesis, characterization of 2-(methacryloyloxy)ethyl-(di-) l-lactate and their application in dextran-based hydrogels. *Polymer* 40, 6877-81.
- Casadio YS, Brown DH, Chirila TV, Kraatz H-B, Baker MV. 2010. Biodegradation of poly(2-hydroxyethyl methacrylate) (PHEMA) and poly{(2-hydroxyethyl methacrylate)-co-[poly(ethylene glycol) methyl ether methacrylate]} hydrogels containing peptide-Based cross-linking agents. *Biomacromolecules* 11, 2949-59.
- Chiellini F, Petrucci F, Ranucci E, Solaro R. 2002. Bioerodible hydrogels based on 2-hydroxyethyl methacrylate: Synthesis and characterization. *Journal of Applied Polymer Science* 85, 2729-41.
- Chung C, Burdick JA. 2008. Engineering cartilage tissue. *Advanced Drug Delivery Reviews* 60, 243-62.
- Darwiche S, Scaletta C, Raffoul W, Pioletti DP, Applegate LA. 2012. Epiphyseal chondroprogenitors provide a stable cell source for cartilage cell therapy. *Cell Medicine* 4, 23-32.
- De Jong S, Van Eerdenbrugh B, van Nostrum Cv, Kettenes-Van Den Bosch J, Hennink W. 2001. Physically crosslinked dextran hydrogels by stereocomplex formation of lactic acid oligomers: degradation and protein release behavior. *Journal of Controlled Release* 71, 261-75.
- Drury JL, Mooney DJ. 2003. Hydrogels for tissue engineering: scaffold design variables and applications. *Biomaterials* 24, 4337-51.
- Gellerstedt G. 1992. Gel permeation chromatography. In *Methods in Lignin Chemistry*, 487-97
- Gunatillake PA, Adhikari R. 2003 Biodegradable synthetic polymers for tissue engineering. *Eur Cell Mater* 5, 1-16
- Han Y, Lee E, Ji B. 2008. Mechanical properties of semi-interpenetrating polymer network hydrogels based on poly(2-hydroxyethyl methacrylate) copolymer and chitosan. *Fibers and Polymers* 9, 393-9.
- Hennink W, Van Nostrum C. 2012. Novel crosslinking methods to design hydrogels. *Advanced Drug Delivery Reviews* 64, 223-36.
- Homsy CA. 1970. Bio-Compatibility in selection of materials for implantation. *Journal of Biomedical Materials Research* 4, 341-56.
- Huang J, Ten E, Liu G, Finzen M, Yu W, Lee JS, Saiz E, Tomsia AP. 2013. Biocomposites of pHEMA with HA-TCP (60/40) for bone tissue engineering: Swelling, hydrolytic degradation, and in vitro behavior. *Polymer* 54, 1197-207.
- Jiang X, Lok MC, Hennink WE. 2007. Degradable-brushed pHEMA-pDMAEMA synthesized via ATRP and click chemistry for gene delivery. *Bioconjugate Chemistry* 18, 2077-84.
- Kamath KR, Park K. 1993. Biodegradable hydrogels in drug delivery. *Advanced Drug Delivery Reviews* 11, 59-84.

-
- Moffat KL, Marra KG. 2004. Biodegradable poly(ethylene glycol) hydrogels crosslinked with genipin for tissue engineering applications. *Journal of Biomedical Materials Research Part B: Applied Biomaterials* 71, 181-7.
- Moghadam MN, Kolesov V, Vogel A, Klok H-A, Pioletti DP. 2014. Controlled release from a mechanically-stimulated thermosensitive self-heating composite hydrogel. *Biomaterials* 35, 450-5.
- Naficy S, Brown HR, Razal JM, Spinks GM, Whitten PG. 2011. Progress toward robust polymer hydrogels. *Australian Journal of Chemistry* 64, 1007-25.
- Ng L-T, Swami S. 2005. IPNs based on chitosan with NVP and NVP/HEMA synthesised through photoinitiator-free photopolymerisation technique for biomedical applications. *Carbohydrate Polymers* 60, 523-8.
- Peppas NA, Moynihan HJ, Lucht LM. 1985. The structure of highly crosslinked poly(2-hydroxyethyl methacrylate) hydrogels. *Journal of Biomedical Materials Research* 19, 397-411.
- Peppas NA, Hilt JZ, Khademhosseini A, Langer R. 2006. Hydrogels in biology and medicine: from molecular principles to bionanotechnology. *Advanced Materials* 18, 1345-60.
- Refojo MF. 1967. Hydrophobic interaction in poly(2-hydroxyethyl methacrylate) homogeneous hydrogel. *Journal of Polymer Science Part A-1: Polymer Chemistry* 5, 3103-13.
- Smith MH, South AB, Gaulding JC, Lyon LA. 2009. Monitoring the erosion of hydrolytically-degradable nanogels via multiangle light scattering coupled to asymmetrical flow field-flow fractionation. *analytical chemistry* 82, 523-30.
- South AB, Lyon LA. 2010. Direct observation of microgel erosion via in-liquid atomic force microscopy. *Chemistry of Materials* 22, 3300-6.
- Striegel A, Yau WW, Kirkland JJ, Bly DD. 2009. *Modern size-exclusion liquid chromatography: practice of gel permeation and gel filtration chromatography*: John Wiley & Sons
- Sun JY, Zhao X, Illeperuma WR, Chaudhuri O, Oh KH, Mooney DJ, Vlassak JJ, Suo Z. 2012. Highly stretchable and tough hydrogels. *Nature* 489, 133-6.
- Ulbrich K, Subr V, Seymour LW, Duncan R. 1993. Novel biodegradable hydrogels prepared using the divinyllic crosslinking agent N,O-dimethacryloylhydroxylamine. 1. Synthesis and characterisation of rates of gel degradation, and rate of release of model drugs, in vitro and in vivo. *Journal of Controlled Release* 24, 181-90.
- van Dijk-Wolthuis WNE, Tsang SKY, Kettenes-van den Bosch W.E. Hennink JJ. 1997. A new class of polymerizable dextrans with hydrolyzable groups: hydroxyethyl methacrylated dextran with and without oligolactate spacer. *Polymer* 38, 6235-42.
- Van Tomme SR, van Nostrum CF, de Smedt SC, Hennink WE. 2006. Degradation behavior of dextran hydrogels composed of positively and negatively charged microspheres. *Biomaterials* 27, 4141-8.

-
- Verestiuc L, Nastasescu O, Barbu E, Sarvaiya I, Green KL, Tsibouklis J. 2006. Functionalized chitosan/NIPAM (HEMA) hybrid polymer networks as inserts for ocular drug delivery: Synthesis, in vitro assessment, and in vivo evaluation. *Journal of Biomedical Materials Research Part A* 77, 726-35.
- Vogel A, Pioletti DP. 2011. Thermomechanical hysteresis of biological and synthetic hydrogels: theory, characterisation, and development of a novel deformation calorimeter. PhD thesis, école polytechnique federale de Lausanne

Chapter 6

Conclusion

6.1 Summary of Findings

In this study, we developed a smart drug delivery system based on the dissipative properties of hydrogels. We introduced viscous dissipation as a new environmental variable to trigger a delayed drug release following mechanical loading. The developed hydrogel based on Hydroxyethyl Methacrylate (HEMA), which has high dissipative properties, increases in temperature via viscous dissipation when subjected to cyclic mechanical loading. We showed that such a temperature increase can activate the incorporated thermosensitive nanoparticles, which can trigger the drug release by changing the permeability of HEMA hydrogels when the temperature surpasses a threshold. To reach to this aim, we divided the project into four steps.

In the first step, we estimated the required heat power needed from the hydrogel under mechanical loading to increase the temperature. For this purpose, a FE model was developed to study the heat transfer mechanism in articular cartilage. In particular, we found that the synovial fluid flow could only partially affect the temperature increase in cartilage subjected to dynamic loading. Indeed, a significant temperature increase in the cartilage was observed due to the viscous properties of cartilage itself even when taking the synovial fluid flow into consideration. However, we showed that to reach the required temperature increase in knee cartilage for our proposed drug delivery system, we need a material which can dissipate four times more than cartilage.

In the second step, we developed a HEMA-based hydrogel with high dissipative properties. Here we showed that due to the special properties of HEMA hydrogels, their elastic and viscous properties are tunable by the type and ratio of cross-linker and by the ratio of water. The high dissipative properties of HEMA hydrogels were related to the shape of HEMA monomers and the particular choice of the short-length cross-linker, which could provide high friction under loading. We demonstrated that to increase the dissipative properties of HEMA hydrogels, the hydrophobicity of the structure must be increased. Additionally, short-length cross-linkers must be used to let HEMA chains interact and to increase the friction and dissipation in hydrogel networks under deformation. Based on that, we developed a HEMA-based hydrogel cross-linked with Ethylene glycol di-methacrylate (EGDMA) (6% molar ratio) with an aqueous ratio of 40%, which can provide the required dissipation that we estimated in the first step. We also showed that the high dissipative properties of this hydrogel increase its toughness and resistance to crack propagation, which is necessary to use it in load bearing applications.

In the third step, we demonstrated our proof of concept for the dissipation-driven delayed drug delivery system by combining the developed HEMA-EGDMA hydrogel with poly(N-isopropyl acrylamide) (PNIPAM) nanogel particles. The dissipation of our HEMA hydrogel under mechanical loading was able to increase the temperature from 36°C to 37°C after 5 minutes of cyclic loading. At this temperature, the PNIPAM nanoparticles shrunk and thus increased the void ratio of the hydrogel. Consequently, the permeability of the hydrogel increased and expedited the release of its payload by a factor of 3 compared to when the temperature was lower than 37°C. In this way we could achieve a 5 minutes delay between the initiation of mechanical load and the release of the model drug.

In the last step, we improved the degradation properties of our HEMA-based hydrogel to make it suitable for clinical application. Here, we developed a new biodegradable HEMA-based hydrogel by employing a tetra-functional chain breaker group as a part of the HEMA backbone and a low molecular weight biodegradable cross-linker called N,O-Dimethacryloyl hydroxylamine (DMHA), which provided the same dissipative properties as EGDMA and high mechanical strength. Our results showed that the developed hydrogel underwent long-term degradation with low molecular weight degradation products.

6.2 General Discussion

Local delivery of growth factors by hydrogels is a recent strategy to treat defects in connective tissues like cartilage (Lee et al., 2011, Park et al., 2007, Tayalia and Mooney, 2009). Additionally, mechanical loading has been demonstrated to activate growth factor receptors involved in the healing process of these tissues (Discher et al., 2009, Hiyama et al., 2007, Neu et al., 2007). Based on these findings, several mechanically controlled drug delivery systems were designed (Holme et al., 2012, Korin et al., 2012, Lee et al., 2001). However, a delay of 5 to 20 minutes is necessary for the activation of cell receptors following the initiation of a mechanical stimulation (Tschumperlin et al., 2004). The synergic effect between mechanical loading and activation of growth factor receptors can be maximized by delaying the delivery of the growth factor so that it occurs several minutes after a mechanical stimulation. We used the viscous dissipation of hydrogels as a new environmental variable to control the drug release with mechanical loading and provide such a delay between the initiation of mechanical loading and the release of the drug following the activation of the growth factor receptors.

Our results are especially of great importance since hydrogels are generally known as highly swollen polymer structures with very weak mechanical properties. Here, through studying the structure of hydrogels, we identified parameters that can influence the mechanical properties of hydrogels. The proposed hydrogel met the required elastic and viscous properties needed for a mechanically controlled drug delivery system for cartilage. Its stiffness is close to the stiffness of articular cartilage. From the viscous aspect, such a hydrogel shows very high dissipation and damping properties, which can provide a sufficient temperature increase under load to activate nanoparticles and which can increase the resistance of the hydrogel to cracks and fractures. Furthermore, the long-term degradation properties of the biodegradable version of this hydrogel can reflect the rate of tissue regeneration, provide long-term drug delivery, and support new tissue formation by acting as a scaffold in the defected zone. The dissipative properties of these hydrogels can be modulated to link the duration of the cyclic loading with a targeted increase in temperature. Thus, a tunable delay between the initiation of the mechanical stimulation and the release of a payload can be achieved.

Furthermore, our results showed that the passive release of these hydrogels was insignificant compared to their active release under mechanical loading. We related this to the small mesh size and hydrophobicity of these hydrogels, which cause the hydrogel to exchange less fluid and have less payload release without the application of an external force. However, nanoparticles which can encapsulate the drug and release it based on temperature can give greater control over the passive release of these hydrogels. Indeed, one of the limitations of our study was that the thermosensitive PNIPAM nanoparticles, which we used in this study, could control the drug release by changing the permeability of the HEMA hydrogel when the temperature passed a threshold (i.e. the LCST of nanoparticles). Since the nanoparticles could not encapsulate the drug, the passive release of the drug was highly dependent on the permeability of the HEMA hydrogel at temperatures lower than LCST. Another limitation of our study was that the developed highly dissipative hydrogels (either HEMA-EGDMA or HEMA-DMHA) have a very small mesh size, and we couldn't show the dissipation-driven drug delivery with TGF- β . Indeed, the size of the TGF- β molecules, which have a molecular weight of 25 kDa, is too big for them to be released from the highly dense HEMA hydrogels we developed. Increasing the mesh size of these hydrogels requires decreasing the amount of cross-linker and increasing water ratio, which significantly decreases the amount of hydrogel dissipation.

In the next section, we will propose some solutions to overcome these limitations and improve the proposed smart drug delivery system for a clinical application.

6.3 Future Works

6.3.1 Improvement of the Thermosensitive Nanoparticles

As we discussed before, one of the limitations of our study was the developed thermosensitive nanoparticles. To have more control over the release, especially to prevent passive release, the thermosensitive nanoparticles used in this study should be improved so the drug can be encapsulated and released based on temperature increase. Furthermore, although PNIPAM-based polymers have been previously used as thermosensitive drug carriers, their biocompatibility and biodegradability have not yet been proven (Gong et al., 2013). Therefore, further studies are needed to develop nanoparticles which can encapsulate the drug, are biocompatible, and are biodegradable. Some of proposed solutions for the encapsulation of the drug are (Gong et al., 2013, Hodorog et al., 2012, Klouda and Mikos, 2008):

- Binding the drug molecule to the nanoparticles via thermosensitive bonds, which can be broken when temperature passes the LCST of the thermosensitive bonds.
- Developing self-assembling nanoparticles able to aggregate and encapsulate the drug and disengage and release the drug following temperature increase.
- Developing thermosensitive nanogels in the form of porous shells, which can encapsulate the drug and change porosity and allow drug release following a temperature increase.

6.3.2 Improving the Mesh Size of Hydrogels to Deliver Larger Drugs

To be able to release drug molecules of a larger size like TGF- β , the mesh size of hydrogels needs to be increased. In particular, we found that to release a drug with such a large molecular size, we need to decrease the cross-linker (DMHA) ratio to 1% and increase the water ratio to 65%. We tested the release of Lysozyme proteins (Sigma-Aldrich, St. Louis, MO, USA), which have a molecular size similar to TGF- β , from hydrogels with these ratios (APPENDIX 7.3). The resulting hydrogels were very soft and could not produce the high magnitude of dissipation needed under mechanical loading to activate the nanoparticles. To overcome this problem, we propose a cylindrical double-layer hydrogel structure (Figure 6.1) consisting of two different hydrogel components. The first

component, which is the inner part of the cylinder, is a dense HEMA-based hydrogel with a high cross-linker ratio (10% DMHA) and a low water ratio (40%), which can provide high dissipation and temperature increase under mechanical loading. The second component, which surrounds the dense hydrogel and makes up the outer layer of the cylinder, is a HEMA hydrogel with a low cross-linker ratio (1% DMHA) and a high water ratio (65%) loaded with TGF- β and thermosensitive nanoparticles. With this double-layer system, the temperature of the interior hydrogel with high dissipative properties can be increased under mechanical load, triggering the drug release from the outer layer. In the future, such a system should be characterized and combined with proper thermosensitive nanoparticles.

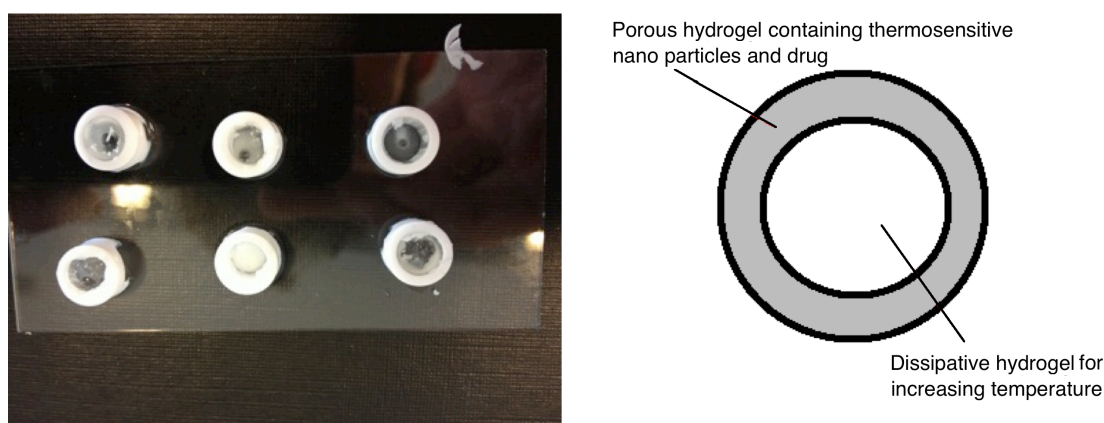


Figure 6.1. Double-layer smart hydrogels to deliver drugs with a large molecular size. These hydrogels consist of two layers: the inner layer is a dense hydrogel providing high dissipation and temperature increase under mechanical loading, and the outer layer is a highly porous structure loaded with thermosensitive nanoparticles and the drug.

6.3.3 HEMA Hydrogels as a Mechanically Controlled Drug Delivery System

We argue that our developed hydrogels can be used as a mechanically controlled drug delivery system even without nanoparticles. In particular, we showed that the amount of cumulative passive release of Lysozyme proteins, from hydrogels after one month is less than 18% of the total encapsulated drug (Figure 6.2A). However, the active release of Lysozyme proteins from hydrogels subjected to 20 minutes of mechanical loading was more than 1% (even after 11 days of incubation), which is a larger release than the total passive release over two days (Figure 6.2B). This suggests that even at later points in time, the active release under mechanical loading is still much greater than the passive release. These results confirm that even without nanoparticles, the pro-

posed HEMA-based hydrogels can be used as a mechanically controlled drug delivery system for applications where a delayed release is not needed. Although such systems have already been developed, when the special properties of the HEMA-based hydrogels we developed are taken into consideration, they may be a very interesting candidates for a mechanically-controlled drug delivery system in a load bearing application. However, further investigation is needed to study the potential application of such a mechanically-driven drug delivery system.

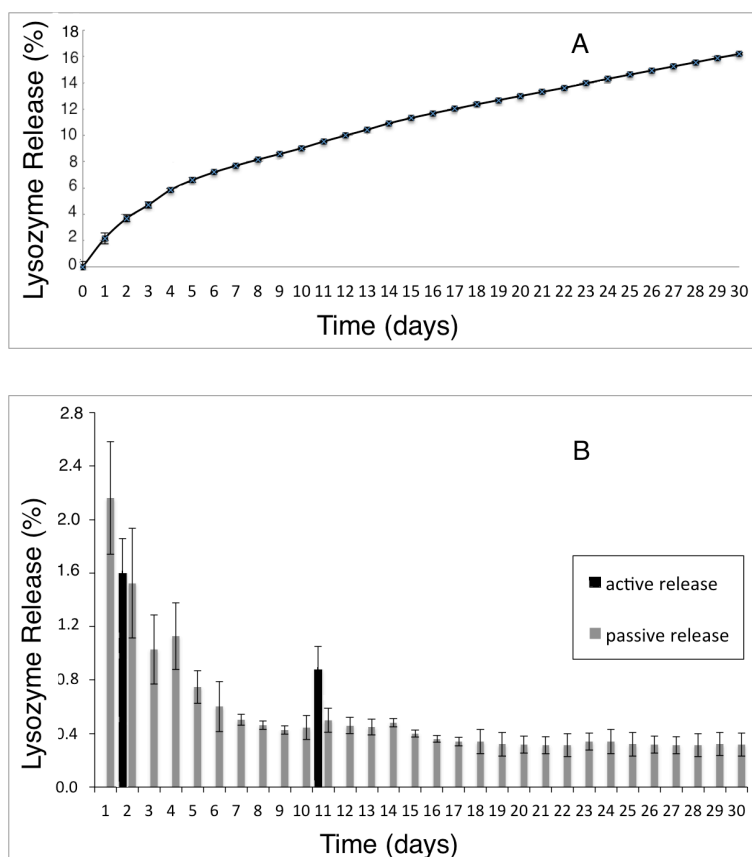


Figure 6.2. Drug release from HEMA-DMHA-Tetrakis hydrogels. Model drug: Lysozyme proteins from chicken egg white. (A) The cumulative passive release over one month. (B) The daily passive release and the release after 20 minutes of mechanical loading at 1.5 Hz and 15% deformation amplitude in the 2nd and 11th days.

6.3.4 Clinical Application

After several discussions with clinicians at the Orthopedic Hospital of Lausanne, we found that our drug delivery system could be implanted in cartilage in both microfracture surgery and mosaicplasty surgery. The shape of the delivery system can be adapted to the defect geometry. It can cover the zone of the microfracture containing the mesenchymal stem cells delivered from the

bone marrow and it can release TGF- β . In small defects the drug delivery system may serve as only one graft, similar to the cartilage plugs used in mosaicplasty. In a mosaicplasty using multiple cartilage plugs, an interesting strategy would be to implant the drug delivery system in the spaces between the cartilage plugs to deliver enough growth factors to the defect zone (Figure 6.3). We call this approach of combining existing cartilage treatments with an innovative drug delivery system “*augmented cartilage repair technique*”. The key aspect of this new technique is the post-surgery mechanical loading. A rehabilitation program will need to be developed in collaboration with the surgeons and the physiotherapists to achieve the required mechanical loading.

Prior to clinical tests, beside other regulatory aspects, the shape of the final system and its fixation in defected cartilage must be defined. For this purpose, the surgical technique can be initially developed on bovine cadaver knee samples and then on human cadaver knees. The suitability of using the smart hydrogel in real knee geometry and how a press-fit of the hydrogel between the osteochondral plugs may increase the primary stability of the mosaicplasty reconstruction should be verified for the success of this technique.

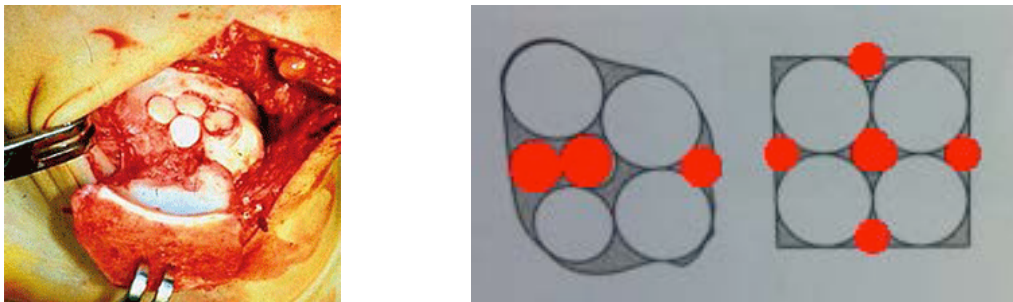


Figure 6.3. Proposed application of mechanically controlled drug delivery system for mosaicplasty. Implanting hydrogel plugs in the spaces between the cartilage plugs of the mosaicplasty to deliver growth factors to the defected zone. Left) a common mosaicplasty surgery (Chuckpaiwong, 2009). Right) proposed augmented cartilage repair technique in mosaicplasty. Red circles: hydrogel plugs, Gray circles: cartilage plugs.

6.4 References

- Chuckpaiwong B. 2009. Surgical treatments of the lateral ankle sprain. Siriraj Medical Journal 61, 104-6.
- Discher DE, Mooney DJ, Zandstra PW. 2009. Growth factors, matrices, and forces combine and control stem cells. Science 324, 1673-7.

-
- Gong C, Qi T, Wei X, Qu Y, Wu Q, Luo F, Qian Z. 2013. Thermosensitive polymeric hydrogels as drug delivery systems. *Current Medicinal Chemistry* 20, 79-94.
- Hiyama A, Mochida J, Iwashina T, Omi H, Watanabe T, Serigano K, Iwabuchi S, Sakai D. 2007. Synergistic effect of low-intensity pulsed ultrasound on growth factor stimulation of nucleus pulposus cells. *Journal of Orthopaedic Research* 25, 1574-81.
- Hodorog ADR, Ibanescu C, Danu M, Simionescu BC, Rocha L, Hurduc N. 2012. Thermo-sensitive polymers based on graft polysiloxanes. *Polymer Bulletin* 69, 579-95.
- Holme MN, Fedotenko IA, Abegg D, Althaus J, Babel L, Favarger F, Reiter R, Tanasescu R, Zaffalon PL, Ziegler A, Muller B, Saxer T, Zumbuehl A. 2012. Shear-stress sensitive lenticular vesicles for targeted drug delivery. *Nature Nanotechnology* 7, 536-43.
- Klouda L, Mikos AG. 2008. Thermoresponsive hydrogels in biomedical applications. *European Journal of Pharmaceutics and Biopharmaceutics* 68, 34-45.
- Korin N, Kanapathipillai M, Matthews BD, Crescente M, Brill A, Mammoto T, Ghosh K, Jurek S, Bencherif SA, Bhatta D, Coskun AU, Feldman CL, Wagner DD, Ingber DE. 2012. Shear-activated nanotherapeutics for drug targeting to obstructed blood vessels. *Science* 337, 738-42.
- Lee K, Silva EA, Mooney DJ. 2011. Growth factor delivery-based tissue engineering: general approaches and a review of recent developments. *Journal of the Royal Society Interface* 8, 153-70.
- Lee KY, Peters MC, Mooney DJ. 2001. Controlled drug delivery from polymers by mechanical signals. *Advanced Materials* 13, 837-9.
- Neu CP, Khalafi A, Komvopoulos K, Schmid TM, Reddi AH. 2007. Mechanotransduction of bovine articular cartilage superficial zone protein by transforming growth factor beta signaling. *Arthritis and Rheumatism* 56, 3706-14.
- Park H, Temenoff JS, Tabata Y, Caplan AI, Mikos AG. 2007. Injectable biodegradable hydrogel composites for rabbit marrow mesenchymal stem cell and growth factor delivery for cartilage tissue engineering. *Biomaterials* 28, 3217-27.
- Tayalia P, Mooney DJ. 2009. Controlled growth factor delivery for tissue engineering. *Advanced Materials* 21, 3269-85.
- Tschumperlin DJ, Dai G, Maly IV, Kikuchi T, Laiho LH, McVittie AK, Haley KJ, Lilly CM, So PT, Lauffenburger DA, Kamm RD, Drazen JM. 2004. Mechanotransduction through growth-factor shedding into the extracellular space. *Nature* 429, 83-6.

Chapter 7

APPENDIX

7.1 APPENDIX for Chapter 3

7.1.1 Supplementary Tables

Table 1S. Combination of parameters and volumetric material composition to synthesize HEMA hydrogels with different cross-linkers.

	Sample	HEMA [μl]	EGDMA [μl]	TEGDM [μl]	PEGDM 550 [μl]	PEGDM 750 [μl]	Water [μl]
20% water	S1	880	56	0	0	0	220
4% cross-linker	S2	880	0	80	0	0	220
	S3	880	0	0	150	0	220
	S4	880	0	0	0	200	220
20% water	S5	880	84	0	0	0	220
6% cross-linker	S6	880	0	120	0	0	220
	S7	880	0	0	230	0	220
	S8	880	0	0	0	300	220
40% water	S9	880	56	0	0	0	590
4% cross-linker	S10	880	0	80	0	0	590
	S11	880	0	0	150	0	590
	S12	880	0	0	0	200	590
40% water	S13	880	84	0	0	0	590
6% cross-linker	S14	880	0	120	0	0	590
	S15	880	0	0	230	0	590
	S16	880	0	0	0	300	590
50% water	S17	880	56	0	0	0	880
4% cross-linker	S18	880	0	80	0	0	880
	S19	880	0	0	150	0	880
	S20	880	0	0	0	200	880
50% water	S21	880	84	0	0	0	880
6% cross-linker	S22	880	0	120	0	0	880
	S23	880	0	0	230	0	880
	S24	880	0	0	0	300	880

Table 2S. Mesh size of HEMA-EGDMA hydrogels. The mesh size of HEMA hydrogels increases by decreasing cross-linker (EGDMA) percentage and increasing water content. The mesh size was quantified from the relation between the tensile modulus of hydrogels and their swelling properties.

EGDMA concentration mol%	Water concentration volume %	Average mesh size (nm)
1	40	4.3 ± 0.18
2	40	2.0 ± 0.23
4	40	1.6 ± 0.15
6	40	1.1 ± 0.16
2	50	5.2 ± 0.25
4	50	2.1 ± 0.18
6	50	1.4 ± 0.11

7.1.2 Supplementary Methods: Mesh Size Measurement

The elastic behavior of hydrogels can be used to elucidate their structure by utilizing the rubber-elasticity theory. Here one form of the rubber-elasticity theory is presented as (Peppas et al, 2006):

$$\tau = \frac{\rho RT}{\overline{M}_c} \left(1 - \frac{2\overline{M}_c}{\overline{M}_n} \right) \left(\alpha - \frac{1}{\alpha^2} \right) \left(\frac{v_{2,s}}{v_{2,r}} \right)^{1/3} \quad (7.1)$$

Where ρ is the density of the polymer, R is the gas constant, T the temperature in K, \overline{M}_c is the molecular weight between the cross-links, \overline{M}_n the molecular weight of the polymer chains, $v_{2,r}$ the polymer volume fraction in the relaxed state and $v_{2,s}$ the polymer volume fraction in the swollen state. τ is the stress applied to the polymer sample and α is the deformation ratio (deformed length/initial length). To more accurately measure the volume fraction of polymer in gel, we used the buoyancy method. The buoyancy of the gel was measured with a density determination kit in ethanol on a Mettler-Toledo balance (Mettler-Toledo, Greifensee, Switzerland). The stress and deformation ratio tensile load was applied on each sample with a Instron E3000 linear mechanical testing machine (Norwood, MA, USA).

The mesh size was found using the following equation:

$$\epsilon = v_{2,s}^{1/3} \times \frac{2\overline{M}_c \overline{C}_n}{\overline{M}_r} \times l \quad (7.2)$$

Where ϵ is the mesh size, M_r is the molecular weight of HEMA monomer, C_n is the Flory characteristic ratio (6.2 for HEMA) and l the length of the bond along the polymer backbone (1.54 Å).

7.2 APPENDIX for Chapter 4

7.2.1 Supplementary Figures

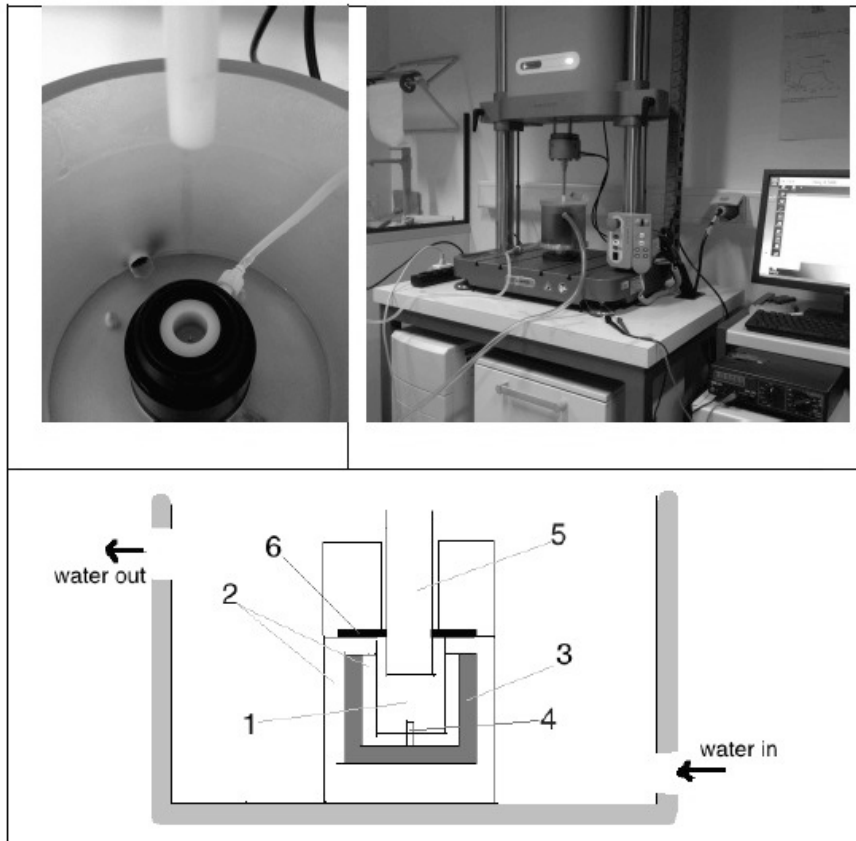


Figure 15. Thermally isolated system used for measuring payload release from hydrogel under mechanical loading. The system consists of a test chamber (1) with two layer walls (2), where vacuum can be created in the gap between the two walls (3) to have a highly insulated system. A thermistor in the center of the chamber monitors the temperature during the test (4). Mechanical loading is applied directly on the sample in the test chamber with a piston (5) passing through a diaphragm (6). The initial temperature of the test chamber can be set by thermostated water circulation around the chamber.

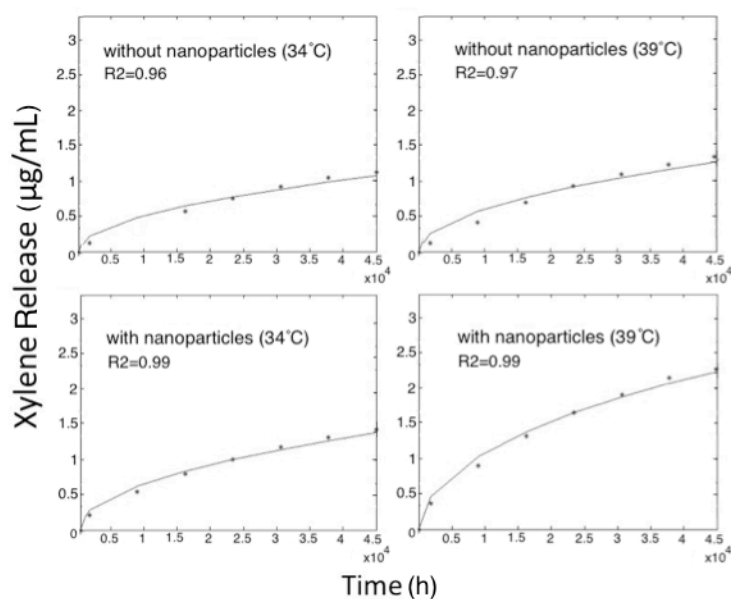


Figure 2S. Xylene Cyanole FF release from films and curve fitting for diffusion coefficient D_{eff} calculation. D_{eff} was calculated by fitting Equation (4.2) to experimental data from desorption bath using a least squares method implemented in MATLAB. The values of R^2 was comprised between 0.96 and 0.99 indicating the good quality of the curves fitting.

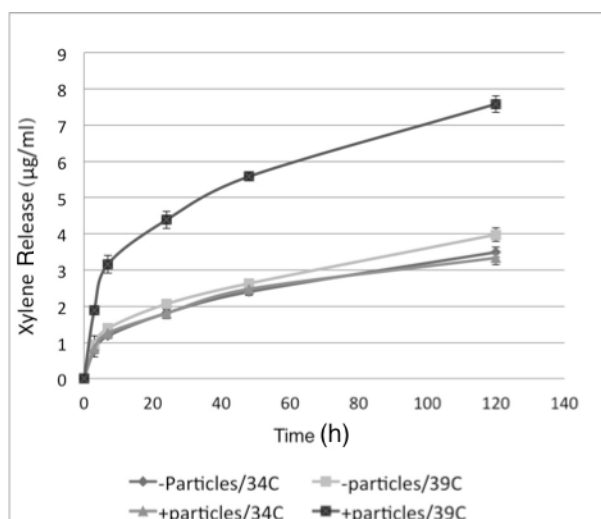


Figure 3S. Passive release of Xylene Cyanole FF from the smart hydrogel controlled by temperature. Cumulative passive dye release from the smart hydrogel at 34 and 39°C from gels with and without nano particles. The passive xylene release was 2.45 times (145%) higher at 39°C than at 34°C when nanoparticles are present in the hydrogel. Conversely, no significant difference in passive dye release at two different temperatures was noted in the absence of nanoparticles.

7.3 APPENDIX for Chapter 6

7.3.1 Supplementary Methods: Lysozyme Release from HEMA-DMHA-Tetrakis Hydrogels

We optimized the structure of HEMA-DMHA-Tetrakis hydrogels to control their mesh size so that they could release drugs with larger molecular sizes. We studied the release of Lysozyme proteins (Lysozyme from chicken eggs, 14.6 kDa, Sigma-Aldrich, St. Louis, MO, USA) as a model drug from HEMA-DMHA-Tetrakis hydrogels. Lysozyme molecules have a molecular size (molecular radius = 1.7 nm) similar to TGF- β (molecular radius = 1.9 nm) and are much less expensive for laboratory experiments. We prepared HEMA hydrogels (6 samples for each hydrogel type) with different ratios of DMHA cross-linker (1, 2, and 5% mol) while for each DMHA ratio the water content varied as 55, 60, 65, and 70% of total volume of the mixture. We added 2 mg/ml of Lysozyme proteins to the hydrogel composition before polymerization and we followed the same polymerization procedure explained in Chapter 5.3.3. The hydrogels were kept in 5 mL PBS and incubated at 37°C. The PBS was changed every day and the release of proteins in the PBS was measured every day with a lysozyme assay following the standard manufacturer protocol (*Micrococcus lysodeikticus* ATCC, Sigma, St. Louis, MO, USA) and an absorbance reading at 590 nm with a spectrophotometer (Wallac Victor2, 1420, Turku, Finland).

Since decreasing the amount of cross-linker and increasing the water ratio decreases the mechanical stiffness and dissipation of hydrogels (Chapter 3), we targeted a hydrogel structure with the highest possible cross-linker ratio and lowest possible water content that could still release Lysozyme proteins. We did not observe any drug release from hydrogels containing less than 65% water and more than 1% cross-linker, or the release ended after several days. Therefore, we chose a hydrogel structure with 1% cross-linker and a 65% water ratio as an optimum structure, which can release the protein and had the highest mechanical properties of the hydrogels we tested. We studied the release of Lysozyme from this hydrogel over 30 days (Section 6.3.3, Figure 6.2)

7.4 Reference

Peppas NA, Hilt JZ, Khademhosseini A, Langer R. 2006. Hydrogels in biology and medicine: from molecular principles to bionanotechnology. *Advanced Materials* 18, 1345-60

Curriculum Vitae

Mohamadreza Nassajian Moghadam

Chemin de Bonne-esperance 14, 1006, Lausanne, Switzerland

+41 78-930.90.98

Nassajian@gmail.com

Sex: male, **Status:** single, **Age:** 29, **Nationality:** Iran

Profile

Managing projects in biomaterial development, smart drug delivery systems, tissue engineering and biomechanics, Bio-instruments design and development.
Strong, adaptable communication of technical concepts to broad audience. International and multidisciplinary experiences.

Work Experiences

2010-now

[Laboratory of biomechanical orthopaedics \(LBO\), EPFL Lausanne Switzerland](#)

Developing a smart biomaterial for mechanically-controlled drug delivery. The result of the work was published in top journals of field and received worldwide medias feedback ([Sciencedaily media](#))

2008-2010

[Faculty member: Feiz Institute of Higher Education, Isfahan, Iran](#)

Consulting and holding university courses in Applied Mathematics and Differential Equations. A remarkable managing and organization experience.

2007

[Research Center for Science and Technology In Medicine \(RCSTIM\), Tehran](#)

Leading project in design and manufacturing of a new laparoscopic trocar for improving dialysis catheter placement in laparoscopy surgery.

Education

2010-2014

[PhD in mechanics Ecole Polytechnique Fédérale de Lausanne \(EPFL\)](#)

Thesis topic: Self-heating hydrogel for mechanically-controlled drug delivery system.

2007-2010

[Master of Science in biomechanics Sharif University of Technology \(SUT\)](#)

Thesis topic: A biomechanical model for evaluation of shoulder function: detecting the relationship between muscles activation patterns using muscle synergies.

2002-2007

[Bachelor of Science in mechanical engineering Sharif University of Technology](#)

Thesis topic: A finite element model for analysis of undersea pipeline With S-lay method.

Key skills

[Communication and management skills](#)

- Project leadership in bio-instruments design and manufacturing.
- Strong, adaptable communication to clinical and engineering audience and scientists with different background.
- Strong management and organization skills obtained through academic consulting, teaching university courses supervising master and bachelor students.

[Technical skills](#)

Material science and chemistry skills:

- Synthetic techniques and characterization of biomaterials, spectrophotometry, polymerization techniques, UV polymerization, specialist in synthesis and characterization of hydrogels.

Bioengineering skills:

- Tissue engineering: cell culture and treatment, cell encapsulation, biocompatibility study of biomaterial, RNA extraction, gene expression, histology of biomaterial and biological tissues,
- Advanced microscopy skills: confocal microscopy, super-resolution microscopy STED, electron microscopy SEM,
- Musculoskeletal modelling, bio-sensors and bio-instrument design.

Mechanical engineering skills:

- Specialist in mechanical characterization of soft and non-linear materials, viscoelastic and poroelastic, finite element modelling, hydraulics and pneumatics, Micro fluid modelling, machine design and development.

Obtained professional trainings

2013	Biomedical approaches for drug evaluation l'Institut de Pathologie CHUV, Lausanne, Switzerland
2013	Super-resolution microscopy Leica STED workshop Bioimaging and Optics Platform (PT-BIOP), EPFL, Lausanne, Switzerland
2013	Effective presentation in the life and natural sciences Conférence Universitaire de Suisse Occidentale (CUSO), Lausanne, Switzerland
2012	Materiomics: Multi-scale Mechanics of Biological Materials and Structures International Centre for Mechanical Sciences (CISM), Udine, Italy
2011	Computational Biomechanics workshop Spine FX, Initial Training Network, Vienna, Austria
2011	Interdisciplinary training for young scientists: Growth and dissolution of solids on the molecular, cellular and atomic scale Suisse national Science foundation (SNSF), Lugano, Switzerland

Publications

- M. Nassajian Moghadam, V. Kolesov, H.-A. Klok and D. Pioletti. **Controlled release from a mechanically-stimulated thermosensitive self-heating composite hydrogel**, *Biomaterials*, vol. 35, p. 450-455, 2014.
- M. Nassajian Moghadam and D. Pioletti. **Improving hydrogels' toughness by increasing the dissipative properties of their network**, *Journal of the Mechanical Behavior of Biological Materials*, vol. 41, p. 161-167, 2015.
- M. Nassajian Moghadam, P. Abdel-Sayed, V Malfroy Camine and D. Pioletti **Impact of synovial fluid flow on temperature regulation in knee cartilage**, accepted to *Journal of Biomechanics*.
- M. Nassajian Moghadam and D. Pioletti. **Biodegradable HEMA-based hydrogels with enhanced mechanical properties**, submitted to *Acta Biomaterialia*.
- P. Abdel-Sayed, M. Nassajian Moghadam, R. Salomir, D. Tchernin and D. Pioletti. **Intrinsic viscoelasticity increases temperature in knee cartilage under physiological loading**, *Journal of the Mechanical Behavior of Biomedical Materials*, vol. 30, p. 123-130, 2014.
- P. Abdel-Sayed, A. Vogel, M. Nassajian Moghadam and D. Pioletti. **Cartilage self-heating contributes to chondrogenic expression**, *European Cells and Materials*, vol. 26, p. 171-178, 2013.
- M. Nassajian Moghadam, K. Aminian, M. Asghari, M. Parnianpour, **How well do the muscular synergies extracted via non-negative matrix factorisation explain the variation of torque at shoulder joint?**, *Computer Methods in Biomechanics and Biomedical Engineering*, vol 16, p. 291-301, 2013.
- E. Rashedi, K. Khalaf, M. Nassajian Moghadam, B. Nasserolelami, M. Parnianpour, **How does CNS address the kinetic redundancy in lumbar spine? 3 dimensional isometric exertions with 18 Hill based muscle fascicles at L4/L5 Level**, *Journal of Engineering in Medicine*, vol 224, p.487-

501, 2010.

M. Nassajian Moghadam, V. Kolesov, H.-A. Klok and D. Pioletti. **Controlled release by hydrogel dissipative properties** 41st Annual Meeting & Exposition of the Controlled Release Society, in the Hilton Chicago in Chicago, Illinois, USA, 2014.

M. Nassajian Moghadam and D. Pioletti, **Degradation study of mechanically-controlled drug delivery system for knee cartilage** 14th european Cells and Materials Meeting, Davos, Switzerland, 2014.

M. Nassajian Moghadam, V. Kolesov, H.-A. Klok and D. Pioletti. **Drug Delivery System Based On Hydrogel Dissipative Properties**. In proceeding of: 60th annual meeting of orthopedic research society, At New Orleans, USA, 2014.

P. Abdel-Sayed, M. Nassajian Moghadam, R. Salomir, and D. Pioletti. **Intrinsic Viscoelasticity Increases Temperature In Knee Cartilage Under Physiological Loading**. In proceeding of: 60th annual meeting of orthopedic research society, At New Orleans, USA, 2014.

M. Nassajian Moghadam, D. Pioletti. **Quantification of viscous dissipation properties of HEMA hydrogels as a tough biomaterial**, 19th european society of biomechanics, At Patras, Greece, 2013.

M. Nassajian Moghadam, D. Pioletti. **Numerical simulation of the heat power required for a thermosensitive drug delivery system in knee cartilage**, 10th Computer Methods in Biomechanics and Biomedical Engineering, At berlin, 2012.

M. Nassajian Moghadam, M. Asghari, K. Aminian, M. Parnianpour, **How Well Does The Muscular Synergies Extracted Via Non-Negative Matrix Factorization Explain The Variation Of Torque at Shoulder Joint?** ASME 2010, 10th Biennial Conference on Engineering Systems Design and Analysis, Istanbul, Turkey, 2010.

M. Nassajian Moghadam, M. Asghari, K. Aminian, M. Parnianpour. **Application of Non-negative factorization to extract small muscular synergies to balance external bi-axial moments isometrically by a redundant validated 3D biomechanical shoulder model**, ISME, Tehran, Iran, 2010.

Media feedback

Arthrose: comme un clou dans genou, **canal 9, Suisse TV**, 2013

L'EPFL opère une percée dans le traitement de l'usure du cartilage, **RTS Info, Suisse TV**, 2013.

Une nouvelle technique pour sauver les genou, **24 Heures, Suisse daily newspaper**, 2013.

L'EPFL met au point un matériau intelligent pour le cartilage du genou, **Le Temps, Suisse daily newspaper**, 2013.

Innovative Concept for Knee Cartilage Treatment, **ScienceDaily**, 2013

EPFL: un matériau intelligent pour traiter le cartilage du genou, **Agence Télégraphique Suisse**, 2013.

Ein Medikament, das durch Bewegung zu wirken beginnt, **Thurgauer Zeitung**, 2013.

"Intelligentes" Material gibt beim Gehen Wirkstoff ins Knie ab, **Schweizerische Depeschagentur**, 2013.

Ein Medikament, das durch Bewegung zu wirken beginnt, **St. Galler Tagblatt**, 2013.

Nano-Medikament für geschädigte Knieknorpel, **Tages Anzeiger**, 2013.

Neues Material für kaputte Knie, **20 Minuten, Suisse daily newspaper**, 2013.

Nano-Medikament für geschädigte Knieknorpel. **Der Bund**, 2013.

Innovative concept for knee cartilage treatment, **theVisualMD**, 2013.

Researchers reveal Innovative concept for knee cartilage treatment, **Phys.org**, 2013.

Language skills

Percian: mother tongue **English:** fluent **French:** intermediate **Arabic:** intermediate **German:** beginner
